Title

Sing-Cell Lipidomic Analysis and Cytotoxicity Studies of Microorganisms Enabled by Plasmonics-Enhanced MALDI-MS

Author

Li, Bochao

Publication Date

2022

UNIVERSITY OF CALIFORNIA
RIVERSIDE

Sing-Cell Lipidomic Analysis and Cytotoxicity Studies of Microorganisms Enabled by Plasmonics-Enhanced MALDI-MS

A Dissertation submitted in partial satisfaction
of the requirements for the degree of

Doctor of Philosophy

in

Environmental Toxicology

by

Bochao Li

December 2022

Dissertation Committee:

Dr. Quan Cheng, Chairperson
Dr. Wenwan Zhong
Dr. Ying-Hsuan Lin

The Dissertation of Bochao Li is approved:

Committee Chairperson

University of California, Riverside

Acknowledgments

Five years ago, I made the decision to study abroad, which allowed me to learn diverse cultures, meet with diverse people, and improve my ability to do scientific research. I am glad I made that decision, which immensely helped me grow. Foremost, I would like to express the most profound appreciation to my advisor Professor Quan (Jason) Cheng, for the continuous support of my Ph.D. study and research, as well as his patience, motivation, enthusiasm, and immense knowledge. His guidance helped me in all the research and writing this thesis. He has instructed me on conducting research and delivering it in the most concise manner. Working and studying under his guidance was a great privilege and honor. I am incredibly grateful for what he has offered me. I could not have imagined having a more excellent advisor and mentor for my Ph.D. study.

My sincere thanks also goes to my thesis and guidance committee members, Professor Wenwan Zhong, Professor Ying-Hsuan Lin, and Professor Yinsheng Wang, for their words of encouragement, various support from unexpected sources, and insightful comments on my Ph.D. study. In addition, I would like to extend my thanks to past and present group members of the Cheng Lab for their direct or indirect contributions to the completion of my Ph.D. It is enjoyable to work with this group of highly motivated individuals. The biggest help in my early time was from Peter V. Shanta, who showed me the ropes and trained me on the tools. I also want to thank Zhengdong Yang and Daniel D. Stuart for their direct contributions to some of my research. A special thanks to Zhengdong Yang, who also provided great help to let me adapt to living in a foreign county.

Lastly, and most importantly, I would like to give special thanks to my parents for their love, care, and sacrifices in educating and preparing me for my future. I am very thankful for their continuing support in completing this research work. Their love and encouragement accompanied me to overcome countless difficulties and frustrations, and sustained me this far. I would also like to thank my grandmother for her unconditional love, care, and encouragement. I am grateful for her company for most of my childhood.

Copyright Acknowledgements

The text and figures in Chapter 2 is reprinted with permission from Chem. Res. Toxicol. 2022, 35, 4, 606–615. The corresponding author, Professor Quan Cheng, directed and supervised the research that formed the basis of that chapter.

The platform established in this work is based on the previous research I collaborated on with Peter V. Shanta. Anal. Chem. 2020, 92, 9, 6213–6217; Environ. Sci. Technol. 2021, 55, 15, 10558–10568

This dissertation is dedicated

To my Father, Qunying Li

and

To my Mother, Renfen Ju.

ABSTRACT OF THE DISSERTATION

Sing-Cell Lipidomic Analysis and Cytotoxicity Studies of Microorganisms Enabled by Plasmonics-Enhanced MALDI-MS

by

Bochao Li

Doctor of Philosophy, Graduate Program in Environmental Toxicology
University of California, Riverside, December 2022
Dr. Quan Cheng, Chairperson

Lipidomics is the comprehensive study of cellular lipids on a large scale based on analytical chemistry principles and technological tools. It provides in-depth understanding of subtle alterations of lipids in cells in response to internal and/or external stimuli, such as environmental stress, diseased condition, drug treatment, and genetic mutation. Mass spectrometry (MS) has been recognized as a vital technique for lipidomics, and MALDI-MS is particularly attractive due to the speed, sensitivity, resolution and throughput benefits. Single-cell lipidomics addresses lipidome characterization at a single cell level, but its study has been largely hindered by complex structural diversity of lipids and limited sample amounts. This thesis describes the methodology development specifically for lipidomic study at the single cell level with a novel, high performing MALDI-MS platform enhanced by plasmonic substrates. The lipid profiling and analysis were applied to a series of cells, including algae, bacteria, and virus from clinical samples.

Chapter Two describes a microchip-based MALDI-MS method to investigate the cytotoxic effects of herbicides on algae through single-cell lipid profiling in combination

with machine learning (ML). The exposure of algal species *Selenastrum capricornutum* to different common herbicides and the resulting cytotoxic behaviors under stressed conditions were characterized. A lipid library for *S. capricornutum* has been established. Machine learning algorithms were applied to the classification of herbicide impact and identification of lipid species affected by the chemical exposure, leading to accurate identification of previously hidden cytotoxic differences.

Chapter Three describes the use of gold nanofilm/MALDI-MS for untargeted lipidomic analysis of *E. coli.* Lipid profiling was performed with intact cells to understand the cellular response to antibiotic treatment (colistin), and statistical models were utilized for classification, variability, and reproducibility assessment. A number of lipids were evaluated as potential biomarkers for indicating gram-negative bacterial response to colistin.

Chapter Four describes a MALDI-MS study with photosensitizer-induced signal enhancement for bacterial lipidomic profiling at both bulk and single cell level. Unique metabolite profiles were constructed by MS measurements and assisted by various statistical models including PLS-DA and LDA. The combination of photosensitizer and fluorescence localization allows discrimination of different bacterial species, providing a potential approach for bacterial identification without a proliferation process.

Chapter Five describes the application of a novel plasmonic chip (Al-chip) with MALDI-MS for virus analysis through lipid profiling. Al-chip delivered higher sensitivity and thus better MS signals than traditional MALDI stainless steel plate. Clinical samples of COVID-19 nasal swabs were investigated by running lipid metabolite profiling to

evaluate the feasibility of high throughput screening of viral infection. A comprehensive data processing and statistical analysis was utilized to reveal key changes among different lipid metabolites and evaluate their potential as diagnostic markers identifying positive and negative samples for rapid COVID-19 screening.

Contents

List of Figures

Chapter 1

Introduction

Metabolomics is a field of study that measures a large number of metabolites simultaneously. Metabolites are small biomolecules that include amino acids, carbohydrates, and lipids. They serve as precursors, intermediates, and end products in biological activities.[1] When found in a biological sample they give a ”fingerprint” of ongoing biological processes. In addition, growing evidence indicates that metabolites directly activate cellular signaling cascades and affect several biological processes, including epigenetic mechanisms and post-translational changes.[2] Thus, metabolomics information may explain the link between cellular activities, metabolic pathways and disease-related molecular processes. An important branch of metabolomics is lipidomics, a study of cellular lipids on a large scale based on analytical chemistry principles and technological tools, in particular mass spectrometry. Figure 1.1 shows the relationship of the genome, transcriptome, proteome and metabolome (lipidome).

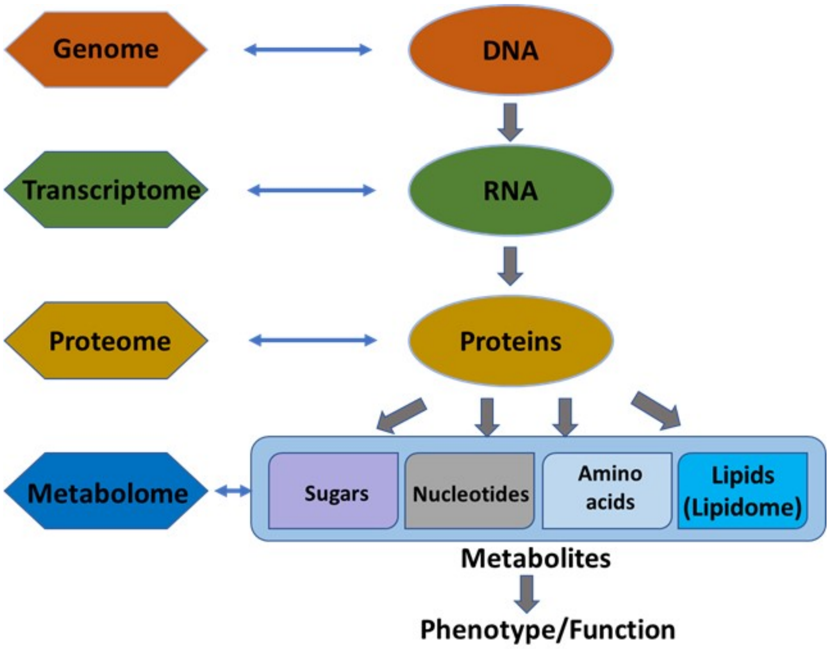

Figure 1.1: General schema showing the relationships of the genome, transcriptome, proteome, and metabolome (lipidome).

It is understood that single cells exhibit metabolic differences from ostensibly homogenous cell groups. Single-cell metabolomics aims to examine a range of cellular metabolites from single cells to comprehend phenotypic heterogeneity. This is a difficult task because of the low analyte abundances and limited sample quantities.

There are a number of reasons that make the analysis of metabolites in biological samples challenging. First, the metabolome is highly dynamic: the presence and quantity of metabolites quickly change due to cellular activity or reactions to the chemical and physical microenvironments. Second, metabolite structures vary significantly in terms of combination of isomers and isobars. These structures are difficult to examine because of the stringent requirements of the selectivity of the analytical approach, and the data consists of both known and undiscovered metabolites. It is still difficult to estimate the number and amount of undiscovered metabolites, although new compounds and metabolic pathways are being discovered continuously.[3][4][5] Lastly, since specific metabolites are only present in trace levels and amplification is not feasible, analytical instruments must be very sensitive. Recent advancements in mass spectrometry (MS) technology, such as high mass resolving power and enhanced sensitivity, and the establishment of metabolite databases, make metabolomics research possible. MS can evaluate concurrently hundreds of metabolites, allowing for label-free chemical identification. In addition to sensitivity, the optimal approach for single-cell metabolomics should permit the high-throughput study of many individual cells. This is necessary for determining the technical variability and discovering biological differences associated with biochemical processes.

Despite the importance, single-cell metabolomics, in particular single-cell lipidomics, is far less explored as compared to other "omics". The research has been largely hindered by complex structural diversity of lipids, limited sample amounts, and the availability of proper techniques. This thesis describes the methodology development and its application to lipidomic study at the single cell level based on a novel, high performing MALDI-MS platform that is enhanced by plasmonic substrates. The lipid profiling and analysis are extended and demonstrated with a series of cells, including algae, bacteria, and virus from clinical samples.

1.1 Single-Cell Analysis

Routine bulk scale omics measurements involving the study of a large number of cells, often in millons, are population-averaging procedures that presume that cell populations are homogeneous. Variability or heterogeneity between individual cells is a key characteristic of biological systems.[6] Due to differential control of gene expression, genetically identical but phenotypically various cell types within the same multicellular organism display different phenotypes. Depending on how they adapt to their microenvironment, cells within the same tissue type also may exhibit different phenotypic profiles. For instance, the proximity of cells to blood arteries, other cells, or oxygen gradients may alter, triggering a response from a subset of the population.[7] The capacity to examine single cells with a high throughput may illuminate biological processes concealed by ensemble measurements. This may be particularly useful when attempting to comprehend diseases such as cancer, in which heterogeneity can play a crucial role in disease development and progression.[8] According to some studies, spreading tumor cells or circulating tumor cells following adjuvant treatment predicts a poor prognosis and suggest metastatic development in cancer patients.[9][10][11] Even though it is possible to detect these rare cell populations, advances in single-cell proteomics and metabolomics could provide much-needed insight into the molecular and phenotypic nature of these cells, which are believed to cause significant inter-patient variation in their dormancy or expression.[12]

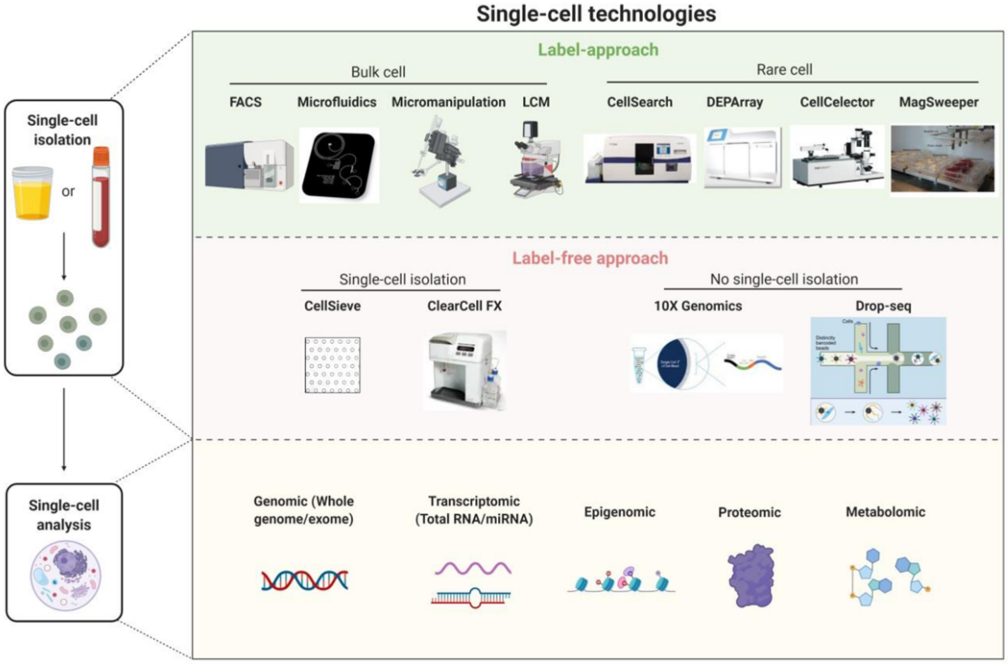

Figure 1.2: An overview of single-cell technologies. Single-cell technologies involve two steps: single-cell isolation followed by single-cell analysis. Single-cell isolation includes label approaches (e.g., FACS, microfluidics, micromanipulation, LCM, CellSearch, DEPArray, CellCelector, and MagSweeper) and label-free approaches (e.g., CellSieve and ClearCell FX). Some single-cell technologies such as 10× genomics and drop-seq do not involve single-cell isolation before single-cell analysis. Single-cell analysis techniques include genomics (whole genome/exome), transcriptomics (total RNA/miRNA), epigenomics, proteomics and metabolomics. FACS, flow assisted cell sorting, LCM, laser capture microdissection. Reprinted with permission from reference [13].

Analyzing single cells also can reveal uncultivable microorganisms that impact community stability and resiliency in microbiomes of diverse ecosystems.[14] However, microbial cells pose a unique challenge due to their size, ranging from 1/1000th to 1/10000th of eukaryotic cells. Improved techniques for analyzing such small samples will provide critical insights, for instance, into the context of host-pathogen interactions, especially for intracellular pathogens. Critical distinctions between uninfected cells and early-, mid-, and late-infection within a population of cells are often averaged using traditional techniques, resulting in the loss of essential cell-cell communication and infection processes. A key obstacle to microbiome proteomics research is the sheer quantity of different species at varying concentrations, which may impede detection efficiency and false-discovery control.[15] Microdissection of microbiome and biofilm samples proves better than the processing exceedingly small samples because it considerably improves the investigation into the homogeneity of species that exist simultaneously. Figure 1.2 shows the technologies involving single-cell isolation and single-cell analysis.[13]

1.1.1 Single-Cell Analytical Techniques

Fluorescence Detection

Early investigations into single cells primarily relied on the observation under a light microscope. The fluorescence method is a classic technique of analysis.[16][17][18] Basically, it uses a fluorescence derivatization reaction to change chemically a non-fluorescent substance and convert it into a fluorescent substance by adding a reagent. Two main types of fluorescence-derived reagents currently used in single-cell analysis are: fluorescent-generated and fluorescent-labeling reagents. The fluorescence-generating reagent is a non-fluorescent reagent that reacts with the intracellular components to generate fluorescent substances. For example, in the presence of the nucleophile reagent, cyanide ion (CN-), 2,3-naphthalenedicarboxaldehyde can react with intracellular amino acids to generate polyaromatic compounds with strong fluorescent properties. The reagent can be used to detect amino acids in cells. In the absence of CN-, it will react with glutathione (GSH) to form isoindole adducts with strong fluorescence, and the content of intracellular glutathione then can be detected by the fluorescence intensity. Fluorescent labeling reagents have strong fluorescent groups, such as fluorescein isothiocyanate (FITC), with both fluorescent groups and reactive groups reacting with NCS in their molecular structure. Through the coupling reaction between the reactive group and the N-terminal amino group of the amino acid, protein or polypeptide in the cell, the substrate is fluoresced for the analysis of these cellular substance. However, this method has two disadvantages: (1) while most molecules in cells are non-fluorescent and need to be labeled, unknown molecules in cells cannot be labeled and detected; (2) fluorescent probes have a certain wavelength range and can only be detected in a limited window, which allows the detection of only 3-4 molecules that do not interfere with each other.

Electrochemical Detection

Electrochemical detectors are suitable for single-cell analysis because of their high sensitivity. They even can be applied as intra- or extracellular probes for the label-free detection of metabolites that are present inside the cell and those that are released into the extracellular microenvironment. However, only electroactive species can be analyzed, which limits the applicability of electrochemical techniques to targeted studies of metabolites in single cells. Various microscale electrochemical methods have been developed to track different physiological processes.[19] For example, the release of metabolites like catecholamines and oxygen can be easily monitored electrochemically.[20]

Electrochemical sensors also can be utilized as detectors following electrophoretic separations. Capillary electrophoresis (CE) combined with less selective electrochemical probes, can serve as a platform for investigating a greater variety of metabolites than electrochemical sensors employed without separation. T.M. Olefirowicz, et al. employed very thin capillaries to collect cytoplasm samples from single snail nerve cells.[21] This was then followed by CE separation and amperometric detection using a two-electrode configuration. This approach revealed excellent selectivity for catecholamine, indolamine, and related metabolites as neurotransmitters. Weng and Jin described a straightforward assay for identifying amino acids in individual lymphocytes using CE coupled with electrochemical detection. It could detect quantities of four amino acids ranging from femtomoles to attomoles.[22] Ai et al. fabricated an amperometric sensor based on the electrochemical deposition of platinum nanoparticles on the surface of carbon fiber microdisk electrodes through nanopores containing a polymer matrix, and then employed it for real-time monitoring of oxidative bursts from single plant protoplasts.[23]

Mass-Spectrometric Detection

Mass spectrometry (MS) is used widely in single-cell analysis due to its benefits of speed, high selectivity, and high sensitivity.[24][25] MS is a label-free analytical technique that identifies virtually any analyte and provides structural information. In addition, methodological advancements have been made to adapt MS for single-cell analysis. Single-cell MS has been demonstrated by a number of examples, using various types of cells.[26][27][28][29] Currently, a variety of ionization methods have been developed that can desorb/ionize various types of samples, including electrospray/nano-electrospray ionization (ESI/Nano-ESI), laser ablation/laser desorption ionization (LA/LDI) and secondary ionization mass spectrometry (SIMS). These ionization techniques can ionize many compounds, including proteins, peptides, esters, and small molecule metabolites.[30][31]

Other Techniques

Spectroscopic techniques also can analyze metabolites in single cells. For instance, the glycogen metabolism of yeast cells has been investigated using single-cell spectroscopy and image analysis.[32] Shinohara and Wang studied the release of dopamine from a mammalian nerve cell following incubation with a drug using an enzyme-catalyzed luminescence method.[33] The approach was very sensitive, quick to measure, and did not need any preparation of the single-cell sample. Goff et al. reported a method for the measurement of ethanol formation in single living cells of unicellular algae by synchrotron Fourier transforms infrared spectromicroscopy.[34] Moreover, using Raman spectroscopy, some studies reported the detection of nucleic bases and amino acids in single cells.[35][36][37][38] Moritz et al. investigated the influence of a drug on the metabolic states of individual *Escherichia coli* cells by analyzing their Raman fingerprints.[39] However, this technique is unable to discriminate between free species and their corresponding macromolecules.

1.1.2 Matrix-Assisted Laser Desorption/Ionization of Single Cell

Matrix-assisted laser desorption/ionization mass spectrometry (MALDI MS), is a widely used technique for analyzing single cells. This technique employs a laser to ablate a sample surface covered with a chemical matrix that absorbs light.[40][41] The matrix selection for the study of metabolites is critical in MALDI. The matrix must allow for the ionization of the species of interest through charge transfer while producing few but well-characterized peaks that do not interfere with endogenous species collected from cells. In addition, the matrix must generate crystals small enough to preserve single-cell resolution.

Profiling single cells based on their positional coordinates could improve throughput since less surface area is evaluated. Krismer et al. used microscale sample preparation for high throughput MALDI-MS screening of single algal cells.[42] They used a stainless steel microarray slide, 300 m in diameter and 720 m from center to center, to load droplets carrying single cells into 1430 wells using a spotting robot. The cell metabolism then was inhibited by submerging the microarray in liquid nitrogen, which aids cell lysis via the production of ice crystals. Monitoring the cell-loaded microarray concurrently with confocal fluorescent microscopy confirmed the effectivity of loading single cells before matrix application and MALDI analysis of cellular positions. The mass spectrum was collected from a single algal cell as well as a bulk cell spectrum, highlighting some of the discovered molecular species.[42] The authors note that the single-cell and bulk-cell spectra have the same peak composition. But the relative abundance of identified species differs owing to the heterogeneity of the bulk cell mixture's cells. This approach was subsequently used to investigate phenotypic changes in *C. reinhardtii* algal cells that were isoclonal and genetically heterogeneous.[43] Twenty-six metabolites, such as chlorophyll and triacylglycerol, were measured in thousands of single cells. By cultivating cells under varying nitrogen conditions, the researchers discovered that genetically heterogeneous cultures exhibited more phenotypic flexibility than isoclonal cultures, which indicates the significance of the phenotype to biological function.[43] Cell nuclei were tagged with a fluorescent tag for optical imaging. The generated fluorescence image provided relative coordinates for each cell in comparison to the etched marks on the glass slide. For MS profiling, the MALDI laser was directed to the exact coordinates of each cell.

1.1.3 Technical Challenges

The size and volume of a single cell may vary by order of magnitude depending on the organism and type of cell. Microorganisms such as *Bacillus subtilis*, *Staphylococcus aureus*, and *Escherichia coli* often have individual cell volumes ranging from 0.4 to 3 μm^3.[8][44] Human cell types can vary by multiple orders of magnitude, with erythrocytes, HeLa cells, and oocytes having respective volumes of around 100,3000 and 4×10^6 μm^3. Specialized tools and methods for sample preparation and analysis are required for measuring the size of a single cell. It may be necessary to separate and isolate specific cells using specialized methods depending on the cells of interest. Ideally, these strategies will introduce as few artifacts as possible during the process. Detecting and quantifying biomolecules of interest in the small sample volume of a single cell requires highly sensitive measuring.

The development of whole-genome and whole transcriptome amplification (WGA/ WTA) has enabled the study of single-cell genomics and transcriptomics despite the trace amount of genetic material contained in a cell.[45] The availability of commercial kits and the common use of unique molecular identifiers (UMIs) to barcode individual RNA molecules have enabled the investigation of genome and transcriptome sequences in single cells.[46] In contrast, mass spectrometry-based single-cell omics technologies focus on proteins, metabolites, and lipids are less mature but are new and promising domains. Unlike DNA and RNA, biomolecules such as proteins, metabolites, and lipids cannot be amplified. Therefore, one must work with the quantity existing in the cell and focus on improving the intrinsic sensitivity of the technique of analysis. So far, the majority of single cell MS-based omics research has been on proteomics, partly because this discipline is more developed than metabolomics and lipidomics.

1.2 Plasmonic Substrates for MALDI- TOF-MS

1.2.1 Principle and Mechanism of MALDI-TOF-MS

In MALDI-MS, the analyte of interest indirectly is desorbed and ionized by a laser pulse aimed at the matrix (and ionizing agent in certain circumstances) when a laser beam is directed at a specified area where the sample is attached. Consequently, this approach can create ions with a high mass (soft ionization). A selected matrix must have a high absorption coefficient at the precisely applied wavelength to accomplish effective ionization of the sample.[47] The matrix first serves as a separator for the analyte as a result of matrix isolation, a phenomenon that minimizes intermolecular tensions.[47] Therefore, it inhibits the development of clusters inside the analyte. Upon laser irradiation, the matrix begins to function properly in the gentle ionization of the analyte by absorbing most of the photon energy. As a result, the matrix shields the analyte from direct laser irradiation. The absorbed energy causes the matrix to become excited. The matrix then undergoes a phase transition from solid to gas due to this excitation, and a thick cloud of gas escapes the vacuum chamber. A collision between neutral analyte molecules and matrix ions generates the final ionized analyte product.[47]

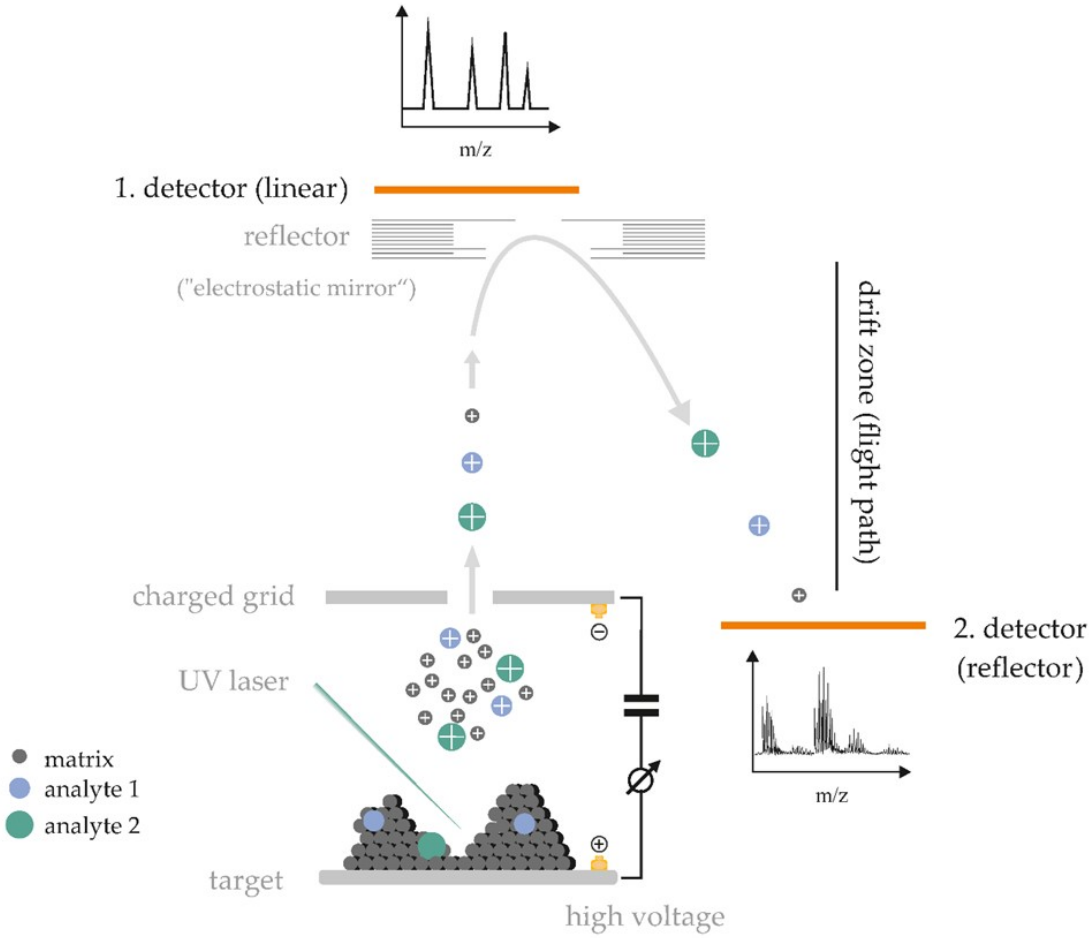

Figure 1.3: Simplified schema of the positive ionization matrix-assisted laser desorption/ ionization-time-of-flight (MALDI-TOF) process occurring in the mass spectrometer. The influence of the detection using either the linear or the reflector mode is emphasized in the figure. Reprinted from reference [47].

Laser irradiation results in the soft ionization of the analyte molecules. The accelerated and directed ions may be matrix ions, analyte ions, or ionized fragments of analyte molecules towards the drift zone. This area is much bigger than the ionization or acceleration zones. As Figure 1.3 shows, the ion detector is situated at the end of the flight path and can record the flight duration and intensity of the individual ions that arrive at the ion detector. As anticipated, larger analyte ions need more time to reach the detector, but lighter ions cover the same distance in less time. Following the equation below, the ratio of mass per charge (m/z) may be calculated using the instrument's recorded data.

$$\mathrm{m/z = 2\,eE(t/d)^2}$$

In this equation, m represents the mass of the ionized molecule, and z represents the number of electrons removed from the molecule. In the equation, E is the accelerating voltage, e is the elementary charge, t is the time of flight, and d is the length of the drift zone.

Initially, MALDI devices were based on the linear ToF spectrometer. In the linear mode, ions of varying masses approach the detector depending on how long it takes them to traverse the drift zone. As predicted, heavier ions arrive at the detector later than their lighter counterparts. Therefore, heavier ions possess greater m/z values than lighter ions. Reflection mode, a more sophisticated method, was used to compensate for the linear mode's lack of resolution. This advanced technology is comprised of ion mirrors and electric fields that repel the ions back into the drift zone and compel them to return to the detector, which now is located on the other side of the flight path. Figure 1.3 represents the schematic explanation of the principle of MALDI-TOF-MS [48]

1.2.2 MALDI Matrix

An appropriate MALDI (UV) matrix possesses the following characteristics: 1). The matrix must have substantial absorption at the laser's emission wavelength, 337 or 355 nm. Because ionization efficiency (and consequently ion production) improves the matrix absorption coefficient, all documented organic matrices feature an aromatic ring structure with delocalized electrons. This is why 2,5-DHB is useful as a MALDI matrix.[49] Although extinction coefficients are frequently obtained in a solution, MALDI matrix absorption characteristics should be assessed in the solid state.[49] It is not an issue if the monochromatic laser light does not match the matrix's UV maximum since UV absorptions are wide. As a result, optimized matrices for 337 nm lasers may be employed at 355 nm. 2). The matrix should have a high sensitivity and an excellent signal-to-noise ratio (S/N) for the analytes of interest. 3)An excellent MALDI matrix has a low background. Low background signals limit interference between the matrix and analyte ions. It is important to note that oligomers of the matrix are often generated in the gas phase.[50][51] Most matrices generate signals at m/z ratios greater than their initial molecular weight. These distinctive matrix peaks may be exploited as calibrant peaks.[52] 4). An ideal matrix should isolate produced ions and inhibit analyte cluster formation, such as dimer formation. These clusters would complicate spectra and reduce sensitivity. 5). Crystallization between the matrix and the analyte results in co-crystals that must be equally homogenous and feasible. Enhancing the crystal's homogeneity is crucial since it impacts the repeatability of the recorded MALDI mass spectra from "shot to shot".

Carboxylic acids are commonly employed as matrix chemicals due to their acidity, which promotes the formation of H^+ adducts - many matrices are derived from cinnamic or benzoic acids. As sodium is a pervasive element, Na^+ adducts are also detected. K^+ ions are relatively plentiful within cells, which frequently result in K^+ adducts in biological samples. In addition to the increased formation of H^+ adducts, there is another reason to utilize carboxylic acids: the presence of the π-electron system makes conventional matrices very soluble in organic solvents. Since MALDI MS is used primarily to examine polar molecules, such as peptides, which seldom are seldom soluble in organic solvents, water is an essential component of the most popular solvent systems. The presence of polar groups, such as carboxylic acids, improves the solubility of the matrix in water.

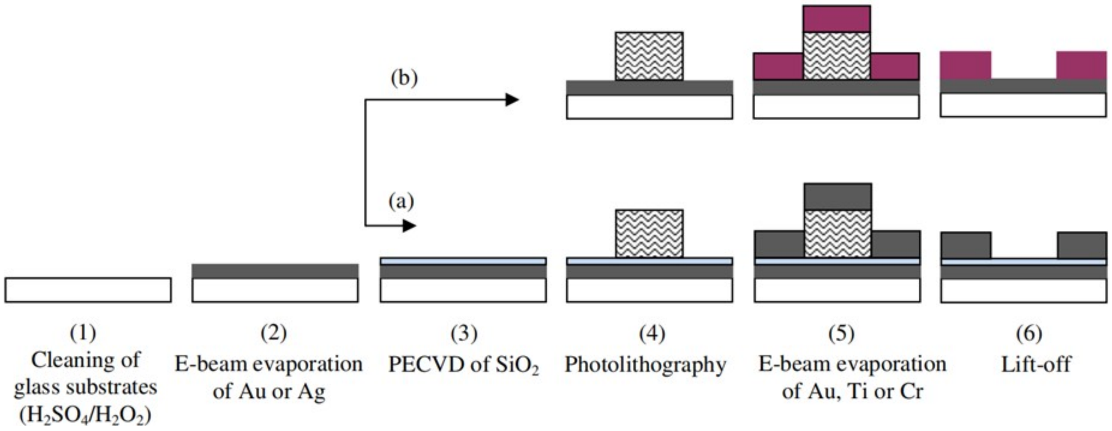

Figure 1.4: Fabrication procedure of the micropatterned resonance SPRi array. (1) BK7 glass slides were cleaned in a hot (ca. 90 °C) bath of piranha (3:1 H2SO4:H2O2) for about 30 min. The substrates were copiously rinsed with water, dried with a nitrogen stream, and dehydrated in a 70 °C oven for 1 h. (2) Deposition of 2 nm chromium adhesion layer, followed by a 51± 2 nm gold or silver layer via e-beam evaporation. (3) Deposition of 3-6 nm silicon dioxide by plasma enhanced chemical vapor deposition (PECVD) at 300 °C. (a) Hydrophilic microarray, (b) hydrophobic microarray for thiol-based surface chemistry. For simplification purposes, the adhesion layer (Cr or Ti) is not represented. Reprinted with permission from reference [53]. Copyright @ 2011 American Chemical Society.

1.2.3 Design and Properties of Plasmonic Substrates

Previous studies in our lab have described microarray substrates with a thin gold or aluminum film, showing high performance for SPR imaging.[53][54] The fabrication of gold microchips is schematically represented in Figure 1.4, and the optical images of the microarray chips are shown in Figure 1.5.[53] Briefly, it entails the deposition of two metal layers on a glass substrate: the first layer is flat and facilitates the development of SPP, while the second layer serves as an electromagnetic barrier, defining the geometry and providing a hydrophobic, nonfouling surface. This layer has a high reflectivity to permit the saturation of the background signal though attenuated total reflection, a high imaginary component of the refractive index, and a suitable thickness to prevent SPR excitation. This gold layer could be substituted with chromium, titanium, nickel, or aluminum. Microarrays with a diameter of 800 m were created and described. Two 800 μm microarrays with various surface characteristics were made. First, titanium surrounds hydrophobic gold wells. This surface is for SAM or thiol-based chemistry. The second microarray has hydrophilic wells enclosed by a hydrophobic gold layer for bioabsorption and membrane investigations. In the latter situation, the chip needs plasma-enhanced chemical vapor deposition (PECVD) to add a thin hydrophilic surface of silicon dioxide to the wells for improved wetting. Both chips could be simply functionalized by immersion in the desired solution, eliminating the need for costly arraying equipment. In contrast, chips with gold islands on glass substrates were also produced using the same method.

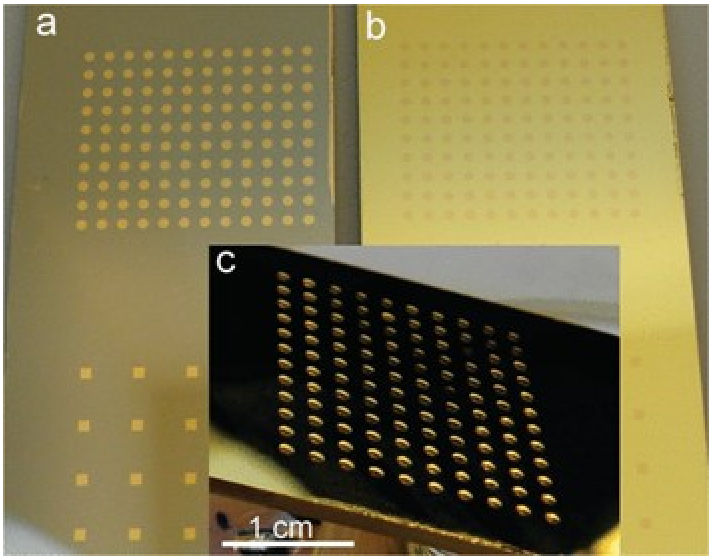

Figure 1.5: Optical images of the micropatterned resonance SPRi chips. The array has a size of 2 cm^2, containing 12 × 10 microwells of 800 μm diameter each. a: hydrophobic gold chip, b: hydrophilic silica chip, c: hydrophilic chip after rapid immersion in PBS buffer. The wells are instantaneously filled with the aqueous solution. Reprinted with permission from reference [53]. Copyright @ 2011 American Chemical Society.

As for the lipid analysis, the 50 nm gold substrate was selected as an essential feature of the substrate design based on three benefits/analytical merits: (i) enhanced fluorescence signal[55][56][57] due to surface plasmon coupling with fluorophore emission, (ii) enhanced MS/MS signal due to rapid thermalization of excited electrons (i.e., hot electron transfer)[58] and generation of laser-induced plasma at near gold ablation thresholds,[59] and (iii) surface robustness to oxidation, sample processing, and sample archiving. Photolithography and e-beam evaporation were used to fabricate gold chips. Well size was carefully considered, allowing for easier cell identification, high-throughput analysis, and easy interaction with MALDI-MS software. Nanovolume sampling and cell isolation needed a well diameter $\leq 800\ \mu$m with a periodicity of 3 mm. Based on the benefits mentioned above, the gold microarray chips were applied to the lipid study of microorganisms in Chapter 2, 3, and 4.

A recent study from our group reported an SPR sensor with aluminum thin films using the standard Kretschmann configuration that gold films dominated previously.[54] In bulk and surface testing, Al films demonstrated exceptional sensitivity. Fabrication was achieved by electron-beam physical vapor deposition (EBPVD), which allowed Al films to oxidize in air to form a nanofilm of Al_2O_3. These films yielded robust stability for sensing applications in buffered solutions. Figure 1.6 depicts a summary of the fabrication.[54] Photolithographic patterning and multiple deposition stages are used to construct 15 nm-thick wells with 800 nm diameter and 150 nm thick walls. The aluminum layer, which is 150 nm thick, dampens effective plasmonic absorption, leaving microwells as the only plasmonically active regions. The Al/Al_2O_3 layer significantly reduced nonspecific binding from proteins in human serum compared to Au. Further characterization shows a broader working range than Au films for SPR imaging analysis. When combined with its economic and manufacturing advantages, Al thin-film has the potential to be a highly favorable plasmonic substrate for a variety of biosensing demands in SPR configurations. Based on the benefits of the plasmonic substrate with Al thin-film, it was further applied to MALDI-MS performance investigation, which will be demonstrated in Chapter 5.

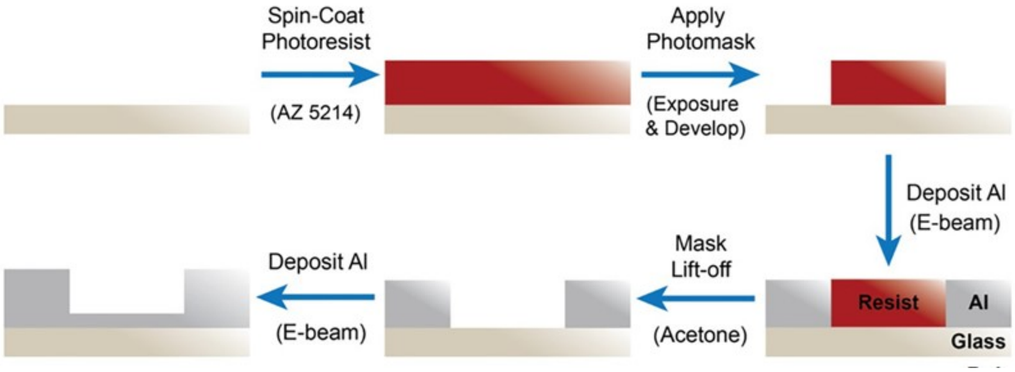

Figure 1.6: Fabrication scheme of the microarray substrate. Reprinted with permission from reference [54]. Copyright @ 2020 American Chemical Society.

1.3 Lipid Analysis based on Mass Spectrometry

Lipidomics is the large-scale profiling and quantification of biogenic lipid molecules. It entails comprehensive lipid pathway investigation and physiological relevance interpretation based on analytical chemistry and statistical analysis.[60] [61] In lipidomics research, a large amount of information that quantitatively depicts spatial and temporal changes in the content and composition of lipid molecular species is accumulated and correlated to disturbances by diseases, drugs, and the environment.

1.3.1 Lipid Classes and Structural Diversity

Lipids are structural and functional molecules that serve crucial biological functions in cellular barriers, membrane matrices, energy storage, and signaling. Their diverse structures and physiochemical characteristics provide critical biological roles in various cellular activities. Lipids are classified as hydrophobic or amphiphilic molecules based on their biosynthetic and chemical structures. Biogenic lipid molecules are composed entirely or partially of two types of biochemical building blocks: ketoacyl and isoprene groups[62][63] According to this classification, lipids are classified into eight classes: fatty acyls (FAs), glycerolipids (GLs), glycerophospholipids (GPs), sphingolipids (SPs), sterol lipids (STs), prenol lipids (PR), saccharolipids (SLs), and polyketides(PK)[62][63] Chemical structures representative of these groups are illustrated in Figure 1.7.[64] Each category has hundreds of thousands of lipid molecules detailed in the Lipid Metabolite and Pathways Strategy (LIPID MAPS) database.

The structural variety of lipids endows lipid molecular entities with a wide range of physiological functions. For example, triacylglycerols (TAGs) are cells' primary energy storage molecules. Long-chain fatty acids (LCFAs) perform crucial functions in controlling energy metabolism.[65] Eicosanoids, lysophospholipids (LPLs), and phosphoinositides (PIs) are lipid molecules that act as signaling messengers in cellular metabolic processes.[66] Furthermore, lipid composition is strongly linked to the physical features of the cellular membrane. For example, the relative size of the head group and the length of the FA chain have an influence on cellular membrane curvature and fission,[67] which may affect the activity and localization of membrane proteins.[68][69] Most natural lipids are composed of diverse hydrophobic fatty acyl chains and polar head groups connected to distinct lipid backbone structures (e.g., glycerol and sphingoid bases). The structural diversity of the lipidome arises from variations in the type of head groups, the length of the fatty acyl chain, the level of unsaturation, double bond location, cis-trans geometric isomerism, branched functional groups in the fatty acyl chains, and the type of covalent bond linked to the head groups, namely ester (acyl-), ether (alkyl-), and vinyl-ether (alkenyl-). Figure. 1.8 depicts the diversity and complexity of lipid structures using GPs and SPs.[70]

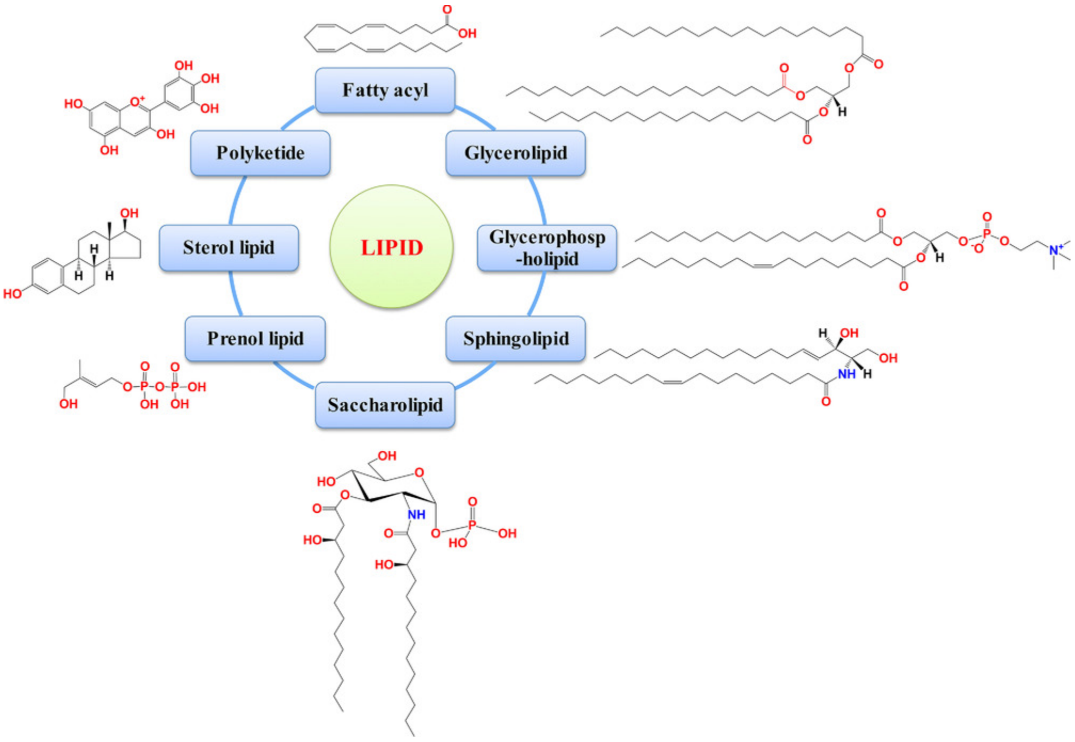

Figure 1.7: Eight categories of lipids with their representative chemical structures. Reprinted with permission from reference [64]. Copyright ©2017 WILEY-VCH Verlag GmbH & Co. KGaA, Weinheim

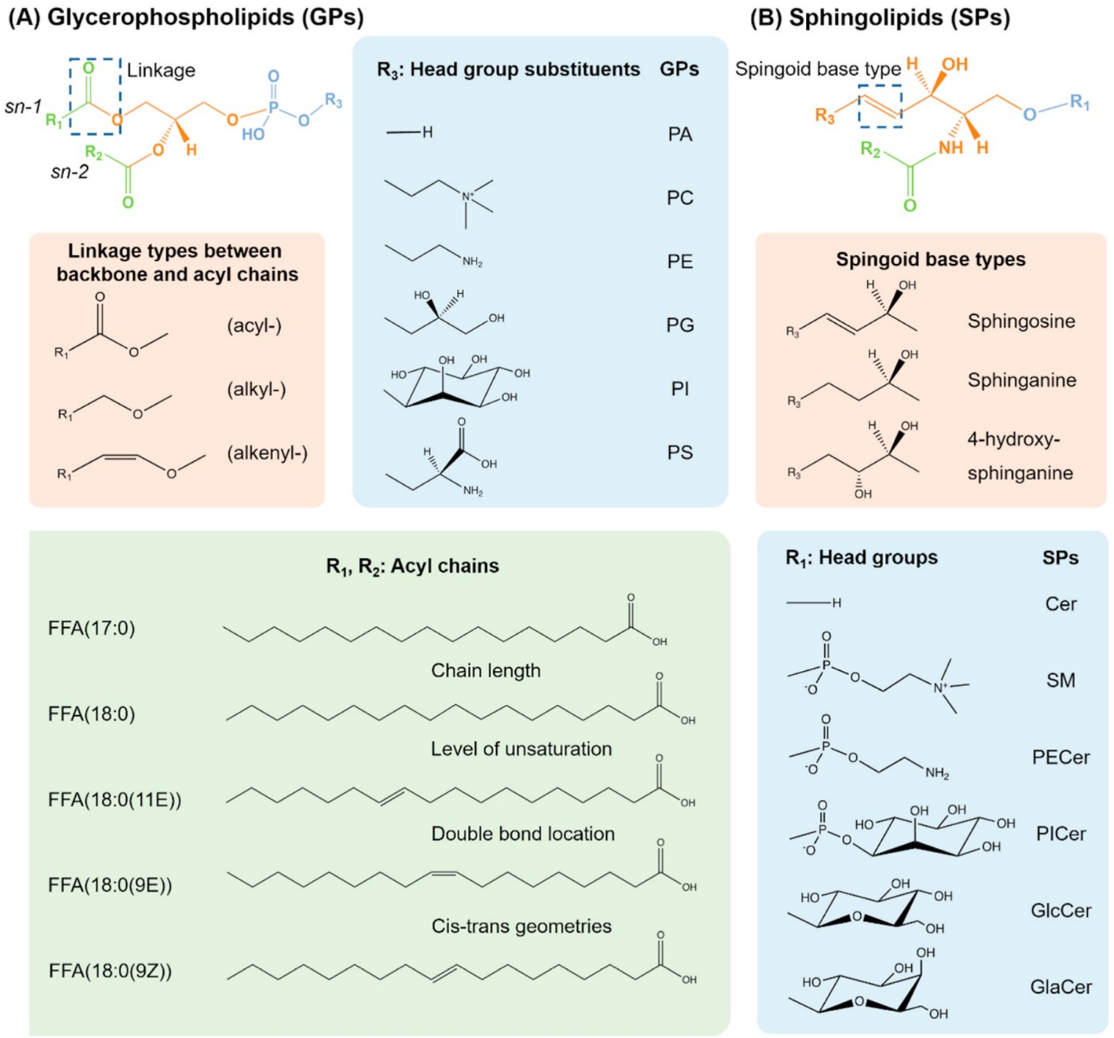

Figure 1.8: The illustration of the diversity and complexity of lipid structures by taking GPs and SPs as examples. GPs structure diversity lies in the variety of head group, fatty acyl chains at the sn-1 and sn-2 positions as well as the linkage between glycerol backbone and sn-1 fatty acids. The head group generally represents phosphate group, phosphatidylcholine, phosphatidylethanolamine, phosphatidylglycerol, phosphatidylinositol and phosphatidylserine, which respectively defines the classes of GPs as PA, PC, PE, PG, PI and PS, etc. Another aspect of diversity stems from three different linkage: ester (acyl-), ether (alkyl-) and vinyl-ether (alkenyl-). Besides, the fatty acyl chains also vary in chain length, level of unsaturation, double bond location and cis-trans geometries. Similarly, combinations of different structures of head group, sphingoid based type and N-acyl chain constitute tens of thousands of SPs. Reprinted with permission from reference [70]. Copyright © 2020 Elsevier B.V.

1.3.2 Data Processing and Analysis

The study of lipidomics, particularly non-targeted lipid analysis, has created massive volumes of data, which require bioinformatics methods to assist in data processing and obtaining significant biological information. Several types of data-processing software are available, such as Progenesis from Waters and Clinpro from Bruker. Some organizations, such as the lipid metabolite and pathways strategy (LIPID MAPS), the Human Metabolome Database (HMDB), provide free access to their databases. In addition, several online platforms, such as MetaboAnalyst, were created to offer free data processing assistance. More functional lipidome can be discovered using analytical tools, which will considerably improve knowledge of disease processes and further the development of lipidomics.

Data Pre-Processing

Data pre-processing is a comprehensive procedure to extract useful metabolomic information from raw data. First, noise and background signals need to be removed. Random noise and background signals from the ambient environment may interfere with cells' "true" metabolomic fingerprints. To eliminate such interference, all acquired signals must be filtered with a set threshold to exclude the random noise generated by the instrument. Background signal also must be removed. In addition, attention should be given to the selection of noise threshold. For unnecessarily high criteria can exclude valuable metabolomic data. Second, the intensity of ions needs to be normalized, and the normalized intensities of ions can then be associated with their relative abundances in various cells. After data pre-processing, complex raw data is transformed into simpler data matrices consisting of observed cellular metabolites and their normalized intensities.

Univariate Analysis

Univariate statistical analysis is required to disclose the alteration of cellular metabolites corresponding to a particular biological process (e.g., drug treatment and environmental stress). This method identifies the difference between metabolite, namely, upregulation or downregulation, and prospective metabolomic biomarkers in single-cell metabolomics; theses biomarkers are features of groups of cells with certain biological properties. Similar to traditional LC-MS/MS metabolomic data analysis, the t-test is frequently employed to identify compounds with substantially different relative abundances between two groups. The compounds with positive test findings (p-value $\leq$ 0.05) are considered metabolomic biomarkers. Analysis of variance (ANOVA) is the preferred statistical tool for identifying biomarkers among several research groups when examining complicated systems with more than two groups of single cells. Similar to the t-test, data normality needs to be extensively evaluated before performing either parametric (i.e., One-way) or non-parametric (i.e., Welch's) ANOVA. Univariate analysis is a strong and common way to find metabolomic biomarkers. However, it can not handle all the metabolic patterns.

Multivariate Analysis

Multivariate analysis handles single-cell metabolomics data by analyzing all factors (i.e., metabolites and their abundances). Multivariate analysis projects high-dimensional raw data into lower-dimensional space (e.g., 2D or 3D space) uses fewer variables, and preserve most of the information. This decreases the raw data's dimensionality yet retains essential information about cell activities. Complex cellular metabolomic profiles may be seen in 2D or 3D, allowing intuitive cell heterogeneity display. Unsupervised and supervised techniques are the two forms of multivariate analysis. Unsupervised approaches, including k-means clustering, Principal Component Analysis (PCA), and t-Distributed Stochastic Neighbor Embedding (t-SNE), reduce the dimensionality of the original data by grouping items with greater similarities in the high dimensional space in a linear or non-linear manner. In contrast, supervised approaches, such as partial least squares discriminant analysis (PLS-DA) as shown in Figure 1.9[71], orthogonal projections to latent structures discriminant analysis (OPLS-DA), and random forest (RE), need prior knowledge of the group characteristics of individual cells. The grouping information will be utilized to apply the appropriate group labels to all subsequent single cells in the training data set.

Advanced Data Analysis

There are more advanced data analysis approaches that have been recently introduced. Due to its high efficiency, artificial intelligence (AI) has been used to analyze single-cell metabolomics data. AI depends on computational resources to "teach" models using a variety of algorithms and gradually approaches the underlying complexity of the investigated object, which is often difficult to study with each interaction of "training". Among all AI approaches, machine learning (ML) has its advantages for single-cell based studies. Complex mathematical models can be developed by combining traditional statistical analysis with modern algorithms. These models can be classified into supervised and unsupervised models. So far, only supervised machine learning algorithms have been employed in single-cell metabolomics research. The obtained datasets are separated into two sets in those models: the training set and the validation set. The training data is used to build multiple ML models iteratively using a variety of algorithms such as random forest (RF), support vector machine (SVM), logistic regression (LR), and artificial neural network (ANN). The validation set is used to evaluate the model's ability to predict the group attribute of foreign objects. The ML models could yield excellent prediction accuracy of an unknown single-cell phenotype based on its integral metabolomic profile if the training set contained a significant number of single cells.

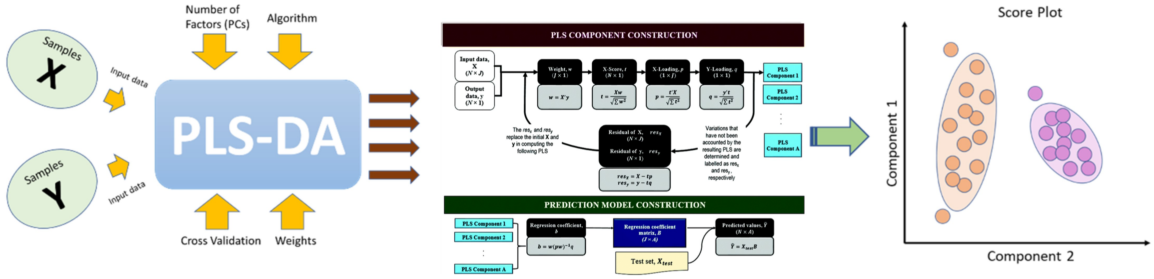

Figure 1.9: Schematic flow of computational steps in estimating the A PLS components using PLS1-DA algorithm. N: number of samples, J: number of variables; X: input data; y: output data; x_{test}: test sample. Reprinted with permission from reference [71].

1.4 Aplications of MALDI-MS in Diverse Fields

1.4.1 Microbial identification using MALDI-MS

In the past, bacterial culture and biochemical testing were frequently employed to detect pathogens with distinct morphological features, such as bacteria, yeasts, and fungi. Methods based on traditional morphology and staining were also employed to identify bacteria. However, due to their lengthy turnaround times and laborious process, these approaches do not rapidly and accurately identify of pathogenic bacteria according to current requirements of clinical microbiology laboratories. Since the 1960s, molecular diagnostic techniques, such as 16S or 18S rRNA gene sequencing, real-time polymerase chain reaction (PCR) tests, and multilocus sequencing typing (MLST),[72] have been employed to identify bacteria. Although molecular technology-based approaches have significantly decreased detection time, there is still a need to lower detection costs through simplified procedures with large-scale clinical applications. Motivated by this need and drawing on the technical features of MALDI-TOF MS, bacterial cell molecular mass fingerprinting by MALDI-TOF MS has been developed during the past several years to enable rapid and accurate identification of bacteria in clinical microbiology laboratories. Bacterial mass fingerprinting technologies, such as VitekMS created by BioMérieux and MALDI Biotyper developed by Bruker Daltonics Corp, were implemented into commercial instruments for routine clinical applications. During MALDI-TOF MS-based bacterial identification, entire bacterial cells or whole cell extracts are deposited on the MALDI plate, followed by a matrix and MS analysis. Fingerprints of the cellular molecular mass are derived mainly from the most abundant small proteins or polypeptides, particularly ribosomal proteins. Different species with varied mass patterns were discovered. Pattern matching makes it feasible to identify bacteria at the species level.

1.4.2 MALDI-MS Investigations Targeting SARS-CoV-2

Using MALDI-TOF technology, researchers have studied and analyzed several viruses, including human herpesviruses, influenza viruses, and diseases associated with severe enterovirus infections, such as echovirus, coxsackievirus A and B, and poliovirus.

[73][74][75][76][77] Currently, MALDI-MS approaches have been tested to detect SARS-Cov-2 based on "biotyping" and "genotyping" strategies. One research is based on "proteotyping" with high-resolution MALDI-FTICR at the peptide level,[78] while several investigations employed "biomolecular host profiling" to identify biomarkers produced after SARS-CoV-2 infection. [79][80][81][82][83].

Figure 1.10 below illustrates the general workflow [84] SARS-CoV-2 patients and control volunteers were enrolled, and samples were collected using several sampling protocols. Following that, biomolecules (RNA or proteins) were extracted based on the MALDI-MS techniques utilized (proteotyping, biotyping, genotyping, and biomolecular host profiling). The samples were subsequently subjected to MALDI-MS analysis. Finally, the data was analyzed through online or in-house database searching or machine learning techniques, identify SARS-CoV-2 infection. We have started the proof-of-concept investigations using MALDI-MS and the biomolecular host profiling methods to evaluate host response to forecast infection. It could potentially become an exciting alternative to the present testing methods (PCR and immunoassay) for identifying SARS-CoV-2 infected patients. However, viral load varies among infected people, particularly between symptomatic and asymptomatic subjects, resulting in a broad variation of host responses. The development of MS-based technologies and associated multi-omics methods needs additional testing before they could become a reference approach for preparation of future outbreaks.

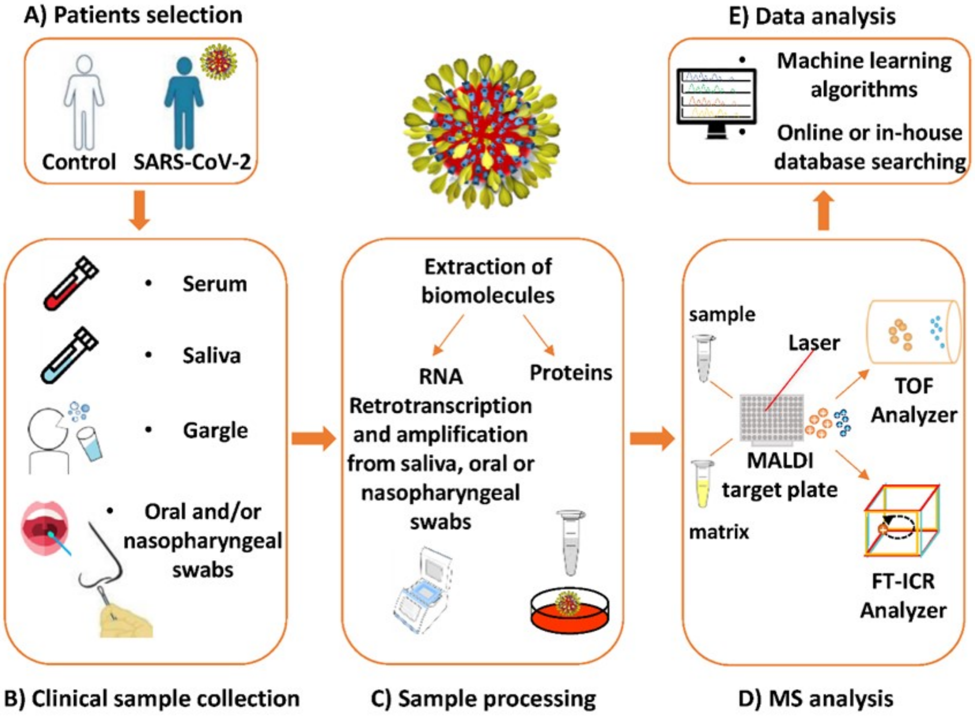

Figure 1.10: Workflow of main MALDI MS-based investigations targeting SARS-CoV-2. (A) Control subjects and (PCR-diagnosed) SARS-CoV-2 patient enrollment. (B) Clinical sample (serum, saliva, gargle, oral, and/or nasopharyngeal swab) collection from control subjects and SARS-CoV-2 patients. (C) Sample processing based on the extraction of RNA or proteins. RNAs are retro-transcripted and amplified from saliva, oral, and/or nasopharyngeal swabs in genotyping methods; proteins are extracted from body fluid samples or from cell-cultured SARS-CoV-2 samples in the proteotyping and biotyping methods; in the case of biomolecular host profiling methods, proteins are extracted from bodily fluids. (D) MS analysis based on the ionization in a MALDI source and the separation of the ions into two different types of analyzers: TOF and FT-ICR. (E) Data analysis using online or in-house database searching or machine learning algorithms for the detection of SARS-CoV-2 infection. Reprinted from reference [84]

.

References

[1] Samy Emara, Sara Amer, Ahmed Ali, Yasmine Abouleila, April Oga, and Tsutomu Masujima. Single-cell metabolomics. *Metabolomics: from fundamentals to clinical applications*, pages 323–343, 2017.

[2] Caroline H Johnson, Julijana Ivanisevic, and Gary Siuzdak. Metabolomics: beyond biomarkers and towards mechanisms. *Nature reviews Molecular cell biology*, 17(7):451–459, 2016.

[3] Nicola Zamboni, Alan Saghatelian, and Gary J Patti. Defining the metabolome: size, flux, and regulation. *Molecular cell*, 58(4):699–706, 2015.

[4] Daniel A Dias, Oliver AH Jones, David J Beale, Berin A Boughton, Devin Benheim, Konstantinos A Kouremenos, Jean-Luc Wolfender, and David S Wishart. Current and future perspectives on the structural identification of small molecules in biological systems. *Metabolites*, 6(4):46, 2016.

[5] Megan R Showalter, Tomas Cajka, and Oliver Fiehn. Epimetabolites: discovering metabolism beyond building and burning. *Current opinion in chemical biology*, 36:70–76, 2017.

[6] Steven J Altschuler and Lani F Wu. Cellular heterogeneity: do differences make a difference? *Cell*, 141(4):559–563, 2010.

[7] Sui Huang. Non-genetic heterogeneity of cells in development: more than just noise. *Development*, 136(23):3853–3862, 2009.

[8] Ibiayi Dagogo-Jack and Alice T Shaw. Tumour heterogeneity and resistance to cancer therapies. *Nature reviews Clinical oncology*, 15(2):81–94, 2018.

[9] Stephan Braun, Florian D Vogl, Bjørn Naume, Wolfgang Janni, Michael P Osborne, R Charles Coombes, Günter Schlimok, Ingo J Diel, Bernd Gerber, Gerhard Gebauer, et al. A pooled analysis of bone marrow micrometastasis in breast cancer. *New England journal of medicine*, 353(8):793–802, 2005.

[10] Stephan Braun, Christina Kentenich, Wolfgang Janni, Florian Hepp, Johann de Waal, Fritz Willgeroth, Harald Sommer, and Klaus Pantel. Lack of effect of adjuvant chemotherapy on the elimination of single dormant tumor cells in bone marrow of high-risk breast cancer patients. *Journal of clinical oncology*, 18(1):80–80, 2000.

[11] Daniel F Hayes, Massimo Cristofanilli, G Thomas Budd, Matthew J Ellis, Alison Stopeck, M Craig Miller, Jeri Matera, W Jeffrey Allard, Gerald V Doyle, and Leon WWM Terstappen. Circulating tumor cells at each follow-up time point during therapy of metastatic breast cancer patients predict progression-free and overall survival. *Clinical Cancer Research*, 12(14):4218–4224, 2006.

[12] Klaus Pantel, Ruud H Brakenhoff, and Burkhard Brandt. Detection, clinical relevance and specific biological properties of disseminating tumour cells. *Nature Reviews Cancer*, 8(5):329–340, 2008.

[13] Michelle Hong, George He, Siting Goh, Alvin Wei Xiang Low, Kae Jack Tay, Tony Kiat Hon Lim, Joe Yeong, Li Yan Khor, and Tong Seng Lim. Biomarkers for precision urothelial carcinoma diagnosis: Current approaches and the application of single-cell technologies. *Cancers*, 13(2):260, 2021.

[14] EK Khlestkina and VK Shumny. Prospects for application of breakthrough technologies in breeding: The crispr/cas9 system for plant genome editing. *Russian Journal of Genetics*, 52(7):676–687, 2016.

[15] Pey Yee Lee, Siok-Fong Chin, Hui-min Neoh, and Rahman Jamal. Metaproteomic analysis of human gut microbiota: where are we heading? *Journal of biomedical science*, 24(1):1–8, 2017.

[16] Bo Huang, Hazen Babcock, and Xiaowei Zhuang. Breaking the diffraction barrier: super-resolution imaging of cells. *Cell*, 143(7):1047–1058, 2010.

[17] Peter Kner, Bryant B Chhun, Eric R Griffis, Lukman Winoto, and Mats GL Gustafsson. Super-resolution video microscopy of live cells by structured illumination. *Nature methods*, 6(5):339–342, 2009.

[18] Jun Liu and Stanley Misler. α-latrotoxin-induced quantal release of catecholamines from rat adrenal chromaffin cells. *Brain research*, 799(1):55–63, 1998.

[19] Lan Huang and Robert T Kennedy. Exploring single-cell dynamics using chemically-modified microelectrodes. *TrAC Trends in Analytical Chemistry*, 14(4):158–164, 1995.

[20] DM Cannon Jr, N Winograd, and AG Ewing. Quantitative chemical analysis of single cells. *Annual Review of Biophysics and Biomolecular Structure*, 29:239, 2000.

[21] Teresa M Olefirowicz and Andrew G Ewing. Capillary electrophoresis in 2 and 5. mu. m diameter capillaries: application to cytoplasmic analysis. *Analytical chemistry*, 62(17):1872–1876, 1990.

[22] Qianfeng Weng and Wenrui Jin. Assay of amino acids in individual human lymphocytes by capillary zone electrophoresis with electrochemical detection. *Analytica chimica acta*, 478(2):199–207, 2003.

[23] Feng Ai, Hong Chen, Shu-Hui Zhang, Sheng-Yi Liu, Fang Wei, Xu-Yan Dong, Jie-Ke Cheng, and Wei-Hua Huang. Real-time monitoring of oxidative burst from single plant protoplasts using microelectrochemical sensors modified by platinum nanoparticles. *Analytical chemistry*, 81(20):8453–8458, 2009.

[24] Renato Zenobi. Single-cell metabolomics: analytical and biological perspectives. *Science*, 342(6163):1243259, 2013.

[25] Stanislav S Rubakhin, Elena V Romanova, Peter Nemes, and Jonathan V Sweedler. Profiling metabolites and peptides in single cells. *Nature methods*, 8(4):S20–S29, 2011.

[26] Liang Li, Rafael E Golding, and Randy M Whittal. Analysis of single mammalian cell lysates by mass spectrometry. *Journal of the American Chemical Society*, 118(46):11662–11663, 1996.

[27] Dario Anselmetti. *Single cell analysis: technologies and applications*. John Wiley & Sons, 2009.

[28] Stanislav S Rubakhin and Jonathan V Sweedler. Characterizing peptides in individual mammalian cells using mass spectrometry. *Nature protocols*, 2(8):1987–1997, 2007.

[29] PA Van Veelen, CR Jimenez, KW Li, WPM Geraerts, UR Tjaden, and J Van der Greef. New advanced analytical tools in peptide/protein research: matrix assisted laser desorption mass spectrometry. *Journal of controlled release*, 29(3):223–229, 1994.

[30] Jessica A Stolee and Akos Vertes. Toward single-cell analysis by plume collimation in laser ablation electrospray ionization mass spectrometry. *Analytical chemistry*, 85(7):3592–3598, 2013.

[31] Peter Nemes, Amina S Woods, and Akos Vertes. Simultaneous imaging of small metabolites and lipids in rat brain tissues at atmospheric pressure by laser ablation electrospray ionization mass spectrometry. *Analytical chemistry*, 82(3):982–988, 2010.

[32] Gearoid Cahill, Padraig K Walsh, and Dan Donnelly. Determination of yeast glycogen content by individual cell spectroscopy using image analysis. *Biotechnology and bioengineering*, 69(3):312–322, 2000.

[33] Hiroaki Shinohara and Feifei Wang. Real-time detection of dopamine released from a nerve model cell by an enzyme-catalyzed luminescence method and its application to drug assessment. *Analytical sciences*, 23(1):81–84, 2007.

[34] Kira L Goff, Luca Quaroni, and Kenneth E Wilson. Measurement of metabolite formation in single living cells of chlamydomonas reinhardtii using synchrotron fourier-transform infrared spectromicroscopy. *Analyst*, 134(11):2216–2219, 2009.

[35] Ryan Buckmaster, Fareid Asphahani, Myo Thein, Jian Xu, and Miqin Zhang. Detection of drug-induced cellular changes using confocal raman spectroscopy on patterned single-cell biosensors. *Analyst*, 134(7):1440–1446, 2009.

[36] Martin Hedegaard, Christoph Krafft, Henrik J Ditzel, Lene E Johansen, Søren Hassing, and Jurgen Popp. Discriminating isogenic cancer cells and identifying altered unsaturated fatty acid content as associated with metastasis status, using k-means clustering and partial least squares-discriminant analysis of raman maps. *Analytical chemistry*, 82(7):2797–2802, 2010.

[37] Antje Hermelink, Angelika Brauer, Peter Lasch, and Dieter Naumann. Phenotypic heterogeneity within microbial populations at the single-cell level investigated by confocal raman microspectroscopy. *Analyst*, 134(6):1149–1153, 2009.

[38] K Christian Schuster, Ingo Reese, Eva Urlaub, J Richard Gapes, and Bernhard Lendl. Multidimensional information on the chemical composition of single bacterial cells by confocal raman microspectroscopy. *Analytical chemistry*, 72(22):5529–5534, 2000.

[39] Tobias J Moritz, Douglas S Taylor, Christopher R Polage, Denise M Krol, Stephen M Lane, and James W Chan. Effect of cefazolin treatment on the nonresonant raman signatures of the metabolic state of individual escherichia coli cells. *Analytical Chemistry*, 82(7):2703–2710, 2010.

[40] Linwen Zhang and Akos Vertes. Single-cell mass spectrometry approaches to explore cellular heterogeneity. *Angewandte Chemie International Edition*, 57(17):4466–4477, 2018.

[41] Troy J Comi, Thanh D Do, Stanislav S Rubakhin, and Jonathan V Sweedler. Categorizing cells on the basis of their chemical profiles: progress in single-cell mass spectrometry. *Journal of the American Chemical Society*, 139(11):3920–3929, 2017.

[42] Jasmin Krismer, Jens Sobek, Robert F Steinhoff, Stephan R Fagerer, Martin Pabst, and Renato Zenobi. Screening of chlamydomonas reinhardtii populations with single-cell resolution by using a high-throughput microscale sample preparation for matrix-assisted laser desorption ionization mass spectrometry. *Applied and environmental microbiology*, 81(16):5546–5551, 2015.

[43] Jasmin Krismer, Manu Tamminen, Simone Fontana, Renato Zenobi, and Anita Narwani. Single-cell mass spectrometry reveals the importance of genetic diversity and plasticity for phenotypic variation in nitrogen-limited chlamydomonas. *The ISME journal*, 11(4):988–998, 2017.

[44] Petra Anne Levin and Esther R Angert. Small but mighty: cell size and bacteria. *Cold Spring Harbor perspectives in biology*, 7(7):a019216, 2015.

[45] Iain C Macaulay and Thierry Voet. Single cell genomics: advances and future perspectives. *PLoS genetics*, 10(1):e1004126, 2014.

[46] Lieselot Deleye, Laurentijn Tilleman, Ann-Sophie Vander Plaetsen, Senne Cornelis, Dieter Deforce, and Filip Van Nieuwerburgh. Performance of four modern whole genome amplification methods for copy number variant detection in single cells. *Scientific reports*, 7(1):1–9, 2017.

[47] Kuang Jen Wu and Robert W Odom. Peer reviewed: characterizing synthetic polymers by maldi ms. *Analytical chemistry*, 70(13):456A–461A, 1998.

[48] Jenny Leopold, Yulia Popkova, Kathrin M Engel, and Jürgen Schiller. Recent developments of useful maldi matrices for the mass spectrometric characterization of lipids. *Biomolecules*, 8(4):173, 2018.

[49] V Horneffer, K Dreisewerd, H-C Lüdemann, F Hillenkamp, M Läge, and K Strupat. Is the incorporation of analytes into matrix crystals a prerequisite for matrix-assisted laser desorption/ionization mass spectrometry? a study of five positional isomers of dihydroxybenzoic acid. *International journal of mass spectrometry*, 185:859–870, 1999.

[50] Jürgen Schiller, Rosmarie Süß, Beate Fuchs, Matthias Müller, Marijana Petković, Olaf Zschörnig, and Hanka Waschipky. The suitability of different dhb isomers as matrices for the maldi-tof ms analysis of phospholipids: which isomer for what purpose? *European Biophysics Journal*, 36(4):517–527, 2007.

[51] William J Perry, Nathan Heath Patterson, Boone M Prentice, Elizabeth K Neumann, Richard M Caprioli, and Jeffrey M Spraggins. Uncovering matrix effects on lipid analyses in maldi imaging mass spectrometry experiments. *Journal of mass spectrometry*, 55(4):e4491, 2020.

[52] Anu Teearu, Signe Vahur, Uku Haljasorg, Ivo Leito, Tõiv Haljasorg, and Lauri Toom. 2, 5-dihydroxybenzoic acid solution in maldi-ms: ageing and use for mass calibration. *Journal of Mass Spectrometry*, 49(10):970–979, 2014.

[53] Abdennour Abbas, Matthew J Linman, and Quan Cheng. Patterned resonance plasmonic microarrays for high-performance spr imaging. *Analytical chemistry*, 83(8):3147–3152, 2011.

[54] Alexander S Lambert, Santino N Valiulis, Alexander S Malinick, Ichiro Tanabe, and Quan Cheng. Plasmonic biosensing with aluminum thin films under the kretschmann configuration. *Analytical chemistry*, 92(13):8654–8659, 2020.

[55] Takatoshi Kaya, Tomonori Kaneko, Shun Kojima, Yukito Nakamura, Youichi Ide, Kenji Ishida, Yoshihiko Suda, and Katsuko Yamashita. High-sensitivity immunoassay with surface plasmon field-enhanced fluorescence spectroscopy using a plastic sensor chip: Application to quantitative analysis of total prostate-specific antigen and galnacβ1–4glcnac-linked prostate-specific antigen for prostate cancer diagnosis. *Analytical chemistry*, 87(3):1797–1803, 2015.

[56] Jing Liu, Rolf Lauterbach, Harald Paulsen, and Wolfgang Knoll. Immobilization of light-harvesting chlorophyll a/b complex (lhciib) studied by surface plasmon field-enhanced fluorescence spectroscopy. *Langmuir*, 24(17):9661–9667, 2008.

[57] Thorsten Liebermann and Wolfgang Knoll. Surface-plasmon field-enhanced fluorescence spectroscopy. *Colloids and Surfaces A: Physicochemical and Engineering Aspects*, 171(1-3):115–130, 2000.

[58] Jicheng Duan, Matthew J Linman, and Quan Cheng. Ultrathin calcinated films on a gold surface for highly effective laser desorption/ionization of biomolecules. *Analytical chemistry*, 82(12):5088–5094, 2010.

[59] Rosa Pilolli, Francesco Palmisano, and Nicola Cioffi. Gold nanomaterials as a new tool for bioanalytical applications of laser desorption ionization mass spectrometry. *Analytical and bioanalytical chemistry*, 402(2):601–623, 2012.

[60] Markus R Wenk. The emerging field of lipidomics. *Nature reviews Drug discovery*, 4(7):594–610, 2005.

[61] Andrew D Watson. Thematic review series: systems biology approaches to metabolic and cardiovascular disorders. lipidomics: a global approach to lipid analysis in biological systems. *Journal of lipid research*, 47(10):2101–2111, 2006.

[62] Eoin Fahy, Shankar Subramaniam, H Alex Brown, Christopher K Glass, Alfred H Merrill, Robert C Murphy, Christian RH Raetz, David W Russell, Yousuke Seyama, Walter Shaw, et al. A comprehensive classification system for lipids1. *Journal of lipid research*, 46(5):839–861, 2005.

[63] Eoin Fahy, Shankar Subramaniam, Robert C Murphy, Masahiro Nishijima, Christian RH Raetz, Takao Shimizu, Friedrich Spener, Gerrit van Meer, Michael JO Wakelam, and Edward A Dennis. Update of the lipid maps comprehensive classification system for lipids1. *Journal of lipid research*, 50:S9–S14, 2009.

[64] Ting Hu and Jin-Lan Zhang. Mass-spectrometry-based lipidomics. *Journal of separation science*, 41(1):351–372, 2018.

[65] Manabu T Nakamura, Barbara E Yudell, and Juan J Loor. Regulation of energy metabolism by long-chain fatty acids. *Progress in lipid research*, 53:124–144, 2014.

[66] Richard W Gross and Xianlin Han. Lipidomics at the interface of structure and function in systems biology. *Chemistry & biology*, 18(3):284–291, 2011.

[67] Robert Ernst, Christer S Ejsing, and Bruno Antonny. Homeoviscous adaptation and the regulation of membrane lipids. *Journal of molecular biology*, 428(24):4776–4791, 2016.

[68] Bruno Antonny. Mechanisms of membrane curvature sensing. *Annual review of biochemistry*, 80:101–123, 2011.

[69] Tobias Baumgart, Benjamin R Capraro, Chen Zhu, and Sovan L Das. Thermodynamics and mechanics of membrane curvature generation and sensing by proteins and lipids. *Annual review of physical chemistry*, 62:483, 2011.

[70] Tianrun Xu, Chunxiu Hu, Qiuhui Xuan, and Guowang Xu. Recent advances in analytical strategies for mass spectrometry-based lipidomics. *Analytica Chimica Acta*, 1137:156–169, 2020.

[71] Loong Chuen Lee, Choong-Yeun Liong, and Abdul Aziz Jemain. Partial least squares-discriminant analysis (pls-da) for classification of high-dimensional (hd) data: a review of contemporary practice strategies and knowledge gaps. *Analyst*, 143(15):3526–3539, 2018.

[72] Kui Wang, Changlong Shu, Mario Soberón, Alejandra Bravo, and Jie Zhang. Systematic characterization of bacillus genetic stock center bacillus thuringiensis strains using multi-locus sequence typing. *Journal of invertebrate pathology*, 155:5–13, 2018.

[73] Adriana Calderaro, Maria-Cristina Arcangeletti, Isabella Rodighiero, Mirko Buttrini, Chiara Gorrini, Federica Motta, Diego Germini, Maria-Cristina Medici, Carlo Chezzi, and Flora De Conto. Matrix-assisted laser desorption/ionization time-of-flight (maldi-tof) mass spectrometry applied to virus identification. *Scientific reports*, 4(1):1–10, 2014.

[74] Fernando Cobo. Application of maldi-tof mass spectrometry in clinical virology: a review. *The open virology journal*, 7:84, 2013.

[75] Malin IL Sjoholm, Joakim Dillner, and Joyce Carlson. Multiplex detection of human herpesviruses from archival specimens by using matrix-assisted laser desorption ionization-time of flight mass spectrometry. *Journal of clinical microbiology*, 46(2):540–545, 2008.

[76] Tzu-Chi Chou, Wei Hsu, Ching-Ho Wang, Yu-Ju Chen, and Jim-Min Fang. Rapid and specific influenza virus detection by functionalized magnetic nanoparticles and mass spectrometry. *Journal of nanobiotechnology*, 9(1):1–13, 2011.

[77] Jingzi Piao, Jun Jiang, Bianli Xu, Xiaohong Wang, Yanfang Guan, Weili Wu, Licheng Liu, Yuan Zhang, Xueyong Huang, Pengzhi Wang, et al. Simultaneous detection and identification of enteric viruses by pcr-mass assay. 2012.

[78] Nicholas L Dollman, Justin H Griffin, and Kevin M Downard. Detection, mapping, and proteotyping of sars-cov-2 coronavirus with high resolution mass spectrometry. *ACS Infectious Diseases*, 6(12):3269–3276, 2020.

[79] Fabiane M Nachtigall, Alfredo Pereira, Oleksandra S Trofymchuk, and Leonardo S Santos. Detection of sars-cov-2 in nasal swabs using maldi-ms. *Nature biotechnology*, 38(10):1168–1173, 2020.

[80] Nam K Tran, Taylor Howard, Ryan Walsh, John Pepper, Julia Loegering, Brett Phinney, Michelle R Salemi, and Hooman H Rashidi. Novel application of automated machine learning with maldi-tof-ms for rapid high-throughput screening of covid-19: A proof of concept. *Scientific reports*, 11(1):1–10, 2021.

[81] Meritxell Deulofeu, Esteban García-Cuesta, Eladia María Peña-Méndez, José Elías Conde, Orlando Jiménez-Romero, Enrique Verdú, María Teresa Serrando, Victoria Salvadó, and Pere Boadas-Vaello. Detection of sars-cov-2 infection in human nasopharyngeal samples by combining maldi-tof ms and artificial intelligence. *Frontiers in Medicine*, 8:661358, 2021.

[82] María Florencia Rocca, Jonathan Cristian Zintgraff, María Elena Dattero, Leonardo Silva Santos, Martín Ledesma, Carlos Vay, Mónica Prieto, Estefanía Benedetti, Martín Avaro, Mara Russo, et al. A combined approach of maldi-tof mass spectrometry and multivariate analysis as a potential tool for the detection of sars-cov-2 virus in nasopharyngeal swabs. *Journal of virological methods*, 286:113991, 2020.

[83] Ling Yan, Jia Yi, Changwu Huang, Jian Zhang, Shuhui Fu, Zhijie Li, Qian Lyu, Yuan Xu, Kun Wang, Huan Yang, et al. Rapid detection of covid-19 using maldi-tof-based serum peptidome profiling. *Analytical chemistry*, 93(11):4782–4787, 2021.

[84] Mariaimmacolata Preianò, Serena Correnti, Corrado Pelaia, Rocco Savino, and Rosa Terracciano. Maldi ms-based investigations for sars-cov-2 detection. *BioChem*, 1(3):250–278, 2021.

Chapter 2

Probing Herbicide Toxicity to Algae by Lipid Profiling with Machine Learning and Microchip/MALDI-TOF Mass Spectrometry

2.1 Introduction

The widespread use of herbicides in the agriculture and commercial sectors has led to tens of millions of pounds of herbicides being poured into the aquatic systems in the United States. These herbicides pollute the water environment and are toxic to nontarget organisms, particularly phytoplankton.[1] A number of herbicides are designed to target lipid-based photosystems for invasive plant species; therefore, they can inadvertently affect the photosystems in nontarget vegetation and photoactive microorganisms, causing alterations in species' metabolism pathways. Microalgae are the leading primary producer in aquatic ecosystems, providing main nutrition and energy sources for water food networks.[2] In addition, they play an essential role in the balance and stability of aquatic ecosystems. Changes in algal biomass and community structure are deleterious to higher trophic levels, such as herbivorous zooplankton and fish. Therefore, there is a severe consequence to the function of an entire ecosystem from the adverse effects of herbicides on microalgae.[3]

Cytotoxic effects on algae have been studied by a variety of analytical methods [4][5][6] but only recently have techniques evolved to allow lipid components to be analyzed toward a comprehensive understanding at a system level.[7][8] The compositions of glycerolipids (GL) in microalgae are found to change due to growth and environmental conditions such as light, salinity, temperature, pollutants, and nutrients, causing alternation in both lipid components and content diversity.[9][10][11][12][13] This, in connection with the presence of a large number of different GL molecular species throughout algal organisms, makes them valuable targets for the analysis of algae response to herbicide exposure. Lipidomic studies offer an in-depth understanding of the changes by lipids, both functional and structural, in a cell or organism and their interactions with other molecules in the cell. Many approaches to lipidomic analysis have been established on the basis of chromatography and mass spectrometry, including thin-layer chromatography (TLC), gas chromatography-mass spectrometer (GC-MS), electrospray mass spectrometry (ESI-MS), and nuclear magnetic resonance (NMR). However, these methods typically require tedious separation steps or derivatization procedures in sample preparation. Furthermore, the laborious sample processing steps lead to a loss of time-sensitive information and can be a source of experimental errors. Matrix-assisted laser desorption ionization time-of-flight (MALDI-TOF MS), a method with fast data collection and structural analysis capability, has a considerable advantage in lipid analysis.[14] Several works have utilized MALDI-MS to analyze lipid profiles and monitor lipid response to stress.[15][16][17][18][19] We have recently demonstrated a lipidomic study of algae *Chlamydomonas reinhardtii*, an important algal species for biopharmaceuticals and biofuel, with a gold-microchip enhanced MALDI-MS.[8][20] The plasmonic gold chips provided improved ionization efficiency and autofluorescence for cell localization in the array wells[8], leading to effective lipid profiling at the single cell level. The elimination of conventional extraction, derivation, and separation steps[17][16][18][21][22][23][24] allows for the identification of lipids directly from intact algae without any chemical sample pretreatment or purification.

In this work, we report the use of machine-learning algorithms in combination of MicroChip/MALDI-MS to investigate the cytotoxic effect of herbicides on algae, *Selenastrum capricornutum*. Figure 2.1 shows the overall workflow. *S. capricornutum* was selected for understanding the species-specific lipid response to herbicide treatment as it is a common bioindicator species owing to ubiquitous distribution and has been widely used for bioassays in toxicological risk assessments.[25] Different from *C. reinhardtii*, the lipid profile of this algae has never been fully studied or demonstrated, leaving a knowledge gap for the research associated with its use in toxicity monitoring, biofuel development,[26][27] heavy metal removal and bioremediation[28][29][30][31]. . In addition, different algae species are likely to have perceptible differences in cytotoxic effects from environmental pollutants, and understanding this property will help identify how toxicants uniquely impact ecosystems. Therefore, the study of the *S. capricornutum* system is carefully compared to that of *C. reinhardtii*. We found that by using machine learning algorithms, our platform can effectively identify small differences and subtle effects normally obscured. The method can find broad applications for lipid analysis in many areas, such as drug efficacy, cancer diagnostics, microbial identification, and lipid metabolism pathway studies.

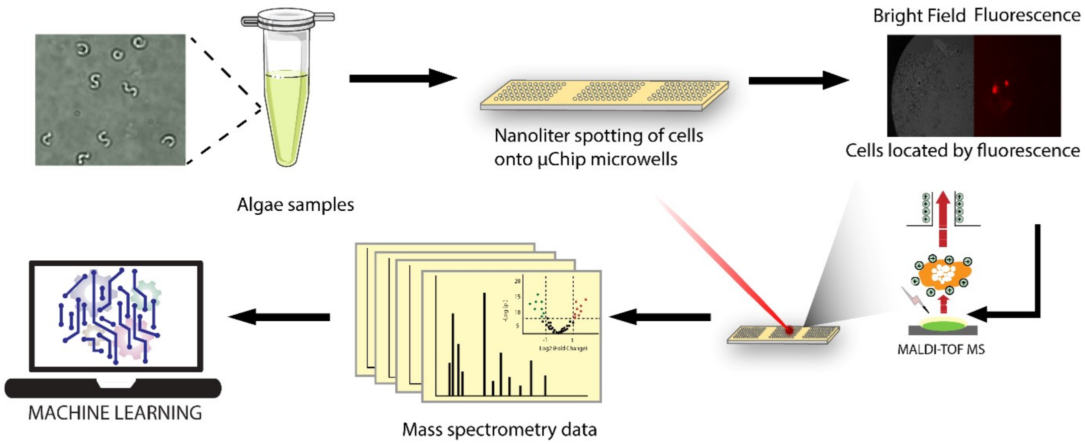

Figure 2.1: Schematic Illustration of Lipidomic Analysis of Algae Exposed to Herbicides Combined with Machine Learning.

2.2 Experimental Section

2.2.1 Reagents

Bioperformance certified dimethyl sulfoxide (DMSO), super dihydroxybenzoic acid (sDHB), acetonitrile (ACN), and trifluoroacetic acid (TFA) were purchased from Sigma Aldrich. High-quality atrazine, clomazone, and norflurazon were purchased from AccuStandard Inc (New Haven, CT, USA). High purity water ($>$18 MΩ cm^{-1}) was from Barnstead E-Pure water purification system. Premium plain BK-7 glass microscope slides came from Fisher Scientific. *Selenastrum capricornutum* bacteria-free UTEX 1648 was purchased from the UTEX culture collection of algae at the University of Texas at Austin. Sterile Algae-Gro freshwater medium was purchased from Carolin Inc.

2.2.2 Algae Culture Condition

The freshwater wild-type algae strain, *S. capricornutum*, was cultured in the freshwater medium at 23±2°C under a "cool white" fluorescent light employing 12/12 h light/dark cycle. The algae growth was measured by counting the number of cells and then monitored by optical density (OD). OD of bulk cultures was measured by the optical density at 600 nm by spectrophotometer (Figure 2.2).

2.2.3 Herbicide Toxicity Test

All tests were conducted after 96 h of exposure to the targeted chemicals. For the toxicity analysis, the cells growing close to the stationary phase were seeded and spiked with different concentrations of the herbicides: atrazine, norflurazon, or clomazone (0.01, 0.1, 1, 10, and 100 mg/L, respectively). After 96 h of exposure at 23±2℃, the growth of cells was monitored by UV-vis spectrometry at 600 nm and plotted against the herbicide dose (Figure 2.3).

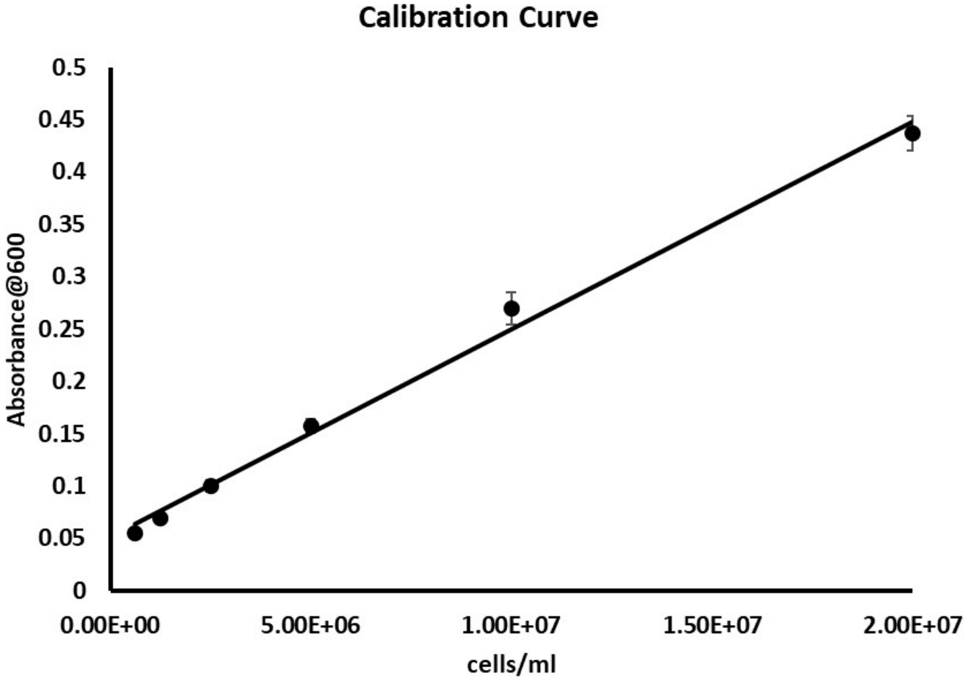

Figure 2.2: Calibration curve that shows the number of cells correlates positively with the absorbance at 600 nm.

2.2.4 Fabrication of Gold Microchip

The gold microchip arrays were fabricated using a previously reported method developed in the lab.[32] Briefly, the photoresist was spun-coated onto glass slides, which had been cleaned with Piranha solution (Caution!), and baked at 110 °C. The chip was then patterned by a mask aligner and UV-light. After another baking step, they were cured using UV light and treated with a developing solution. Next, e-beam deposition was used to deposit different thicknesses of Cr/Au onto the arrays. The photoresist was removed with acetone to afford pristine 50 nm gold well arrays.

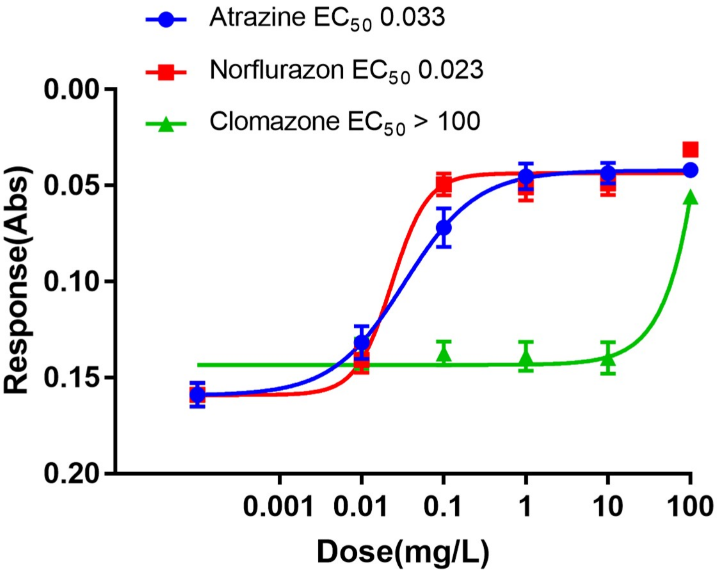

Figure 2.3: Herbicide dose-response curves and algae lipid profiles showing the response to different herbicides.

2.2.5 Sample Preparation

On the basis of the herbicide toxicity tests mentioned above, two concentrations, 0.05 and 0.1 mg/L, were specifically chosen for this work. After 96 h of exposure, cells were washed three times using ultrapure water to remove salt and medium, followed by centrifugation for 8 min at 4000g. After centrifugation, the cells were resuspended with ultrapure water and spotted onto the gold microchip using a nanoliter electrodeposition system. To quench the cells, the microchips loaded with cells were immediately placed into a vacuum desiccator, which stops metabolic changes of the algae. A matrix (sDHB dissolved in acetonitrile, 1% TFA in water (1:2)) was then deposited on the sample by using the same nanoliter deposition system, which allows for the delivery of nanodroplet aliquots (100 nL) with precision and accuracy. The microchips and samples were stored in the desiccator before use.

2.2.6 Mass Spectra Acquisition

MALDI-MS analysis was assisted by fluorescence microscopy to localize the cells in the microarray wells. Fluorescence images of the algae cell, resulting from chlorophyll's autofluorescence, provided direct visualization of the cells on the substrate, which were used to direct laser beams for effective ionization in MALDI-MS experiments (Figure 2.4). An epifluorescence microscope equipped with a TRITC filter cube and a QImaging Retiga 1300 camera was employed to collect fluorescence images. The MALDI-MS analysis was carried out in positive ion mode with a laser fluence of 5000 au on a reflection AB-Sciex 5800 MALDI-TOF instrument. A sample representing m/z values versus intensity (au) is the average of 200 shots from the cluster of a few cells. Precursor ion peaks with high resolution and good s/n values were selected to generate the tandem MS CID-spectra.

2.2.7 MALD-TOF-MS Data Analysis

Data analysis of mass spectra was conducted using the Data Explorer software. Peaks with a signal-to-noise ratio (s/n) of 3 or above were extracted after baseline correction. To perform statistical analysis, the generated lists of m/z and intensity values were imported into MetaboAnalyst 4.0.[33] Volcano plots were generated to search for significant differences between classes of lipids. A lipid library was compiled, and the identification of lipids was assigned on the basis of m/z values, MS/MS data, database search, and literature reference. All values were calculated from ≥20 spectra/samples to generate the charts and for statistical analysis of the results. For machine learning training and testing, data was input into R-studio and analyzied via the cart package.[34][35]

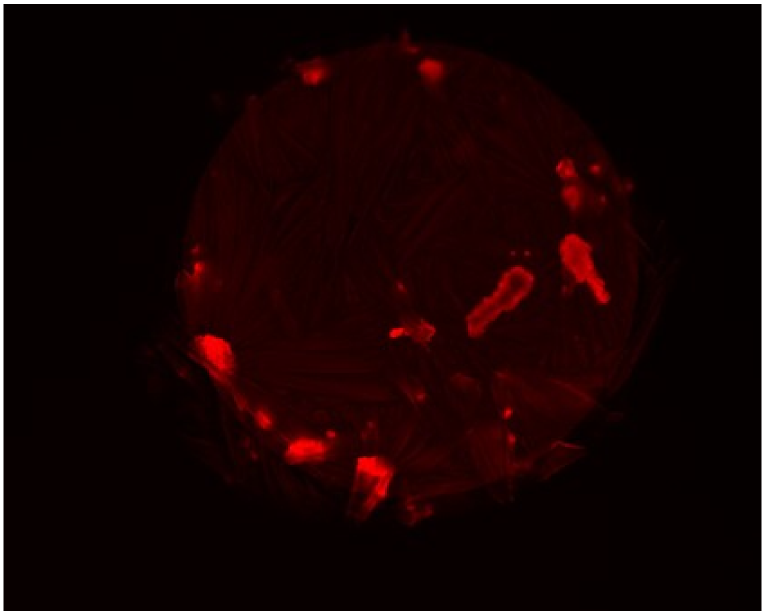

Figure 2.4: Fluorescence images of S.capricornutum in the microarray well of a gold-μchip

2.3 Results and Discussion

To facilitate lipid analysis in unicellular microalgae, we chose the early stationary phase for analysis using a 96 h toxicity bioassay. Given that different lipid classes accumulate under a specific growth stage[36] and there is often a high content of lipid in this stationary phase,[37] this selection is important to the current work and is intentionally done for compatibility with previous study for comparison purposes. Lipid expression profiles of

Selenastrum capricornutum in different growth phases are provided in Figure 2.5. The algae were dosed with different concentrations of three targeted herbicides: atrazine, clomazone, and norflurazon. Figure 2.3 shows the result of a standard 96 h toxicity bioassay.

From Figure 2.3, EC_{50} values for the three herbicides on *S. capricornuim* were determined to be 0.033 mg/L for atrazine, 0.023 mg/L for norflurazon, and >100 mg/L for clomazone. The herbicide concentrations of 0.05 and 0.1 mg/L, moderately higher than the EC_{50} and EC_{90} values respectively, were thus selected to trigger the toxicity effects on the cells. These herbicides are known to target the photosystem of algae but in different ways: atrazine affects photosystem II, while clomazone and norflurazon target the synthesis of pigments (carotenoids and chlorophyll). Chlorophyll in a plastidic membrane is localized and weakly fluorescent; the use of the gold-microchip in combination with its plasmonic effect allows for clear localization of the algae cells even after applying the matrix (Figure 2.4). By contrast, these cells are not traceable on conventional glass slides. The enhancement by the gold-microchip[8] has gas greatly benefited single cell lipid analysis in several ways, primarily from metal enhanced fluorescence[38][39][40][41] and an improved MS signal due to the rapid thermalization of excited electrons.[42]

Figure 2.6 shows the lipid mass fingerprint of the algae from MALDI-TOF-MS and the typical CID-MS spectra of several important lipids. The whole cell lipid profile can be grouped into bands based on inherent similarities in headgroup and m/z ratios (indicated by different colors in Figure 2.6a).). Intraband differences in m/z are a function of fatty acid chain length and degree of unsaturation, represented in shorthand notation by lipid type (carbon number: unsaturation number). MS/MS analysis and literature

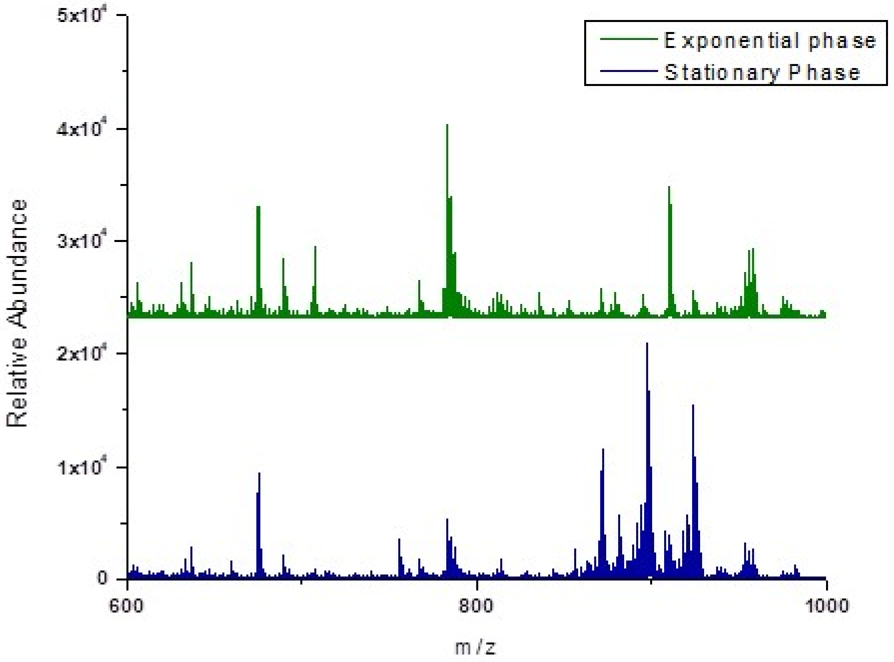

Figure 2.5: Lipid profile of *S. capricornuim* in different growth phases

reference from other algal species[43][44][45][46][47][48] have been used to generate the lipid fingerprint. Representative MALDI-TOF-MS/MS spectra and the assignment of the mass peaks are shown in the Supporting Information (Figure 2.7 and Figure 2.8). Common lipids in *S. capricornutum* include MGDG, TAG, and DGDG, and the composition is slightly different from that in *C. reinhardtii.*[8] Representative structures of common lipid species with fragment locations are shown in Figure 2.6b, where the R_1 and R_2 groups represent acyl chain residues of varying lengths. With the assistance of gold microarrays, we were able to identify 17 monogalactosyl-diacylglycerol (MGDG) lipids, 18 migalactosyl-diacylglycerol (DGDG) lipids, and 33 triacylglycerols (TAG) lipids in *S. capricornutum.* Figure 2.9 is the pie chart that details the lipid species and their identification grouped by subspecies in their respective lipid categories. Among all lipids detected, MGDG (34 : 7), DGDG(36 : 9), and TAG (52 : 4) (chlorophyll a) make up the largest portion within their subspecies group, accounting for about 26%, 18%, and 19% of the group, respectively.

Figure 2.10 shows differentiation in lipid profiles of *S. capricornutum* exposed to herbicide at a concentration of 0.1 mg/L. The difference between clomazone treated and the controls was minimal, while norflurazon and atrazine produced a large decrease in the overall abundance of all DGDG lipids. Norflurazon is a bleaching herbicide that causes the inhibition of the carotenoid pigment biogenesis, leading to irreparable changes to chloroplasts. It has a specific impact on the Δ15-desaturase in the plastids, where the enzyme uses both prokaryotic and eukaryotic monogalactosyldiacylglycerol (MGDG) as substrates. Galactolipids, which include MGDG and DGDG, are the major constituents of photosynthetic membranes in chloroplasts and thylakoids.[47][49] Atrazine is reported to primarily affect the photosynthetic process, cell division, and lipid synthesis in green algae.[50] Specifically, reactive oxygen species (ROS) are overproduced, leading to oxidative damages of cell components (e.g., lipid peroxidation in the membranes).[50] Chloroplast and plasma membrane are the major sites of ROS generation in the microalgae under diverse stress conditions.[51] MGDG and DGDG, which are the major components of photosynthetic membranes in chloroplasts and thylakoids, were observed to decrease after exposure to different concentrations of atrazine (Figure 2.11), which agrees well with the ROS mechanism. When placed under stress conditions, many algae species produce large amounts of neutral

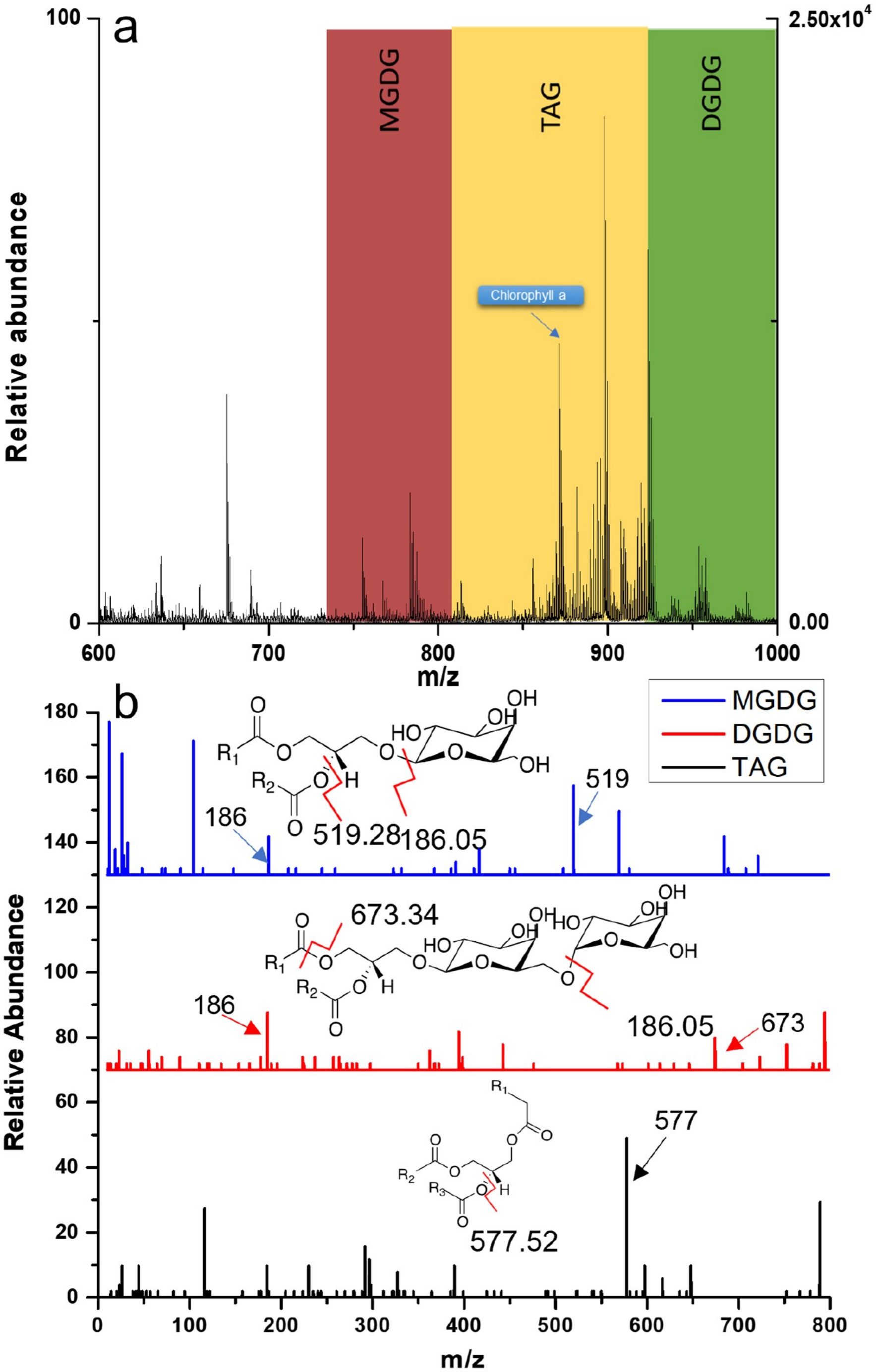

Figure 2.6: (a). MALDI-MS lipid mass fingerprint of *S.capricornutum*. (b). Representative CID-MS spectra of lipids MGDG, DGDG, and TAG.

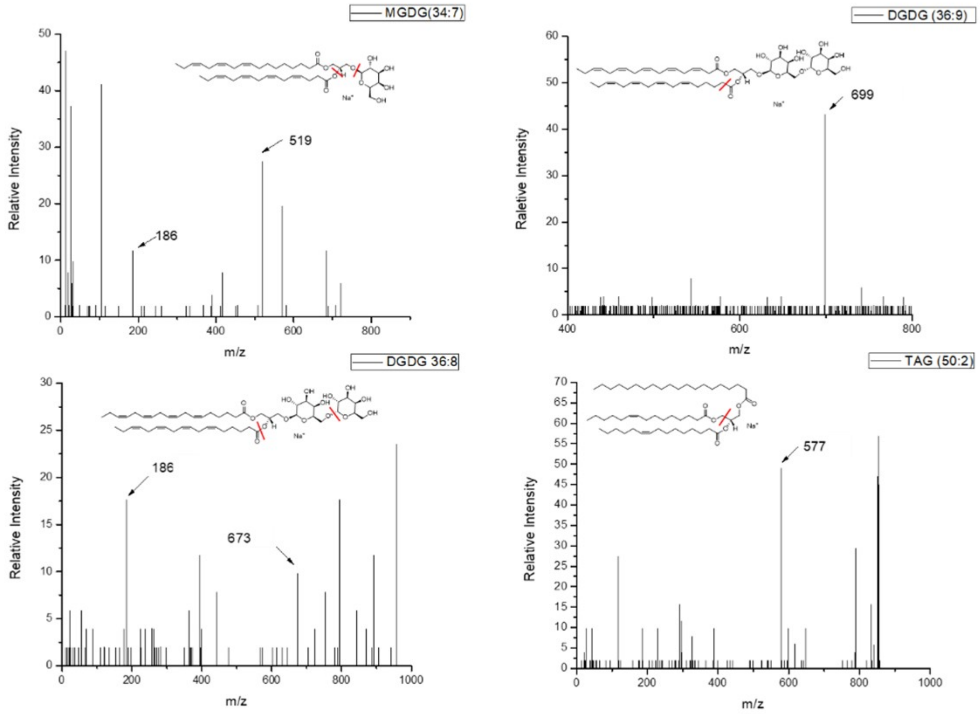

Figure 2.7: Positive-ion MALDI-TOF-MS/MS of MGDG (34:7) DGDG (36:9) DGDG(36:8) and TAG (50:2)

lipids, typically in the form of TAGs as storage products for carbon and energy.[52][53] Some TAG lipids in *S. capricornutum* were observed to increase after exposure to atrazine at the concentration of 1 mg/L (Figure 2.11).

Volcano scatter plots were constructed to further characterize lipid profile changes, which chart significance versus fold-change of a sizable data set (Figure 2.12 and Figure 2.13.). The effect of norflurazon (log_2(FC(norflurazon/control))) is characterized by a significant increase of TAG lipids and a decrease in several DGDG lipids. A significant change threshold of P=0.05 and FC >2 were used to compartmentalize these lipids into

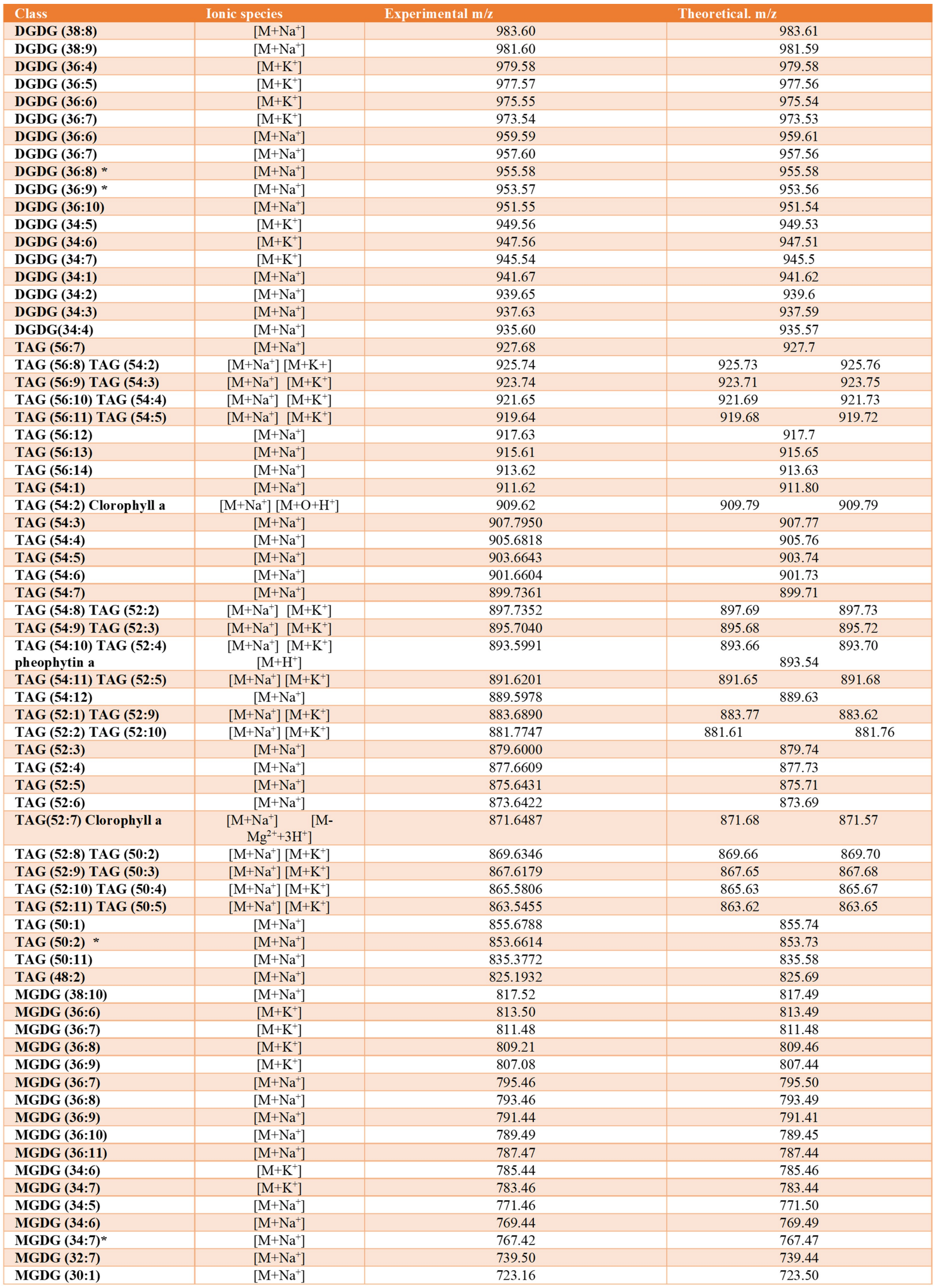

Class	Ionic species	Experimental m/z	Theoretical. m/z	
DGDG (38:8)	[M+Na^{+}]	983.60	983.61	
DGDG (38:9)	[M+Na^{+}]	981.60	981.59	
DGDG (36:4)	[M+K^{+}]	979.58	979.58	
DGDG (36:5)	[M+K^{+}]	977.57	977.56	
DGDG (36:6)	[M+K^{+}]	975.55	975.54	
DGDG (36:7)	[M+K^{+}]	973.54	973.53	
DGDG (36:6)	[M+Na^{+}]	959.59	959.61	
DGDG (36:7)	[M+Na^{+}]	957.60	957.56	
DGDG (36:8) *	[M+Na^{+}]	955.58	955.58	
DGDG (36:9) *	[M+Na^{+}]	953.57	953.56	
DGDG (36:10)	[M+Na^{+}]	951.55	951.54	
DGDG (34:5)	[M+K^{+}]	949.56	949.53	
DGDG (34:6)	[M+K^{+}]	947.56	947.51	
DGDG (34:7)	[M+K^{+}]	945.54	945.5	
DGDG (34:1)	[M+Na^{+}]	941.67	941.62	
DGDG (34:2)	[M+Na^{+}]	939.65	939.6	
DGDG (34:3)	[M+Na^{+}]	937.63	937.59	
DGDG(34:4)	[M+Na^{+}]	935.60	935.57	
TAG (56:7)	[M+Na^{+}]	927.68	927.7	
TAG (56:8) TAG (54:2)	[M+Na^{+}] [M+K+]	925.74	925.73	925.76
TAG (56:9) TAG (54:3)	[M+Na^{+}] [M+K^{+}]	923.74	923.71	923.75
TAG (56:10) TAG (54:4)	[M+Na^{+}] [M+K^{+}]	921.65	921.69	921.73
TAG (56:11) TAG (54:5)	[M+Na^{+}] [M+K^{+}]	919.64	919.68	919.72
TAG (56:12)	[M+Na^{+}]	917.63	917.7	
TAG (56:13)	[M+Na^{+}]	915.61	915.65	
TAG (56:14)	[M+Na^{+}]	913.62	913.63	
TAG (54:1)	[M+Na^{+}]	911.62	911.80	
TAG (54:2) Clorophyll a	[M+Na^{+}] [M+O+H^{+}]	909.62	909.79	909.79
TAG (54:3)	[M+Na^{+}]	907.7950	907.77	
TAG (54:4)	[M+Na^{+}]	905.6818	905.76	
TAG (54:5)	[M+Na^{+}]	903.6643	903.74	
TAG (54:6)	[M+Na^{+}]	901.6604	901.73	
TAG (54:7)	[M+Na^{+}]	899.7361	899.71	
TAG (54:8) TAG (52:2)	[M+Na^{+}] [M+K^{+}]	897.7352	897.69	897.73
TAG (54:9) TAG (52:3)	[M+Na^{+}] [M+K^{+}]	895.7040	895.68	895.72
TAG (54:10) TAG (52:4) **pheophytin a**	[M+Na^{+}] [M+K^{+}] [M+H^{+}]	893.5991	893.66 893.54	893.70
TAG (54:11) TAG (52:5)	[M+Na^{+}] [M+K^{+}]	891.6201	891.65	891.68
TAG (54:12)	[M+Na^{+}]	889.5978	889.63	
TAG (52:1) TAG (52:9)	[M+Na^{+}] [M+K^{+}]	883.6890	883.77	883.62
TAG (52:2) TAG (52:10)	[M+Na^{+}] [M+K^{+}]	881.7747	881.61	881.76
TAG (52:3)	[M+Na^{+}]	879.6000	879.74	
TAG (52:4)	[M+Na^{+}]	877.6609	877.73	
TAG (52:5)	[M+Na^{+}]	875.6431	875.71	
TAG (52:6)	[M+Na^{+}]	873.6422	873.69	
TAG(52:7) Clorophyll a	[M+Na^{+}] [M-Mg^{2+}+3H^{+}]	871.6487	871.68	871.57
TAG (52:8) TAG (50:2)	[M+Na^{+}] [M+K^{+}]	869.6346	869.66	869.70
TAG (52:9) TAG (50:3)	[M+Na^{+}] [M+K^{+}]	867.6179	867.65	867.68
TAG (52:10) TAG (50:4)	[M+Na^{+}] [M+K^{+}]	865.5806	865.63	865.67
TAG (52:11) TAG (50:5)	[M+Na^{+}] [M+K^{+}]	863.5455	863.62	863.65
TAG (50:1)	[M+Na^{+}]	855.6788	855.74	
TAG (50:2) *	[M+Na^{+}]	853.6614	853.73	
TAG (50:11)	[M+Na^{+}]	835.3772	835.58	
TAG (48:2)	[M+Na^{+}]	825.1932	825.69	
MGDG (38:10)	[M+Na^{+}]	817.52	817.49	
MGDG (36:6)	[M+K^{+}]	813.50	813.49	
MGDG (36:7)	[M+K^{+}]	811.48	811.48	
MGDG (36:8)	[M+K^{+}]	809.21	809.46	
MGDG (36:9)	[M+K^{+}]	807.08	807.44	
MGDG (36:7)	[M+Na^{+}]	795.46	795.50	
MGDG (36:8)	[M+Na^{+}]	793.46	793.49	
MGDG (36:9)	[M+Na^{+}]	791.44	791.41	
MGDG (36:10)	[M+Na^{+}]	789.49	789.45	
MGDG (36:11)	[M+Na^{+}]	787.47	787.44	
MGDG (34:6)	[M+K^{+}]	785.44	785.46	
MGDG (34:7)	[M+K^{+}]	783.46	783.44	
MGDG (34:5)	[M+Na^{+}]	771.46	771.50	
MGDG (34:6)	[M+Na^{+}]	769.44	769.49	
MGDG (34:7)*	[M+Na^{+}]	767.42	767.47	
MGDG (32:7)	[M+Na^{+}]	739.50	739.44	
MGDG (30:1)	[M+Na^{+}]	723.16	723.50	

Figure 2.8: A list of m/z value and assignment of the peaks detected in the positive ion MALDI-TOF-MS. Asterisks indicate confirmation of the lipid assignment by MS/MS.Peaks are identified by literature and MS/MS

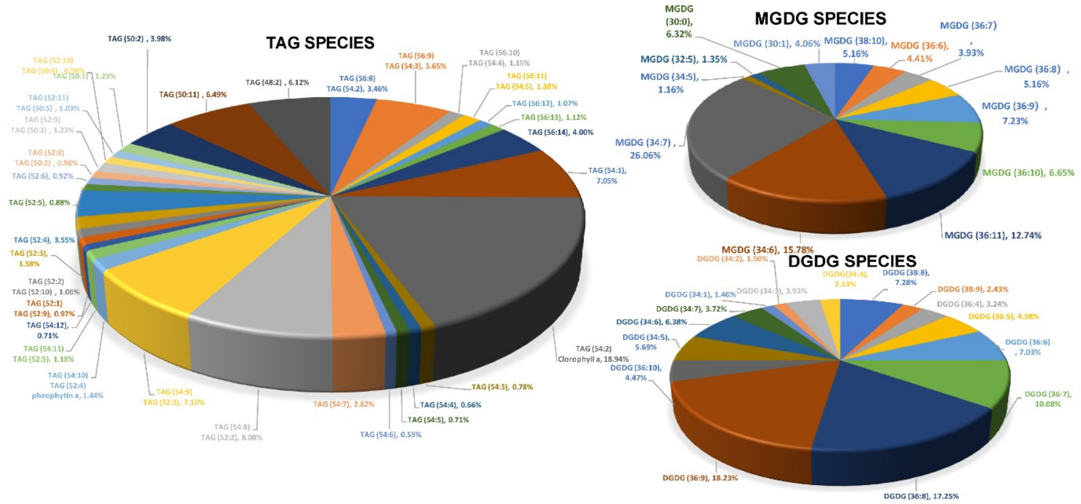

Figure 2.9: Pie charts of lipid species and identified lipids in *S. capricornutum* detected by MALDI-MS.

corners of the volcano plot to indicate a decrease or increase in lipid abundance. An increase in TAG in response to norflurazon can be seen, which is likely a compensatory effect of DGDG decrease and TAG accumulation during the stress conditions, a common phenotypic response in many types of algae.[54] A similar change in TAG was also observed in *C. reinhardtii*, where TAG lipids accumulated after atrazine introduction.[8] Interestingly, *S. capricornutum* is significantly more sensitive to norflurazon while *C. reinhardtii* seems to be more susceptible to atrazine. This indicates that even between similar algae species substantial differences in reaction to herbicides can result. From Figure 2.12 (and Figure 2.13), TAG(52:3) and MGDG(38:10) have a significant increase at 0.1 mg/L norflurazon and atrazine, while MGDG(30:1) and MGDG (38:10) have a marked surge at 0.05 mg/L norflurazon and atrazine. MGDG (38:10) is the only lipid that was found to be sensitive to both herbicides at both concentrations. As a result, it may be utilized as a chemical marker to characterize algae's response to the herbicides. DGDG (34:2), on the contrary, shows a

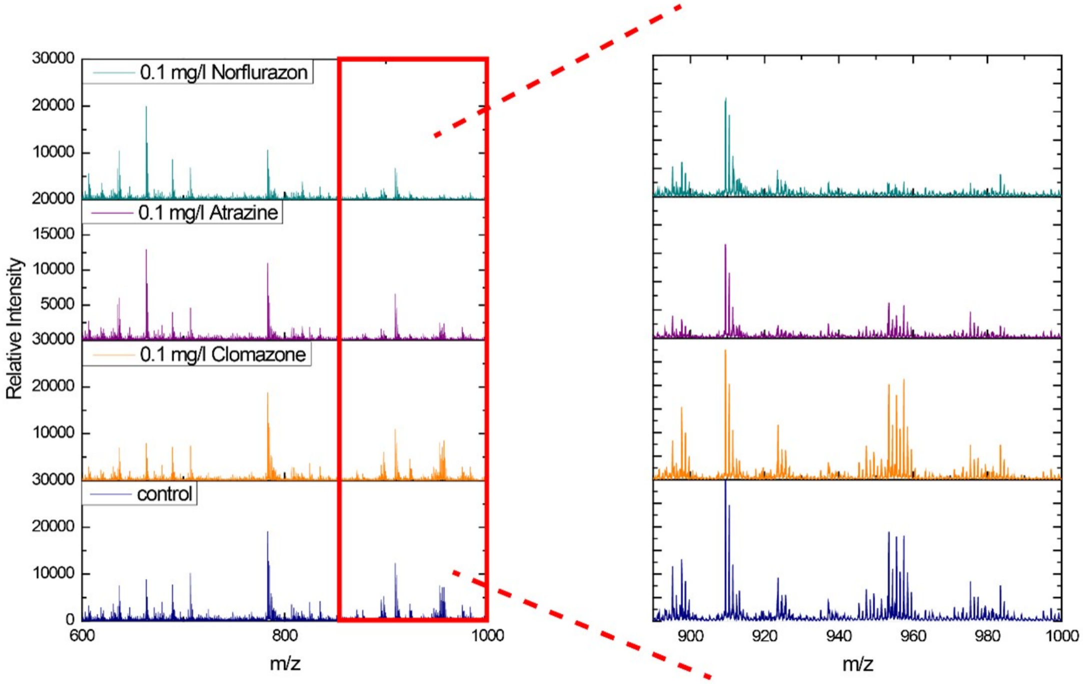

Figure 2.10: Algae lipid profiles showing response to herbicides norflurazon, atrazine, and clomazone compared to the control lipid profile.

dramatic decrease at both concentrations of norflurazon, and could be used as a marker to monitor the specific response to norflurazon.

Additional analysis was conducted for the norflurazon study. The bar graph in Figure 2.14 shows lipid species' distribution at concentrations of 0.05 and 0.1 mg/L of the herbicide. All DGDG lipid species decreased but some of the MGDG lipids increased at the higher concentration. The decrease in DGDG and an increase in MGDG suggest that the stress induced by norflurazon has caused a breakdown of DGDG, converting to its lyso forms like MGDG. This is supported by similar observation in others' work.[55][56] The

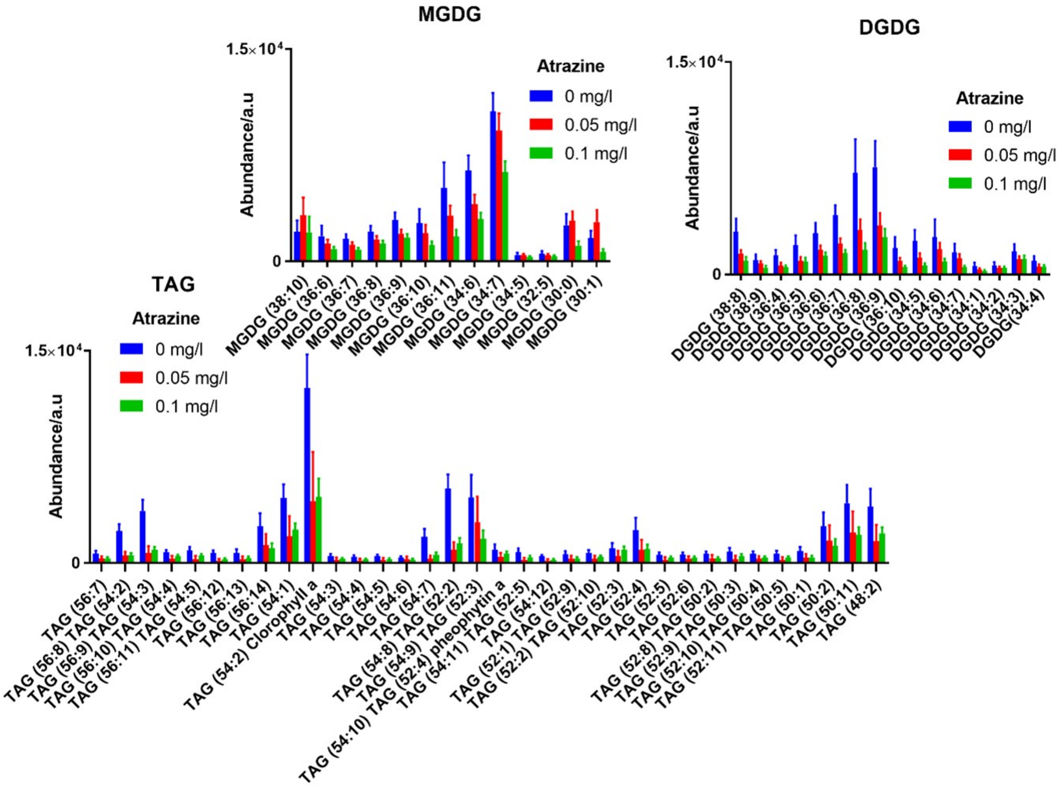

Figure 2.11: Lipidomic response to atrazine. Bars are mean values and SEM 95% is represented by the error bars.

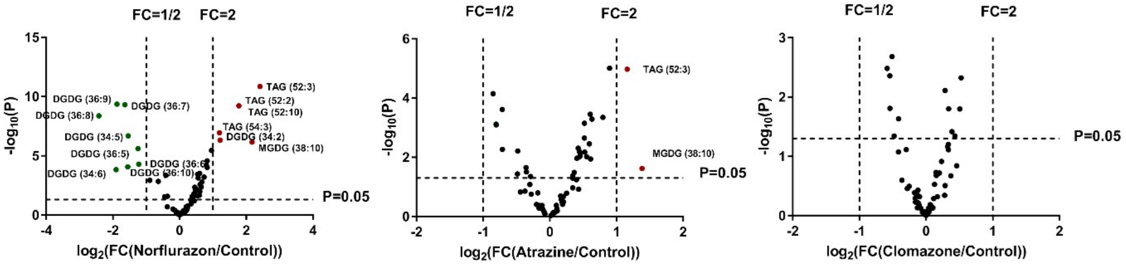

Figure 2.12: Volcano plots of statistical significant lipid variation for herbicide treatment versus control. Data reveals significant changes in the concentration of lipids after 96 h in norflurazon (0.1 mg/L), atrazine (0.1 mg/L), and clomazone (0.1 mg/L)

result can be provisionally considered as the effect of the herbicide on the chloroplastic desaturase pathway.[46][49] However, it is possible that this effect is not a result of direct action of herbicide on the desaturase located in the envelope, but rather indirectly on the

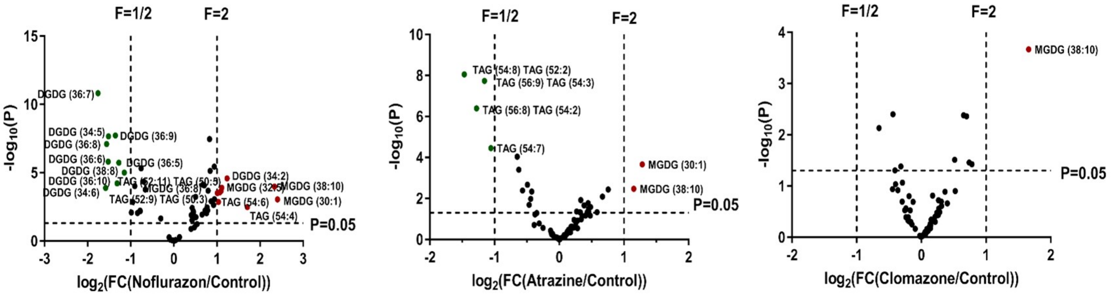

Figure 2.13: Volcano plot of lipid in *S. capricornutum*. Statistical analysis of variation in the data reveals significant changes in concentration of lipids after 96 hours in (a) norflurazon (0.05 mg/l), (b) atrazine (0.05 mg/l), (c) clomazone (0.05 mg/l).

carotenoid biosynthetic pathway. A similar trend for DGDG was observed in response to atrazine's inhibition of plastoquinone binding in PSII (Figure 2.11), causing the disruptions of the lipid supported photosystem complex.

Both norflurazon and clomazone are inhibitors of pigment synthesis; however, their effects on *S. capricornutum* were quite different. Clomazone was found to have little effect on *S. capricornutum*, even at a high concentration (Figure 2.3 and 2.10). Apparently, it inhibits the synthesis of carotenoids in certain types of plants but did not significantly impact algae growth or lipid content. It has been speculated that clomazone needs to be activated by a plant-bioactivation pathway to effectively inhibit photosynthetic organisms, and this is not a valid pathway in algae.[57] Similar effect was observed in *C. reinhardtii*, further suggesting the necessity of plant bioactivation for clomazone inhibition.

To better understand the individual effect of herbicide on *S. capricornutum*, we run in-depth data analysis, in particular partial least squares discriminate analysis (PLS-DA), to separate the herbicide groups into diacritical phenotypic clusters (Figure 2.15). No differentiation between clomazone treatment and the control could be identified; as such,

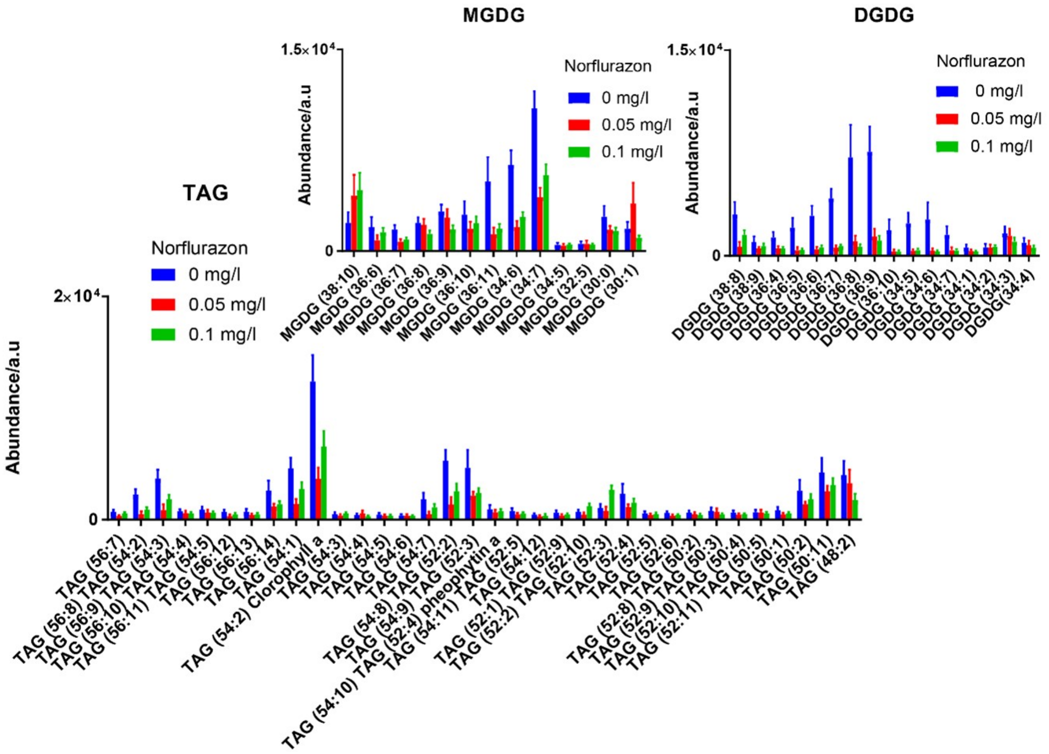

Figure 2.14: Lipidomic response to norflurazon. Bars are mean values, and SEM 95% is represented by the error bars.

clomazone is consistent with control cases in the PLS-DA data. Minimal overlap between atrazine and other treatment cases can be seen. Despite this, Figure 2.15 indicates that lipid profiles resulting from atrazine and norflurazon herbicide treatment can be clearly differentiated from clomazone/control. This further supports the conclusion that clomazone requires plant bioactivation for photosystem inhibition effects. This also demonstrates that lipid clusters can be used to facilitate herbicide classification and may be helpful for the prediction or identification of herbicide contamination in polluted waterways and watersheds.

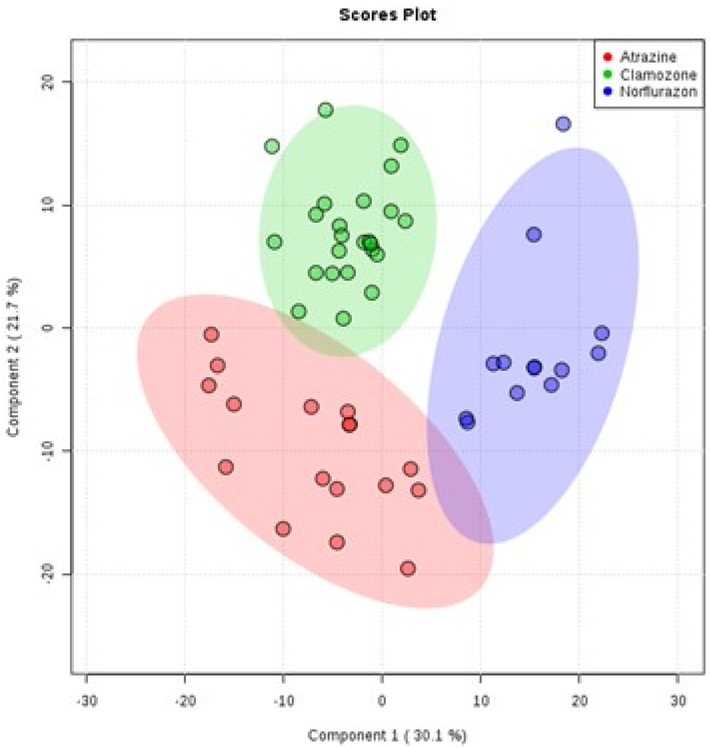

Figure 2.15: PLS-DA separating atrazine, clomazone, and norflurazon treatment cases on the basis of associated lipid profiles. PLS-DA maximizes the covariance between X (data) and Y (group) and is often used in the analysis of large biological data sets. The variance displayed in the plot above is the explained variance for X. A pronounced separation is revealed between the three groups of data. Ellipses indicate 95% confidence fitting.

Further data analysis was performed with a supervised machine learning (ML). ML models were trained and tested to classify the chemical treatment of algae on the basis of resulting lipid profiles. To test the feasibility of ML models to our system, we selected and utilized the caret package[34][35] within R, which contains 238 available models. We then screened these models and assessed if they were compatible with our dataset, which contains mass peaks and associated intensities. In the end, a total of 69 models were found fit. We then split the data 80:20 into training-testing sets and trained each model five times with a random selection of the data and 10-fold cross validation. The accuracies from the testing sets were averaged and utilized to identify 10 algorithms that showed the greatest promise for accurate identification of herbicide treatment effects. These algorithms were then trained and tested 100 times to identify the consistency of model predictions (Figure 2.16).

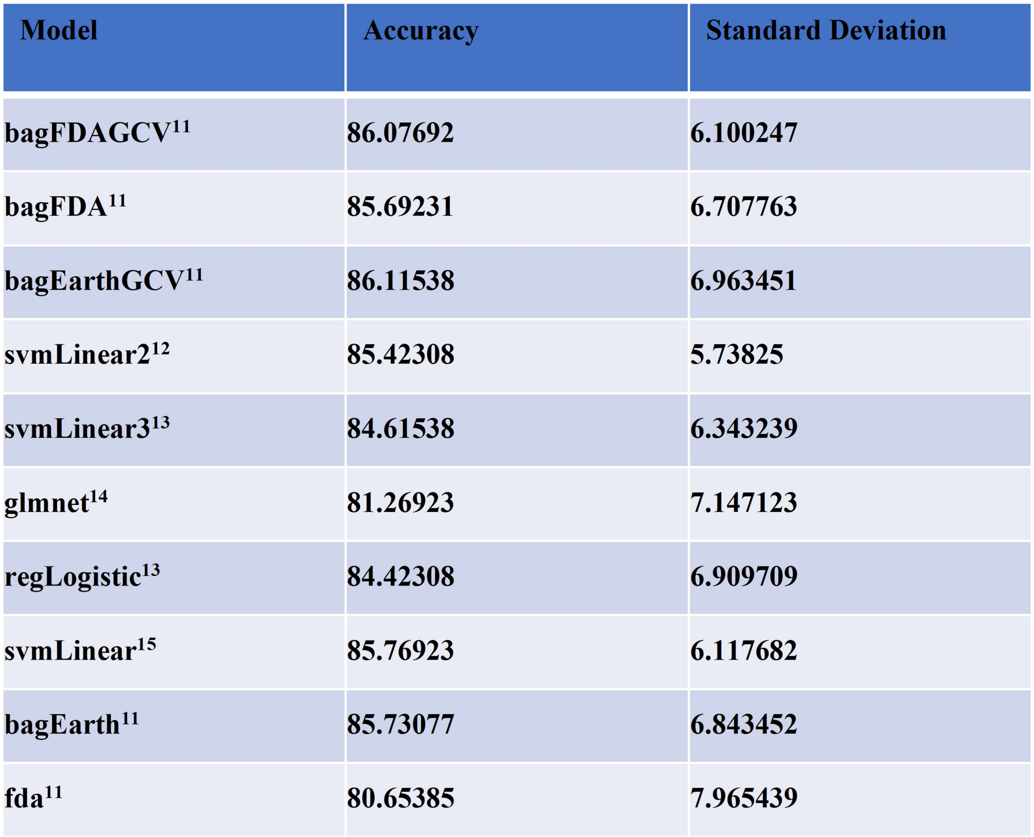

Model	Accuracy	Standard Deviation
bagFDAGCV[11]	86.07692	6.100247
bagFDA[11]	85.69231	6.707763
bagEarthGCV[11]	86.11538	6.963451
svmLinear2[12]	85.42308	5.73825
svmLinear3[13]	84.61538	6.343239
glmnet[14]	81.26923	7.147123
regLogistic[13]	84.42308	6.909709
svmLinear[15]	85.76923	6.117682
bagEarth[11]	85.73077	6.843452
fda[11]	80.65385	7.965439

Figure 2.16: List of the 10 machine learning methods that were chosen based on their accuracy, with average accuracy and standard deviation of repeated model testing results.

From this process, we found that three algorithms, flexible discriminant analysis (FDA), support-vector machines (SVMs), and logistic regression models, yielded the highest accuracy. In particular, the model of svmLinear2[58] demonstrated an accuracy of 85

6% across the 100 training and prediction sets. Figure 2.17 shows the ROC curves for svmLinear2 and a representative confusion matrix. Multiclass ROC curves were calculated and visualized with R package multiROC[59]. The area under the ROC curve represents the diagnostic success of the model for the indicated treatment class. This can be seen with clomazone as the curve has significantly less area than other treatment cases, illustrating the compromised ability to consistently differentiate clomazone treatment. This is further demonstrated in the accompanying confusion matrix (Figure 2.17b) that shows that clomazone and the control have ambiguity in identification while atrazine and norflurazon treatments are identified correctly. Clearly these machine learning models classify herbicide treatment cases using MS-based lipid profiles, and model testing produces consistent and accurate results. What is even more exciting is that the machine learning models could differentiate controls and clomazone treatment cases, which could not be achieved with other statistical methods. It pulls out minute differences in lipid profile caused by clomazone treatment that were not previously identified.

Additional investigation was carried out to identify lipid peak variables that are most important to classification (Figure 2.18) and compare them against those from the volcano plots. For norflurazon, TAG and DGDG lipids found to be significantly increased or decreased in volcano plots were also among the top 20 most important variables for classification, further confirming our findings about these lipid species. For clomazone, DGDG 34:6 and 36:6 appeared to have a significantly large role in the classification of clomazone treated cases, while TAG 54:2 (chlorophyll a) was observed to play a much greater role in the classification of the control cases against clomazone. The result suggests

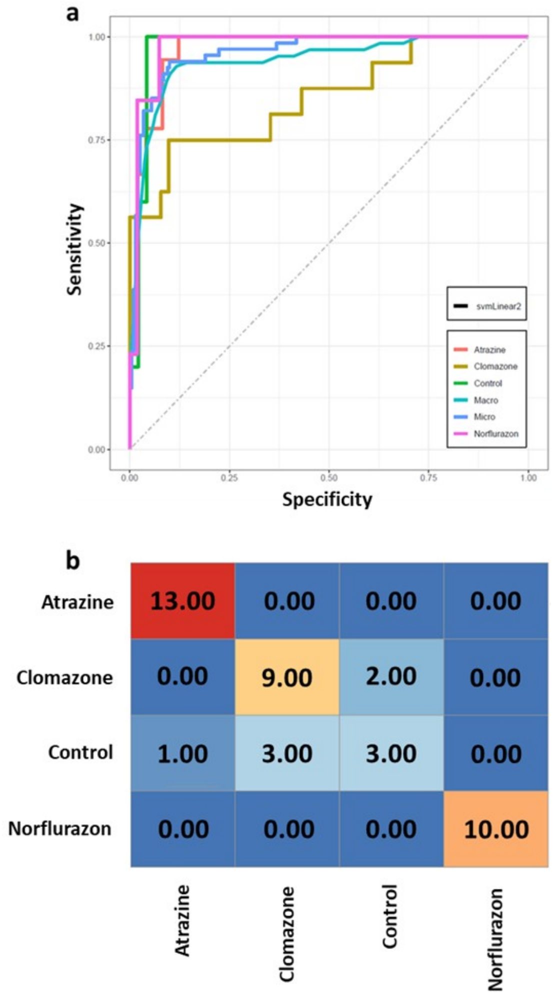

	Atrazine	Clomazone	Control	Norflurazon
Atrazine	13.00	0.00	0.00	0.00
Clomazone	0.00	9.00	2.00	0.00
Control	1.00	3.00	3.00	0.00
Norflurazon	0.00	0.00	0.00	10.00

Figure 2.17: Representative results of svmLinear2 model training and predictions where most misclassifications are isolated to control and clomazone treatment cases as can be seen from the ROC curve of clomazone and confusion matrix results. (a) Multiclass ROC curves of svmLinear2 for each treatment class (calculated via R package multiROC). Macro and micro curves are methods for converting the multi-class classification into a traditional binary classification used in ROC curves. Macro is achieved by averaging all groups and linear interpolation, while micro stacks all groups. (b) Confusion matrix of the model classification results.

that these lipids may be heavily implicated in some ways by clomazone, which imposes very low toxicity to *S. capricornutum*, compared to atrazine and norflurazon.

2.4 Conclusion

In conclusion, we report the use of a direct, label-free analytical platform to identify lipids and classify lipid profiling directly on intact algae cells with gold-microchip enhanced MALDI-TOF mass spectrometry. We have demonstrated that the platform is capable of characterizing differences in lipidomic response to various herbicides, and we have identified some unique effects of herbicides on lipid profiling between algal species. In addition, machine learning is combined with MALDI-MS lipid analysis to classify different treatment groups using diverse models that exhibit high accuracy. A chemical marker of MGDG (38:10) was discovered that could be potentially used for monitoring the response of the cells to the exposure of atrazine and norflurazon. A lipid library for *S. capricornutum* has been constructed for this less studied alga, which contains 63 identified lipids. The study and monitoring of several lipid families, including MGDG, DGDG and TAG, indicate that lipid conversion occurs under herbicide induced stress conditions, which leads to TAG accumulation and DGDG depletion. Aside from algae study, we believe that this method can find broad applications in characterizing other types of cells and their lipid mass fingerprint for global monitoring of environmentally significant molecules.

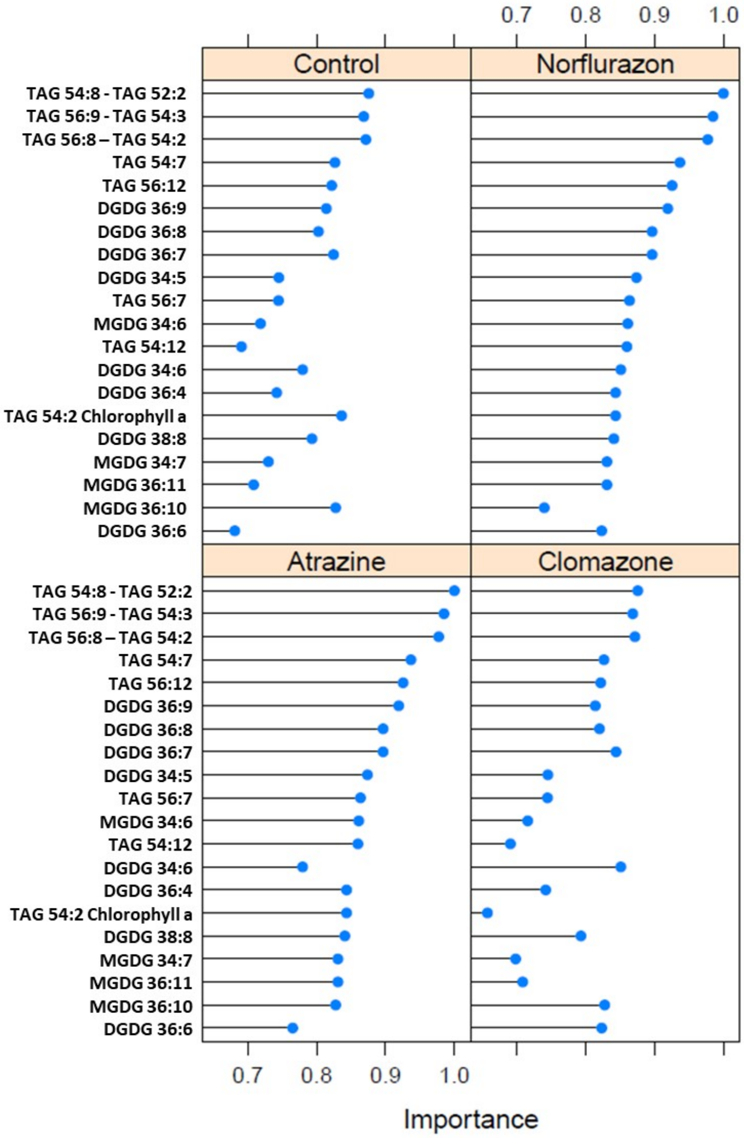

Figure 2.18: The 20 most important variables for treatment classification of algae samples when using the svmLinear2 model.

References

[1] C Walker, R Sibly, S Hopkin, and D Peakall. Fates of organic pollutants in individuals and organisms. *Principl. Fcotoxicol*, 2012:63–93, 2012.

[2] Xiao-e Yang, Xiang Wu, Hu-lin Hao, and Zhen-li He. Mechanisms and assessment of water eutrophication. *Journal of zhejiang university Science B*, 9(3):197–209, 2008.

[3] G Satyavani, G Chandrasehar, K Krishna Varma, A Goparaju, S Ayyappan, P Nee-

lakanta Reddy, and P Balakrishna Murthy. Toxicity assessment of expired pesticides to green algae pseudokirchneriella subcapitata. *International Scholarly Research Notices*, 2012, 2012.

[4] Jawameer R Hama, Dana W Kolpin, Gregory H LeFevre, Laura E Hubbard, Megan M Powers, and Bjarne W Strobel. Exposure and transport of alkaloids and phytoestrogens from soybeans to agricultural soils and streams in the midwestern united states. *Environmental science & technology*, 55(16):11029–11039, 2021.

[5] Beate I Escher, Nadine Bramaz, Rik IL Eggen, and Manuela Richter. In vitro assessment of modes of toxic action of pharmaceuticals in aquatic life. *Environmental science & technology*, 39(9):3090–3100, 2005.

[6] Carolin Riegraf, Georg Reifferscheid, Benjamin Becker, Shimshon Belkin, Henner Hollert, Ute Feiler, and Sebastian Buchinger. Detection and quantification of photosystem ii inhibitors using the freshwater alga desmodesmus subspicatus in combination with high-performance thin-layer chromatography. *Environmental Science & Technology*, 53(22):13458–13467, 2019.

[7] Orane Guillaume-Gentil, Timo Rey, Patrick Kiefer, Alfredo J Ibanez, Robert Steinhoff, Rolf Bronnimann, Livie Dorwling-Carter, Tomaso Zambelli, Renato Zenobi, and Julia A Vorholt. Single-cell mass spectrometry of metabolites extracted from live cells by fluidic force microscopy. *Analytical chemistry*, 89(9):5017–5023, 2017.

[8] Peter V Shanta, Bochao Li, Daniel D Stuart, and Quan Cheng. Plasmonic gold templates enhancing single cell lipidomic analysis of microorganisms. *Analytical chemistry*, 92(9):6213–6217, 2020.

[9] Yaping Kou, Meijing Liu, Peipei Sun, Zhaoqi Dong, and Jin Liu. High light boosts salinity stress-induced biosynthesis of astaxanthin and lipids in the green alga chromochloris zofingiensis. *Algal Research*, 50:101976, 2020.

[10] Yevhen Maltsev, Irina Maltseva, Svetlana Maltseva, John Patrick Kociolek, and Maxim Kulikovskiy. A new species of freshwater algae nephrochlamys yushanlensis sp. nov.(selenastraceae, sphaeropleales) and its lipid accumulation during nitrogen and phosphorus starvation. *Journal of Phycology*, 57(2):606–618, 2021.

[11] Xiaying Xin, Gordon Huang, Chunjiang An, Chen Lu, and Wenhui Xiong. Exploring the biophysicochemical alteration of green alga asterococcus superbus interactively affected by nanoparticles, triclosan and illumination. *Journal of Hazardous Materials*, 398:122855, 2020.

[12] Manisha Nanda, Krishna Kumar Jaiswal, Vinod Kumar, Mikhail S Vlaskin, Pankaj Gautam, Vivekanand Bahuguna, and PK Chauhan. Micro-pollutant pb (ii) mitigation and lipid induction in oleaginous microalgae chlorella sorokiniana uuind6. *Environmental Technology & Innovation*, 23:101613, 2021.

[13] Irina A Guschina, Anthony J Hayes, and Stephen J Ormerod. Polystyrene microplastics decrease accumulation of essential fatty acids in common freshwater algae. *Environmental Pollution*, 263:114425, 2020.

[14] Jurgen Schiller, Rosmarie Suss, Beate Fuchs, Matthias Muller, Olaf Zschornig, and Klaus Arnold. Maldi-tof ms in lipidomics. *Frontiers in Bioscience-Landmark*, 12(7):2568–2579, 2007.

[15] Xiaowei Zhang, Pu Xia, Pingping Wang, Jianghu Yang, and Donald J Baird. Omics advances in ecotoxicology, 2018.

[16] Stephen J Blanksby and Todd W Mitchell. Advances in mass spectrometry for lipidomics. *Annual Review of Analytical Chemistry*, 3:433–465, 2010.

[17] Michal Holcapek, Gerhard Liebisch, and Kim Ekroos. Lipidomic analysis, 2018.

[18] Kui Yang and Xianlin Han. Lipidomics: techniques, applications, and outcomes related to biomedical sciences. *Trends in biochemical sciences*, 41(11):954–969, 2016.

[19] Leona D Scanlan, Alexandre V Loguinov, Quincy Teng, Philipp Antczak, Kathleen P Dailey, Daniel T Nowinski, Jonah Kornbluh, Xin Xin Lin, Erica Lachenauer, Audrey Arai, et al. Gene transcription, metabolite and lipid profiling in eco-indicator daphnia magna indicate diverse mechanisms of toxicity by legacy and emerging flame-retardants. *Environmental science & technology*, 49(12):7400–7410, 2015.

[20] Peter V Shanta, Bochao Li, Daniel D Stuart, and Quan Cheng. Lipidomic profiling of algae with microarray maldi-ms toward ecotoxicological monitoring of herbicide exposure. *Environmental Science & Technology*, 55(15):10558–10568, 2021.

[21] Chin Chye Teo, William Pooi Kat Chong, Eddy Tan, Nurhidayah Binte Basri, Zhen Jie Low, and Ying Swan Ho. Advances in sample preparation and analytical techniques for lipidomics study of clinical samples. *TrAC Trends in Analytical Chemistry*, 66:1–18, 2015.

[22] Yepy H Rustam and Gavin E Reid. Analytical challenges and recent advances in mass spectrometry based lipidomics. *Analytical chemistry*, 90(1):374–397, 2018.

[23] Kamil Jurowski, Kamila Kochan, Justyna Walczak, Małgorzata Barańska, Wojciech Piekoszewski, and Bogusław Buszewski. Comprehensive review of trends and analytical strategies applied for biological samples preparation and storage in modern medical lipidomics: State of the art. *TrAC Trends in Analytical Chemistry*, 86:276–289, 2017.

[24] Antonio Checa, Carmen Bedia, and Joaquim Jaumot. Lipidomic data analysis: tutorial, practical guidelines and applications. *Analytica chimica acta*, 885:1–16, 2015.

[25] DG Heijerick, KAC De Schamphelaere, and CR Janssen. Biotic ligand model development predicting zn toxicity to the alga pseudokirchneriella subcapitata: possibilities and limitations. *Comparative Biochemistry and Physiology Part C: Toxicology & Pharmacology*, 133(1-2):207–218, 2002.

[26] Jeffrey W Moody, Christopher M McGinty, and Jason C Quinn. Global evaluation of biofuel potential from microalgae. *Proceedings of the National Academy of Sciences*, 111(23):8691–8696, 2014.

[27] Baharak Sajjadi, Wei-Yin Chen, Abdul Aziz Abdul Raman, and Shaliza Ibrahim. Microalgae lipid and biomass for biofuel production: A comprehensive review on lipid enhancement strategies and their effects on fatty acid composition. *Renewable and Sustainable Energy Reviews*, 97:200–232, 2018.

[28] Yoong Kit Leong and Jo-Shu Chang. Bioremediation of heavy metals using microalgae: Recent advances and mechanisms. *Bioresource technology*, 303:122886, 2020.

[29] Amin Keyvan Zeraatkar, Hossein Ahmadzadeh, Ahmad Farhad Talebi, Navid R Moheimani, and Mark P McHenry. Potential use of algae for heavy metal bioremediation, a critical review. *Journal of environmental management*, 181:817–831, 2016.

[30] K Suresh Kumar, Hans-Uwe Dahms, Eun-Ji Won, Jae-Seong Lee, and Kyung-Hoon Shin. Microalgae–a promising tool for heavy metal remediation. *Ecotoxicology and environmental safety*, 113:329–352, 2015.

[31] Jing Nie, Yuqing Sun, Yaoyu Zhou, Manish Kumar, Muhammad Usman, Jiangshan Li, Jihai Shao, Lei Wang, and Daniel CW Tsang. Bioremediation of water containing pesticides by microalgae: mechanisms, methods, and prospects for future research. *Science of The Total Environment*, 707:136080, 2020.

[32] Abdennour Abbas, Matthew J Linman, and Quan Cheng. Patterned resonance plasmonic microarrays for high-performance spr imaging. *Analytical chemistry*, 83(8):3147–3152, 2011.

[33] Jasmine Chong, Othman Soufan, Carin Li, Iurie Caraus, Shuzhao Li, Guillaume Bourque, David S Wishart, and Jianguo Xia. Metaboanalyst 4.0: towards more transparent and integrative metabolomics analysis. *Nucleic acids research*, 46(W1):W486–W494, 2018.

[34] Max Kuhn. Building predictive models in r using the caret package. *Journal of statistical software*, 28:1–26, 2008.

[35] Max Kuhn, Jed Wing, Stew Weston, Andre Williams, Chris Keefer, Allan Engelhardt, Tony Cooper, Zachary Mayer, Brenton Kenkel, et al. caret: Classification and regression training. r package version 6.0-86. *Astrophysics Source Code Library: Cambridge, MA, USA*, 2020.

[36] Xiaoling Su, Jilin Xu, Xiaojun Yan, Peng Zhao, Juanjuan Chen, Chengxu Zhou, Fang Zhao, and Shuang Li. Lipidomic changes during different growth stages of nitzschia closterium f. minutissima. *Metabolomics*, 9(2):300–310, 2013.

[37] Shuang Li, Jilin Xu, Jiao Chen, Juanjuan Chen, Chengxu Zhou, and Xiaojun Yan. The major lipid changes of some important diet microalgae during the entire growth phase. *Aquaculture*, 428:104–110, 2014.

[38] Takatoshi Kaya, Tomonori Kaneko, Shun Kojima, Yukito Nakamura, Youichi Ide, Kenji Ishida, Yoshihiko Suda, and Katsuko Yamashita. High-sensitivity immunoassay with surface plasmon field-enhanced fluorescence spectroscopy using a plastic sensor chip: Application to quantitative analysis of total prostate-specific antigen and galnacβ1–4glcnac-linked prostate-specific antigen for prostate cancer diagnosis. *Analytical chemistry*, 87(3):1797–1803, 2015.

[39] Jing Liu, Rolf Lauterbach, Harald Paulsen, and Wolfgang Knoll. Immobilization of light-harvesting chlorophyll a/b complex (lhciib) studied by surface plasmon field-enhanced fluorescence spectroscopy. *Langmuir*, 24(17):9661–9667, 2008.

[40] Thorsten Liebermann and Wolfgang Knoll. Surface-plasmon field-enhanced fluorescence spectroscopy. *Colloids and Surfaces A: Physicochemical and Engineering Aspects*, 171(1-3):115–130, 2000.

[41] Yongxia Zhang, Anatoliy Dragan, and Chris D Geddes. Wavelength dependence of metal-enhanced fluorescence. *The Journal of Physical Chemistry C*, 113(28):12095–12100, 2009.

[42] Jicheng Duan, Matthew J Linman, and Quan Cheng. Ultrathin calcinated films on a gold surface for highly effective laser desorption/ionization of biomolecules. *Analytical chemistry*, 82(12):5088–5094, 2010.

[43] Jasmin Krismer, Jens Sobek, Robert F Steinhoff, Stephan R Fagerer, Martin Pabst, and Renato Zenobi. Screening of chlamydomonas reinhardtii populations with single-cell resolution by using a high-throughput microscale sample preparation for matrix-assisted laser desorption ionization mass spectrometry. *Applied and environmental microbiology*, 81(16):5546–5551, 2015.

[44] Astrid Vieler, Christian Wilhelm, Reimund Goss, Rosmarie Süß, and Jürgen Schiller. The lipid composition of the unicellular green alga chlamydomonas reinhardtii and the diatom cyclotella meneghiniana investigated by maldi-tof ms and tlc. *Chemistry and physics of lipids*, 150(2):143–155, 2007.

[45] Dawei Yang, Donghui Song, Tobias Kind, Yan Ma, Jens Hoefkens, and Oliver Fiehn. Lipidomic analysis of chlamydomonas reinhardtii under nitrogen and sulfur deprivation. *PLoS One*, 10(9):e0137948, 2015.

[46] B Légeret, M Schulz-Raffelt, HM Nguyen, P Auroy, F Beisson, G Peltier, G Blanc, and Y Li-Beisson. Lipidomic and transcriptomic analyses of chlamydomonas reinhardtii under heat stress unveil a direct route for the conversion of membrane lipids into storage lipids. *Plant, cell & environment*, 39(4):834–847, 2016.

[47] Linxing Yao, Jose A Gerde, Show-Ling Lee, Tong Wang, and Kamel A Harrata. Microalgae lipid characterization. *Journal of agricultural and food chemistry*, 63(6):1773–1787, 2015.

[48] Megan A Danielewicz, Lisa A Anderson, and Annaliese K Franz. Triacylglycerol profiling of marine microalgae by mass spectrometry [s]. *Journal of lipid research*, 52(11):2101–2108, 2011.

[49] Laurence Boudière, Morgane Michaud, Dimitris Petroutsos, Fabrice Rébeillé, Denis Falconet, Olivier Bastien, Sylvaine Roy, Giovanni Finazzi, Norbert Rolland, Juliette Jouhet, et al. Glycerolipids in photosynthesis: composition, synthesis and trafficking. *Biochimica et Biophysica Acta (BBA)-Bioenergetics*, 1837(4):470–480, 2014.

[50] MM Nemat Alla and NM Hassan. Changes of antioxidants levels in two maize lines following atrazine treatments. *Plant physiology and biochemistry*, 44(4):202–210, 2006.

[51] Kaushik Das and Aryadeep Roychoudhury. Reactive oxygen species (ros) and response of antioxidants as ros-scavengers during environmental stress in plants. *Frontiers in environmental science*, 2:53, 2014.

[52] Qiang Hu, Milton Sommerfeld, Eric Jarvis, Maria Ghirardi, Matthew Posewitz, Michael Seibert, and Al Darzins. Microalgal triacylglycerols as feedstocks for biofuel production: perspectives and advances. *The plant journal*, 54(4):621–639, 2008.

[53] Yusuf Chisti. Biodiesel from microalgae. *Biotechnology advances*, 25(3):294–306, 2007.

[54] Yanqun Li, Mark Horsman, Nan Wu, Christopher Q Lan, and Nathalie Dubois-Calero. Biofuels from microalgae. *Biotechnology progress*, 24(4):815–820, 2008.

[55] Ouzna Abrous, Ghouziel Benhassaine-Kesri, Antoine Tremolieres, and Paul Mazliak. Effect of norflurazon on lipid metabolism in soya seedlings. *Phytochemistry*, 49(4):979–985, 1998.

[56] D Di Baccio, Mike Frank Quartacci, F Dalla Vecchia, N La Rocca, N Rascio, and Flavia Navari-Izzo. Bleaching herbicide effects on plastids of dark-grown plants: lipid composition of etioplasts in amitrole and norflurazon-treated barley leaves. *Journal of experimental botany*, 53(376):1857–1865, 2002.

[57] Yurdagul Ferhatoglu and Michael Barrett. Studies of clomazone mode of action. *Pesticide biochemistry and physiology*, 85(1):7–14, 2006.

[58] David Meyer, Evgenia Dimitriadou, Kurt Hornik, Andreas Weingessel, Friedrich Leisch, CC Chang, and CC Lin. e1071: Misc functions of the department of statistics, probability theory group (formerly: E1071), tu wien [r package version 1.7-9]. *Comprehensive R Archive Network (CRAN)*, 2021.

[59] RM Wei, JY Wang, and Wei Jia. multiroc: calculating and visualizing roc and pr curves across multi-class classifications. in. *R package version*, 1(1), 2018.

Chapter 3

Lipidomic Analysis of Intact Bacterial Cells Exposed to Antibiotic Using MALDI-MS and Gold Micro-chip

3.1 Introduction

Lipids are essential metabolites that play important roles in cells and can be used to check the metabolic status of cells directly. Their status can change in repose to cellular environment alteration.

Over the past decade, there has been a growing interest in developing analytical methods for lipid analysis that look at bacterial taxonomy, membrane structure, growth changes, metabolic processes, and changes under normal or stressed growth conditions. [1][2] There have been big steps forward in making high-throughput analytical techniques that can identify lipid profiles from complex biological targets and study antibiotic resistance using mass spectrometry. [3][4][5][6] 3-6However, classic lipid analysis techniques (e.g., GC and LC) include long-term extraction, pre-fractionation followed by chromatographic separation and mass spectrometry identification,[7] which require high sample amounts together with time-consuming sample pre-treatments and lead to unavoidable loss of sample. Therefore, among mass spectrometry techniques, matrix-assisted laser desorption/ionization mass spectrometry (MALDI-MS) shows a considerable advantage in lipid analysis because of its fast, convenient and straightforward performance.[8] In addition, it has demonstrated its capability to provide helpful information for identifying and differentiating microorganisms due to its speed and sensitivity which allow rapid analysis with minimal sample preparation. [9][10][11]

Mass spectrometry-based lipidomics has been increasingly popular in the past decade. While most lipidomics work is focused on mammalian and other eukaryotic systems, there is also a growing interest in the exploration of bacterial lipidomics. [12] Lipids in bacteria can be very different from lipids in eukaryotic cells. Still, they are both important for keeping the structure of bacteria intact and protecting them from the surrounding environment. As an essential part of cells, lipids participate in the energy storage process and maintain structural integrity.[13] Additionally, a lot of studies show that many diseases are accompanied by changes in the lipid composition of cells and tissues.[14][15][16] Changes in the lipid profiles can serve as markers for cell regulation processes.[17] There is evidence suggesting that stress condition (e.g. antibiotic treatment) triggers gene expression changes,[18] cell mutations,[19] which further cause morphological changes in the membrane correlated with lipid composition. The composition of lipids in the membrane controls the ability of the cell to withstand or adjust to external factors such as temperature and pH, regulate permeability and active transport, and influence the spatial distribution of proteins throughout the membrane.[20][21]

Bacterial resistance to antibiotics has been a serious issue over the last decades since the number of strains resistant to multiple types of antibiotics has increased each year and spread worldwide. Overcoming this challenge requires developing new modified antimicrobial therapeutics and, more importantly, a better understanding of the cellular response. Colistin is a polymyxin antibiotic with a narrow antibacterial spectrum against Gram-negative bacteria such as Pseudomonas aeruginosa, Acinetobacter baumannii, Klebsiella spp., Escherichia coli, and other Enterobacteriaceae.citefalagas2010resistance Previous studies show that for some multidrug-resistant Gram-negative bacteria, in particular, *Pseudomonas aeruginosa*, *Acinetobacter baumannii*, and *Klebsiella pneumoniae*, polymyxins are seriously considered as last-resort antibiotics.[22][23][24][25] The initial target of colistin is the lipopolysaccharide (LPS) component of the outer membrane of Gram-negative bacteria. Through an electrostatic interaction between positively charged α, γ-dianimobutyric acid (Dab) residues of colistin and negatively charged phosphate groups of lipid A, a key component of the LPS, divalent cations calcium (Ca^{2+}) and magnesium (Mg^{2+}), which normally stabilize the LPS, are displaced from the negatively charged phosphate groups of membrane lipid. Therefore, LPS is destabilized, increasing the permeability of the bacterial membrane.

This leads to leakage of intracellular contents and eventually causes cell death.[26] It should be emphasized here that colistin's mode of action based on membrane lysis death is the most documented explanation, but its ultimate mechanism of action is still unclear.[27][28] Therefore, a study monitoring the changes of lipids in microorganisms as a response to colistin exposures at the molecular level would help rationalize the mechanism behind the colistin-mediated antimicrobial effect.

In this study, we performed MALDI-TOF-MS based on untargeted lipidomics to improve our understanding of the mechanism of action of colistin. We designed to gain insight into alterations in lipids associated with colistin treatment in intact E.coli. A high throughput lable free method of direct lipid analysis by matrix-assisted laser desorption/ionization (MALDI) mass spectrometry (MS) in intact membranes, without prior extraction/separation steps, is described. Multiple metabolic analysis approaches were integrated to analyze the lipid profiling response to antibiotic treatment. We adopted MALDI-MS coupled with gold micro-chips, which enable rapid identification of lipids and profiling phospholipid metabolism in intact cells. Our results showed differences in the spectral pattern of lipids when bacteria were exposed to colistin, suggesting that E.coli responds to colistin by changing the expression of specific classes of lipids.

3.2 Experimental Section

3.2.1 Materials

Super 2,5 - dihydroxybenzoic acid (sDHB), acetonitrile (ACN), colistin sulfate salt (CAS 264-72-8), LB Broth (Miller) medium were purchased from Sigma-Aldrich. BK7 glass microscope slides came from Fisher Scientific. High-purity water (>18 MΩ cm–1) was obtained from a Barnstead E-Pure water purification system. Matrix solutions (sDHB) were prepared in acetonitrile and water (2:1,v/v) at a concentration of 10 mg/ml. The culture medium was autoclaved at 121°C for 30 minutes.

3.2.2 Fabrication of Gold μchip

The gold μchip array were fabricated using the method which we have reported before in the Cleanroom Facility at UCR[29] Briefly, gold micro-chips were fabricated by a photolithographic method. The photoresist was spun-coated onto glass slides which were cleaned with Piranha solution, followed by baked at 110 °C for 1 min. The array was patterned into the photoresist by a mask aligner and UV-light. After another baking step, the micro-chips were cured using UV-flood light and developed with a developing solution (AZ400 : $H_2O = 1 : 400$). Next, e-beam deposition was used to deposit different thicknesses of Cr/Au onto the arrays. The photoresist was removed by acetone. Finally, there is a pristine 50 nm gold well array onto the surface.

3.2.3 Bacterial Strain and Culture Conditions

E.coli ATCC 25922 was purchased from American Type Culture Collection (ATCC, United Stated). For experimental purposes, the microorganism was grown overnight in LB Broth (Miller) growth medium in a 37°C shaker at 220 rpms to early stationary phase, harvested by centrifugation, and resuspended with medium (10^6 cells/mL). 200 μl/well of resuspension was added to a 96-well plate as a control group. The colistin used in the studies was diluted from 256 μg/mL to 0.25 μg/mL in a double dilution. After 18h incubation, cultures in the control and antibiotic treatment groups were harvested by centrifugation at 8000 rpm for 10 minutes, washed three times with deionized water, and finally resuspended in deionized water at $\approx 10^9$ cells/ml. The cell density was evaluated by measuring the turbidity of suspension in an Agilent spectrophotometer (Cary 60 UV-Vis). The standard optical density (OD) value at 600nm of $\approx$1.7 (10^9 cells/ml) for E.coli was selected and used for MALDI-MS acquisition.

3.2.4 Minimum Inhibitory Concentration (MIC) Microbiological Assay

MICs were performed according to the Clinical and Laboratory Standards Institute (CLSI) guidelines. MICs were determined in three replicates on separate days using broth microdilution method in LB medium in 96-well plates. Plates were inoculated with 100 μL of bacterial suspension prepared in LB medium (containing 106 cells/ mL) and 100 μL of LB containing increasing concentrations of colistin (0.25–256 μg/mL) in each well. The MICs were defined as the lowest concentration at which visible growth was inhibited following 18 h incubation at 37 °C. Cell viability was determined by sampling wells at colistin concentrations higher than the MIC.

3.2.5 MALDI-TOF-MS Preparation and Acquisition

1μl of the sample was added to each well of the gold micro-chip, covered with 1μl of sDHB matrix. Experiments were performed using a AB-Sciex 5800 time-of-flight mass spectrometer equipped with a nitrogen UV laser (337nm wavelength). Lipid profiles of E. coli were acquired in negative ion mode with a laser fluence of 5900 au on the reflectron detector.

3.2.6 Data Processing and Statistical Analysis

The raw data was acquired using TOF/TOF Series Explorer software version 4.1.0 (AB Sciex), and raw data were converted to the .mzXML files using conversion software T2D converter. The mzXML data were then exported as a .csv file by the MALDIquant package for further statistical analysis. MetaboAnalyst 5.0 was used for univariate and multivariate statistical analysis. For univariate analysis, the statistical significance of feature was determined between the control and colistin treatment groups using a t-test and fold change. The p-value of 0.05 and fold change > 2 were used as criteria for significant feature selection. For multivariate analysis, partial least squares discriminant analysis (PLS-DA) was used as a supervised method to find significant variables with discriminative power. Lipids were assigned from the LIPIDMAPS[30] database and literature. [31][32][33][34][35]

3.3 Results and Discussion

According to the antibiotic dose-response curve (Figure.3.1), MIC was determined to be 2 μg/ml, consistent with the reported concentration required to kill susceptibility bacteria.[36] 37 Then EC_50 was determined to be 1μg/ml. After 18h incubation, all the data were collected from E.coli treated with and without 1μg/ml colistin, followed used for lipid analysis. Typical mass spectra of the lipid profile from intact E.coli are shown in Figure 3.2. E.coli accumulated three major phospholipids in the membrane. Its predominant lipid is zwitterionic phosphatidylethanolamine (PE) (about 75% of membrane),and additionally, it forms the anionic lipids phosphatidylglycerol (PG, about 20%) and cardiolipin (CL).[13] A drawback of MALDI MS analysis in positive ion mode is represented by ionization suppression effects exerted by phosphatidylcholines, which makes a difficult study of complex lipid mixtures. Such suppression has limitations when analyzing whole cell bacteria since the dominant components in the membrane are phospholipids (PLs), and the two major phospholipids, PE and PG, cannot easily be ionized in positive mode. Therefore, we selected to collect the mass spectra in the negative ion mode to reduce such suppression effects. As is shown in Figure. 3.2, lipid-related differentiation between the control group and antibiotic treatment group can be observed from MALDI-TOF-MS. Our area of interest in the spectra is mainly between 600-2000 m/z since there are interference peaks from the matrix in the front of the area of the spectra (< m/z 600). After treatment, the two groups can be easily distinguished by a visual inspection of the spectra. Inset in Figure. 3.2 shows expanded regions of the spectra from m/z 600 to 1300, where more details of difference can be found.

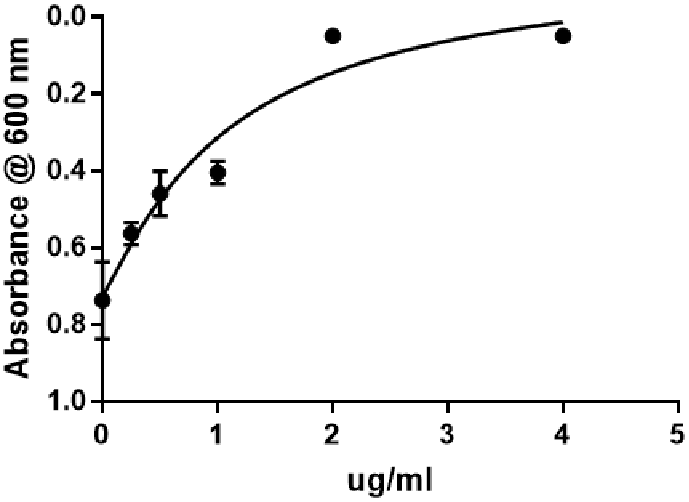

Figure 3.1: Colistin dose-response curve

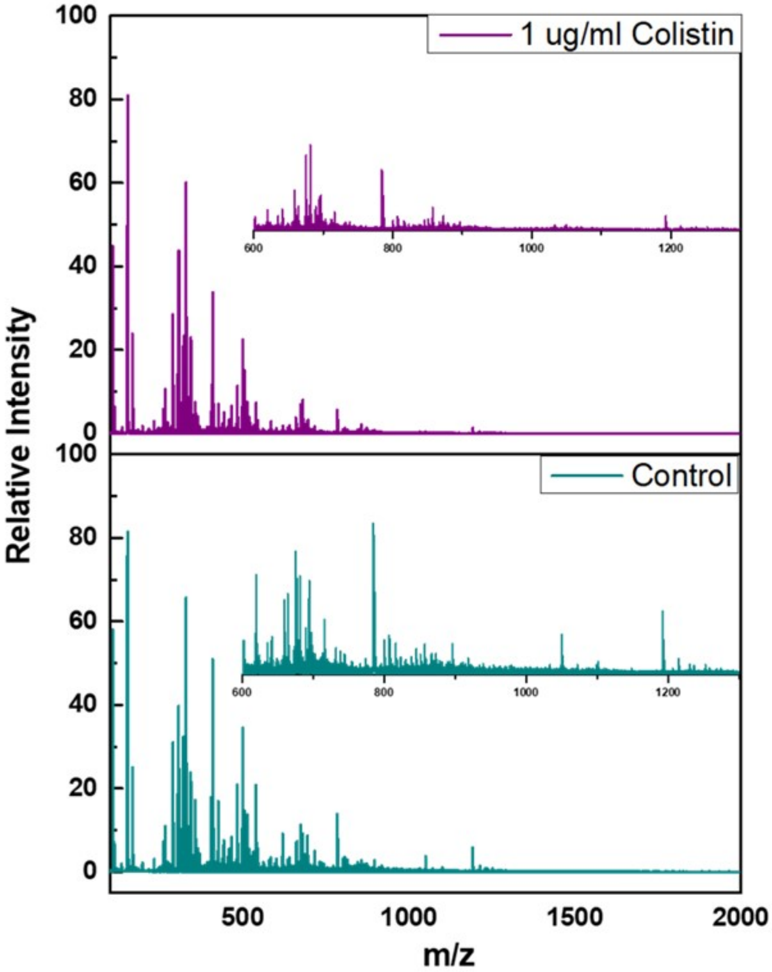

Figure 3.2: MALDI-TOF MS averaged spectra in negative ion mode for lipid profile of intact E.coli with and without antibiotic treatment.

Lipid response resulting from the exposure to colistin was studied. All the data were collected from the bacterial sample spotted on our gold microchips, demonstrating a high throughput, label-free, and enhanced MALDI ionization microarray. The bar graph shows the putatively identified lipid distribution in intact E.coli detected by MALDI-MS on our gold micro-chip (Figure. 3.3).In negative mode, 68 lipids were annotated, belonging to four lipid classes: 28 phosphatidylethanolamines (PEs), 26 phosphatidylglycerols (PGs), 11 phosphatidic acids (PAs), and 3 phosphatidylserines (PSs). To compare the performance of our lipid analysis platform for intact bacteria with the traditional method for lysis cells, we also conducted experiments on lipid extracts on HPLC-MS (Figure. 3.1). A few more lipids, 95 lipid peaks, were found in negative mode, including PE, PG, PS, PA, and CL, since the sample is lipid extracts with higher concentration. Inspection of Figure. 3.3 shows that following an 18 h exposure to colistin, E.coli demonstrates a lipid response to the presence of an antibiotic, resulting in an increase in the number of lipids that are down-regulated compared to those from the control culture. PE has the most extensive alteration among each lipid class, either upregulation or downregulation significantly. A significantly higher quantity of PE(30:2), PE(31:1), PE(32:6), PE(32:5), and PE(32:1) with an antibiotic concentration decrease, while only PE (32:4) increases significantly. PE is a principal phospholipid in bacterial membranes. It can be synthesized either via the Pss (phosphatidylserine synthase) / Psd (phosphatidylserine decarboxylase) pathway[37] or via CL/PE synthase (cardiolipin/ phosphatidylethanolamine synthase)[38]. In the first pathway, Pss condenses serine with CDP-DAG (cytidine diphosphate-diacylglycerol), forming of the anionic lipid PS. Psd then decarboxylates PS to form the zwitterionic lipid PE. Ethanolamine is used as a substrate catalyzed by CL/PE synthase in the second pathway to form PE. One of the main roles of PE in bacterial membranes is to spread out the negative charge caused by anionic membrane phospholipids. In E.coli, it plays a role in supporting active transport by the lactose permease and is involved in other transport systems as well. Besides, it is reported to serve as a 'chaperone' in the assembly of lactose permease and other membrane proteins to guide the proteins' folding path and aid in the transition from the cytoplasmic to the membrane environment. When PE is absent, the transport proteins may have an incorrect tertiary structure and do not function correctly.[39]Moreover, PE enables bacterial multidrug transport to work properly and allows the formation of intermediates required for the transporters to open and close properly.[40] As it is shown in Figure. 3.3, PE significantly decreased concomitantly with the decrease of most of PG, PA, and PS. Among annotated PGs, PG(29:2), PG(29:1), and PG(30:2) have slight increases after exposure to the antibiotic compared with other PGs. Aside from being an important membrane constituent, PG is an essential intermediate in the biosynthesis of many other lipids, especially cardiolipin. It is also important for the optimal functioning of the bacterial machinery and plays a role in protein folding and binding.[41] In E.coli, PG is synthesized by a system of enzymes. Phosphatidylglycerolphosphate synthase (PgsA) condenses glycerol-3-phosphate (G3P) with CDG-DAG leading to the formation of PGP, which in turn is dephosphorylated to PG by three PGP phosphatases (PgpA, PgpB, and PgpC).[42] PG is a direct precursor of CL, whose synthesis is mediated by three CL synthase genes in E.coli. There is conflicting evidence as to whether E.coli absolutely needs PG in its membrane. Studies on mutants lacking PG have shown that its absence can lead to defects in DNA replication and a lack of necessary modifications to the major cellular lipoproteins or proteolipids, which leads to membrane welding and, eventually, cell death. However, some other studies on similar experiments found that PG and CL are dispensable and can be replaced by PE and anionic phospholipids such as phosphatidic acid.[41] PA is the precursor for the biosynthesis of many other lipids. In addition to its role in lipid biosynthesis, PA has been reported to act as a signaling molecule that modulates several aspects of cell biology, including membrane transport, vesicular trafficking, enzyme activity, as well as membrane structure and dynamics.[43]They are also activators of lipid lipid-gated ion channels.[44] In E.coli, formation of PA occurs via the Gro3P (glycerol 3-phosphate) pathway, the first step of acylation catalyzed by Gro3P acyltransferase (Gro3P AT) leads to the formation of 1-acylGro3P which is further acylated to PA by 1-acylGro3P acyltransferase(1-acyl-Gro3P AT).[45] In Figure. 2, all annotated PSs decrease after being exposed to the antibiotic. PS is a key intermediate in the synthesis of phospholipids in E.coli since it is converted to PE, the dominant lipid in the membrane of E.coli. It is formed in E.coli through a displacement of cytidine monophosphate, which is formed from CDP-diacylglycerol by PS synthase, through a nucleophilic attack by the hydroxyl functional group of serine and eventually becomes PE by the enzyme PS decarboxylase. [46]

Statistical analysis of variation in the data indicates significant changes in lipid concentration after exposure to 0.1 μg/ml colistin (Figure 3.4). The volcano plot shows log 2 of the fold change on the x-axis and log10 of the p-value on the y-axis (Figure 3.4a). A significant change threshold of $P = 0.05$ and $FC > 2$ was used to compartmentalize lipids into the upper left and right corners of the volcano plot. Significantly down (green) and up (red) regulated lipids were shown on the top. As shown in Figure 3.4a, compared to the untreated control, E.coli treated with colistin (1μg/ml) significantly reduced PG(30:0), PA(30:1), PA (30:0), PE (30:2), PE (31;1), and PE (32:1), while significantly increase PA (36:3) and PE (32:4). Box-and-whisker plots show the lipid content level of the top four selected lipids with significant differences between the non-treatment and the treatment groups. All of the

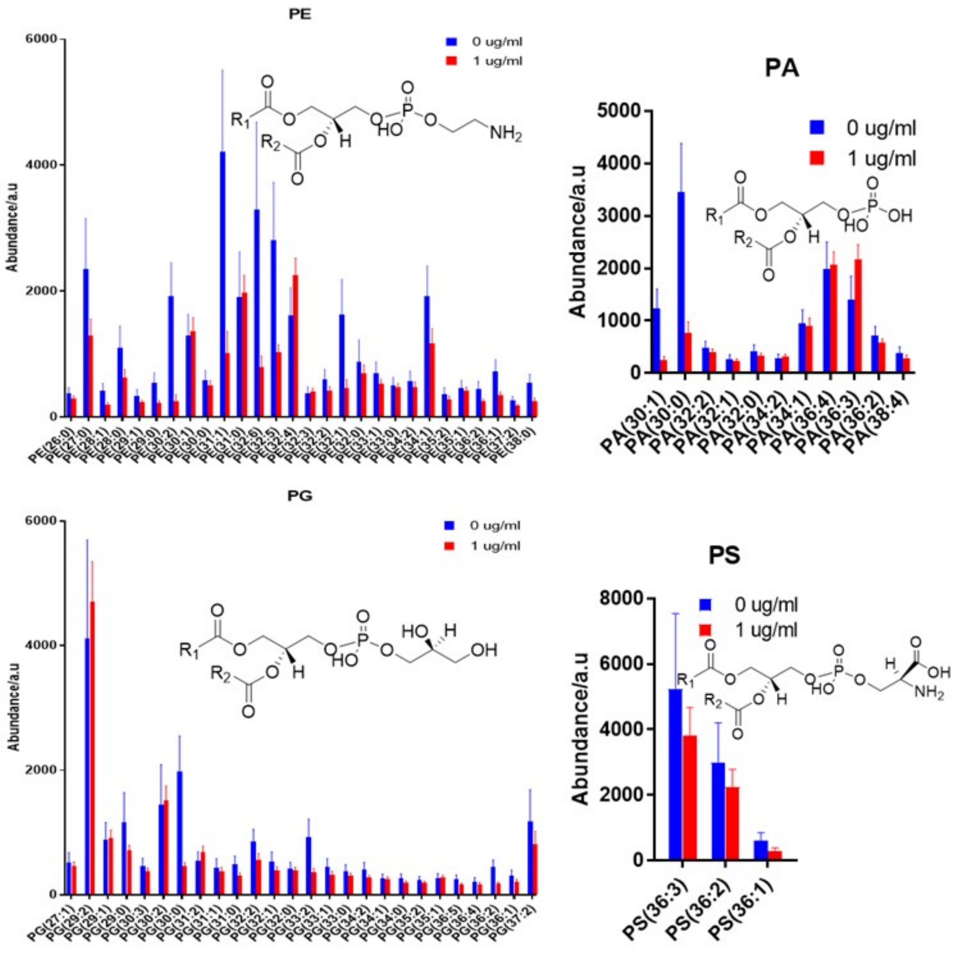

Figure 3.3: Lipid distribution in Intact E.coli with and without antibiotic treatment detected by MALDI-MS on Gold-μChip.Bars are mean values, and SEM 95% is represented by the error bars.

top four selected lipids that change dramatically, PG (30:0), PE (30:2), PA (30:1), and PA (30:0), show a decrease after treatment (Figure 3.4b). Figure 3.4c. shows the specific fold change of each lipid, which has significant down or up regulation, e.g. PE(30:2) decreased to 0.12 fold, and PA(36:3) increased to 2.48 folds. Phospholipids are critical components of bacterial membranes, and are responsible for maintaining membrane integrity and the selective permeability of the outer membrane. [47] In addition, they contribute to cationic peptide resistance, protect bacteria from osmotic stress, and regulate flagellum-mediated motility.[48]

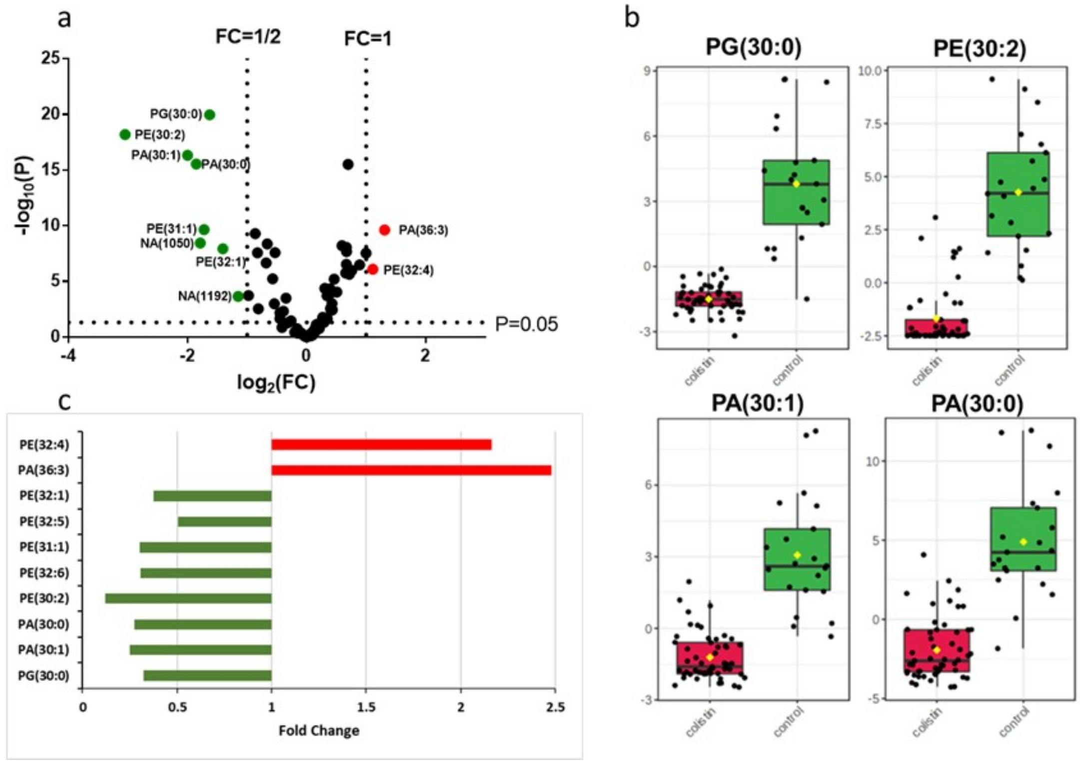

Figure 3.4: Content level change of lipid. a. volcano plot of significant change of lipid content compared to control group. Important features selected by volcano plot with fold change threshold (x) 2 and t-tests threshold (y) 0.05. The red circles represent features above the threshold. Note both fold changes and p values are log transformed. The further its position away from (0,0), the more significant the feature is. b. Box-whisker plots of the top 4 putatively identified lipids that were distinguished between the untreated control group and colistin treated group. c. Fold change for each lipid which has significant changes.

In addition, correlation analysis was conducted, which was used to visualize the overall correlations between different features (Figure 3.5). We look for features showing similarities in their intensity or concentration changes to a feature of interest and determine if certain features show particular patterns under different conditions. It is directly performed against the target feature to identify those peaks that are either positively or negatively correlated. In this figure, the red boxes represent variables with a positive relationship, and the blue boxes represent variables with a negative relationship. Therefore, it shows the changes in which lipids due to the colistin effect are more related to which in others. The hierarchical clustering was also included to show that the features located in the same cluster as the target feature are most similar in intensity or concentration changes.

We also performed a supervised statistical analysis to assess the major changes in lipid analysis between the treatment group and the non-treatment group. As shown in Figure 3.6a, lipid profiles differed in E.coli treated with 0.1μg/ml colistin relative to those without treatment. The PLS-DA shows that the different groups were well-clustered, with a specific lipid profile for each. Group membership (treated with and without colistin) is illustrated by the 95% confidence ellipses calculated from PLS-DA scores. Top15 significant feature peaks show the features which are identified in the PLS-DA analysis (Figure 3.6b). Among the annotated lipids, PG (29:2) and PA (30:0) contribute most to the discrimination of two clusters, which can be considered potential biomarkers for the colistin effect on lipids in E.coli. According to correlation analysis (Figure 3.5), they are most correlated to PE (31:0) and PE (32:6), respectively.

3.4 Conclusion

We developed a direct, label-free analysis platform to identify lipids directly on intact organisims without any chemical treatment or purification, using a gold microchip in combination with MALDI-TOF mass spectrometry. Our gold microarray platform has

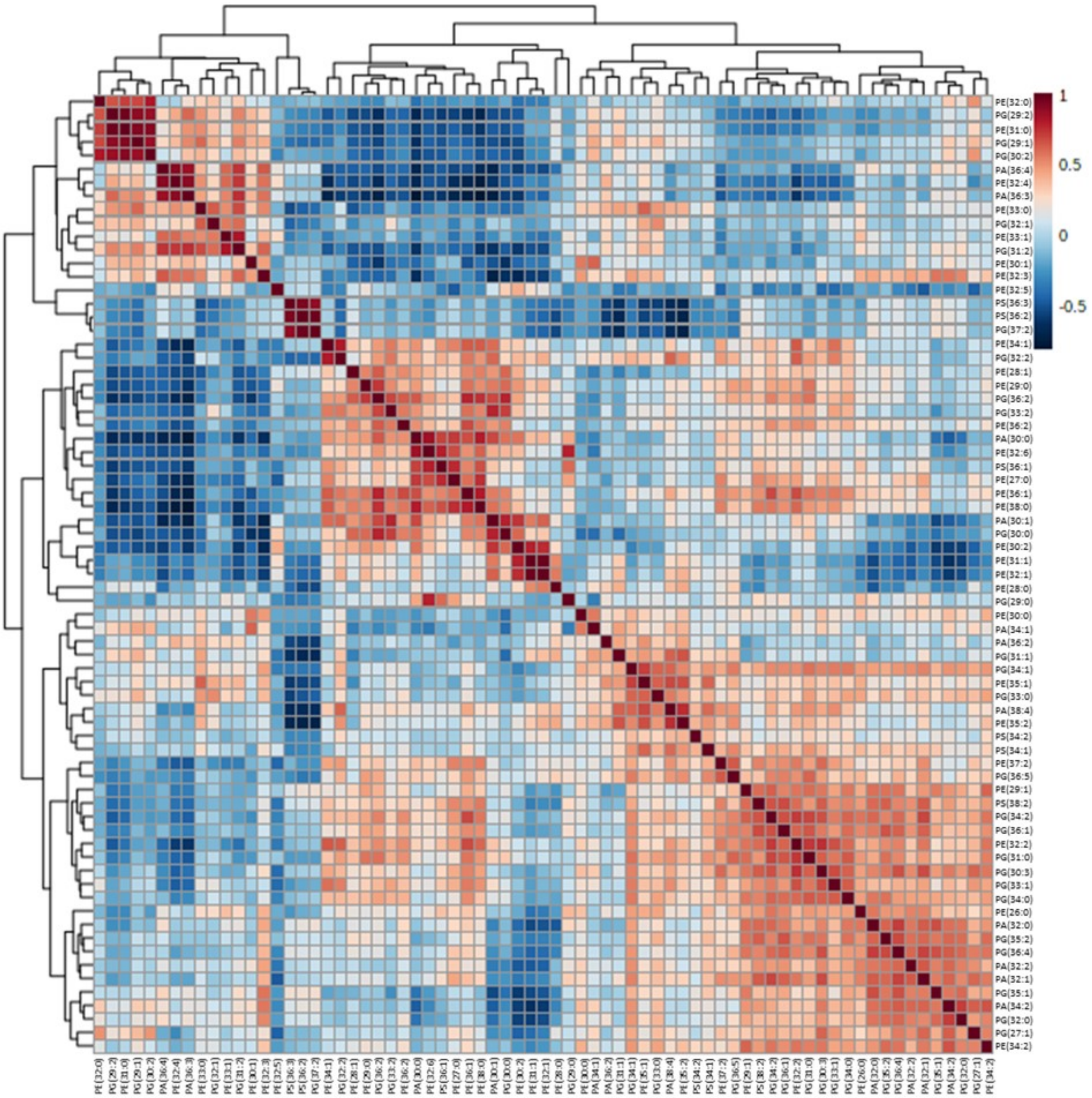

Figure 3.5: Correlation Heatmaps. Heatmap of Pearson correlation between lipids

been reported for lipid analysis of microalgae at a single-cell level. In this study, we further applied it to the lipidomic analysis of E.coli, which is used as a model organism for procaryotic organisms study. Compared to the HPLC-MS, MALDI-TOF-MS is much faster and easier to handle without any sample pre-preparation. Based on the lipid detection

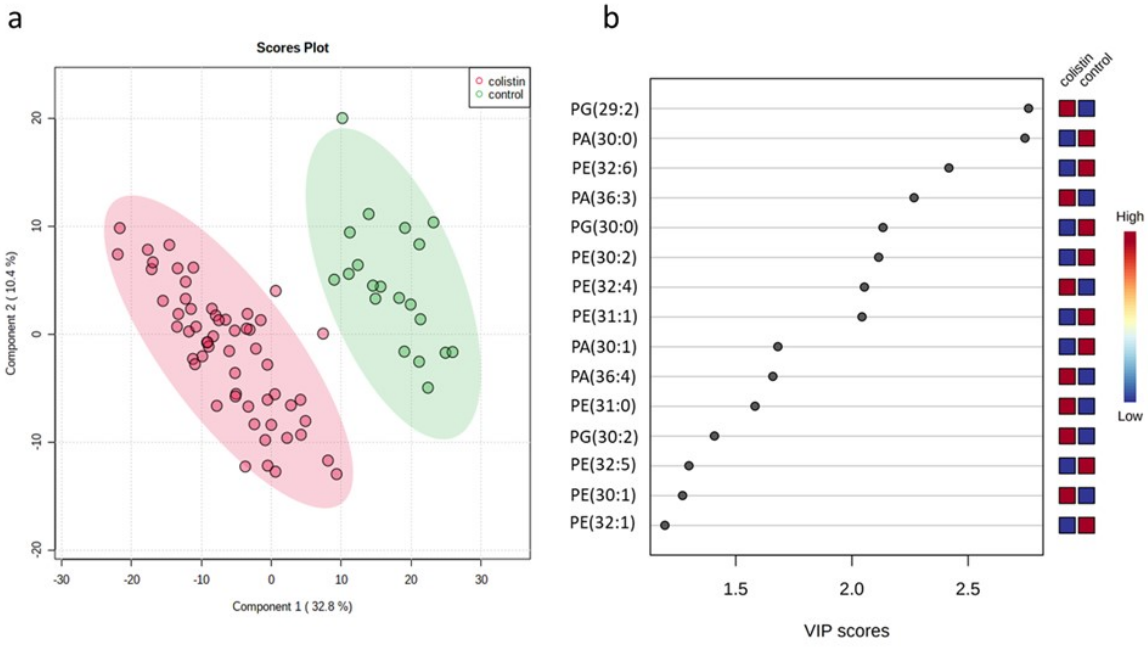

Figure 3.6: Partial least squares-discriminant analysis(PLS-DA). PLS-DA score plot for comparison of E.coli without treatment of colistin and E.coli with treatment of 0.1μg/ml colistin shows the separation achieved according to the lipid profile. Colored circles represent 95% confidence intervals. Colored dots represent individual samples: 32.8% and 10.4% are the scores of component 1 and component 2, respectively, in the PLS-DA analysis. b. Important features identified by PLS-DA. The colored boxes on the right indicate the relative intensity of the corresponding lipid in each group under study. VIP (variable importance in projection) score is a weighted sum of squares of PLS-DA loadings taking into account the amount of explained y-variation in each dimension.

platform we have built, we can also detect the different types of lipids, including 28 PEs, 26 PCs, 11 PAs, 3 PSs based on the MALDI-TOF-MS in the intact E.coli. On the other hand, it is known that the main target for colistin is lipid A of the LPS in Gram-negative bacteria, leading to disruption of the bacterial membrane and resulting in cellular death. However, its ultimate mechanism of action is still unclear. Our results indicate that the lipid expression of E.coli was significantly perturbed by colistin and can be distinguished from those without exposure based on the lipid profiling. The lipidomic analysis would help rationalize the mechanism behind the colistin-mediated antimicrobial effect. PG (29:2) and PA (30:0), the two most critical features of PLS-DA, may serve as potential biomarkers for gram-negative bacterial response to colistin. Since the lipid components and content are various in different bacteria strains, our Gold-μChip lipid analysis platform can be expected to extend to classify and identify different species of bacteria.

References

[1] Cosima Damiana Calvano, Francesca Italiano, Lucia Catucci, Angela Agostiano, Tommaso RI Cataldi, Francesco Palmisano, and Massimo Trotta. The lipidome of the photosynthetic bacterium rhodobacter sphaeroides r26 is affected by cobalt and chromate ions stress. *Biometals*, 27(1):65–73, 2014.

[2] Suresh Kumar Kailasa and Hui-Fen Wu. Surface modified batio3 nanoparticles as the matrix for phospholipids and as extracting probes for llme of hydrophobic proteins in escherichia coli by maldi–ms. *Talanta*, 114:283–290, 2013.

[3] David Gode and Dietrich A Volmer. Lipid imaging by mass spectrometry–a review. *Analyst*, 138(5):1289–1315, 2013.

[4] Melvin Blaze MT, Artem Akhmetov, Berdan Aydin, Praneeth D Edirisinghe, Gulsah Uygur, and Luke Hanley. Quantification of antibiotic in biofilm-inhibiting multilayers by 7.87 ev laser desorption postionization ms imaging. *Analytical chemistry*, 84(21):9410–9415, 2012.

[5] Gerald L Gasper, Lynelle K Takahashi, Jia Zhou, Musahid Ahmed, Jerry F Moore, and Luke Hanley. Laser desorption postionization mass spectrometry of antibiotic-treated bacterial biofilms using tunable vacuum ultraviolet radiation. *Analytical chemistry*, 82(17):7472–7478, 2010.

[6] Walter Florio, Lelio Baldeschi, Cosmeri Rizzato, Arianna Tavanti, Emilia Ghelardi, and Antonella Lupetti. Detection of antibiotic-resistance by maldi-tof mass spectrometry: An expanding area. *Frontiers in cellular and infection microbiology*, 10:572909, 2020.

[7] Emilie Layre and D Branch Moody. Lipidomic profiling of model organisms and the world's major pathogens. *Biochimie*, 95(1):109–115, 2013.

[8] Jurgen Schiller, Rosmarie Suss, Beate Fuchs, Matthias Muller, Olaf Zschornig, and Klaus Arnold. Maldi-tof ms in lipidomics. *Frontiers in Bioscience-Landmark*, 12(7):2568–2579, 2007.

[9] Najla AlMasoud, Yun Xu, Nicoletta Nicolaou, and Royston Goodacre. Optimization of matrix assisted desorption/ionization time of flight mass spectrometry (maldi-tof-ms) for the characterization of bacillus and brevibacillus species. *Analytica Chimica Acta*, 840:49–57, 2014.

[10] Maria-Theresia Gekenidis, Patrick Studer, Simone Wüthrich, René Brunisholz, and David Drissner. Beyond the matrix-assisted laser desorption ionization (maldi) biotyping workflow: in search of microorganism-specific tryptic peptides enabling discrimination of subspecies. *Applied and environmental microbiology*, 80(14):4234–4241, 2014.

[11] Tanis C Dingle and Susan M Butler-Wu. Maldi-tof mass spectrometry for microorganism identification. *Clinics in laboratory medicine*, 33(3):589–609, 2013.

[12] Keerthi Appala, Kingsley Bimpeh, Christian Freeman, and Kelly M Hines. Recent applications of mass spectrometry in bacterial lipidomics. *Analytical and Bioanalytical Chemistry*, 412(24):5935–5943, 2020.

[13] Christian Sohlenkamp and Otto Geiger. Bacterial membrane lipids: diversity in structures and pathways. *FEMS microbiology reviews*, 40(1):133–159, 2016.

[14] Elizabeth Drolle, Alexander Negoda, Keely Hammond, Evgeny Pavlov, and Zoya Leonenko. Changes in lipid membranes may trigger amyloid toxicity in alzheimer's disease. *PloS one*, 12(8):e0182194, 2017.

[15] Noemí Fabelo, Virginia Martín, Raquel Marín, Dolores Moreno, Isidre Ferrer, and Mario Díaz. Altered lipid composition in cortical lipid rafts occurs at early stages of sporadic alzheimer's disease and facilitates app/bace1 interactions. *Neurobiology of aging*, 35(8):1801–1812, 2014.

[16] Celine Fernandez, Marianne Sandin, Julio L Sampaio, Peter Almgren, Krzysztof Narkiewicz, Michal Hoffmann, Thomas Hedner, Björn Wahlstrand, Kai Simons, Andrej Shevchenko, et al. Plasma lipid composition and risk of developing cardiovascular disease. *PloS one*, 8(8):e71846, 2013.

[17] Ashutosh Singh, Vipin Yadav, and Rajendra Prasad. Comparative lipidomics in clinical isolates of candida albicans reveal crosstalk between mitochondria, cell wall integrity and azole resistance. *PloS one*, 7(6):e39812, 2012.

[18] Bénédicte Michel. After 30 years of study, the bacterial sos response still surprises us. *PLoS biology*, 3(7):e255, 2005.

[19] Ryan T Cirz, Jodie K Chin, David R Andes, Valérie de Crécy-Lagard, William A Craig, and Floyd E Romesberg. Inhibition of mutation and combating the evolution of antibiotic resistance. *PLoS biology*, 3(6):e176, 2005.

[20] Yong-Mei Zhang and Charles O Rock. Membrane lipid homeostasis in bacteria. *Nature Reviews Microbiology*, 6(3):222–233, 2008.

[21] Ying-Ying Chang and John E Cronan. Membrane cyclopropane fatty acid content is a major factor in acid resistance of escherichia coli. *Molecular microbiology*, 33(2):249–259, 1999.

[22] Jian Li, Roger L Nation, Robert W Milne, John D Turnidge, and Kingsley Coulthard. Evaluation of colistin as an agent against multi-resistant gram-negative bacteria. *International journal of antimicrobial agents*, 25(1):11–25, 2005.

[23] Rupali Jain and Larry H Danziger. Multidrug-resistant acinetobacter infections: an emerging challenge to clinicians. *Annals of Pharmacotherapy*, 38(9):1449–1459, 2004.

[24] DM Livermore. The need for new antibiotics. *Clinical microbiology and infection*, 10:1–9, 2004.

[25] Matthew E Falagas, Sofia K Kasiakou, and Louis D Saravolatz. Colistin: the revival of polymyxins for the management of multidrug-resistant gram-negative bacterial infections. *Clinical infectious diseases*, 40(9):1333–1341, 2005.

[26] Laurent Poirel, Aurélie Jayol, and Patrice Nordmann. Polymyxins: antibacterial activity, susceptibility testing, and resistance mechanisms encoded by plasmids or chromosomes. *Clinical microbiology reviews*, 30(2):557–596, 2017.

[27] Silpak Biswas, Jean-Michel Brunel, Jean-Christophe Dubus, Martine Reynaud-Gaubert, and Jean-Marc Rolain. Colistin: an update on the antibiotic of the 21st century. *Expert review of anti-infective therapy*, 10(8):917–934, 2012.

[28] Roger L Nation, Tony Velkov, and Jian Li. Colistin and polymyxin b: peas in a pod, or chalk and cheese? *Clinical infectious diseases*, 59(1):88–94, 2014.

[29] Abdennour Abbas, Matthew J Linman, and Quan Cheng. Patterned resonance plasmonic microarrays for high-performance spr imaging. *Analytical chemistry*, 83(8):3147–3152, 2011.

[30] Kara Schmelzer, Eoin Fahy, Shankar Subramaniam, and Edward A Dennis. The lipid maps initiative in lipidomics. *Methods in enzymology*, 432:171–183, 2007.

[31] Fong-Fu Hsu and John Turk. Characterization of cardiolipin from escherichia coli by electrospray ionization with multiple stage quadrupole ion-trap mass spectrometric analysis of [m- 2h+ na]- ions. *Journal of the American Society for Mass Spectrometry*, 17(3):420–429, 2006.

[32] Eugenia Mileykovskaya, Andrea C Ryan, Xi Mo, Chun-Chieh Lin, Khaled I Khalaf, William Dowhan, and Teresa A Garrett. Phosphatidic acid and n-acylphosphatidylethanolamine form membrane domains in escherichia coli mutant lacking cardiolipin and phosphatidylglycerol. *Journal of Biological Chemistry*, 284(5):2990–3000, 2009.

[33] Cosima D Calvano, Carlo G Zambonin, and Francesco Palmisano. Lipid fingerprinting of gram-positive lactobacilli by intact cells–matrix-assisted laser desorption/ionization mass spectrometry using a proton sponge based matrix. *Rapid Communications in Mass Spectrometry*, 25(12):1757–1764, 2011.

[34] CD Calvano, A Monopoli, N Ditaranto, and F Palmisano. 1, 8-bis (dimethylamino) naphthalene/9-aminoacridine: a new binary matrix for lipid fingerprinting of intact bacteria by matrix assisted laser desorption ionization mass spectrometry. *Analytica Chimica Acta*, 798:56–63, 2013.

[35] CD Calvano, RA Picca, E Bonerba, G Tantillo, N Cioffi, and F Palmisano. Maldi-tof mass spectrometry analysis of proteins and lipids in escherichia coli exposed to copper ions and nanoparticles. *Journal of Mass Spectrometry*, 51(9):828–840, 2016.

[36] Michael J Satlin, James S Lewis, Melvin P Weinstein, Jean Patel, Romney M Humphries, Gunnar Kahlmeter, Christian G Giske, and John Turnidge. Clinical and laboratory standards institute and european committee on antimicrobial susceptibility testing position statements on polymyxin b and colistin clinical breakpoints. *Clinical Infectious Diseases*, 71(9):e523–e529, 2020.

[37] Anne DeChavigny, Philip N Heacock, and W Dowhan. Sequence and inactivation of the pss gene of escherichia coli. phosphatidylethanolamine may not be essential for cell viability. *Journal of Biological Chemistry*, 266(8):5323–5332, 1991.

[38] Roman Moser, Meriyem Aktas, Christiane Fritz, and Franz Narberhaus. Discovery of a bifunctional cardiolipin/phosphatidylethanolamine synthase in bacteria. *Molecular microbiology*, 92(5):959–972, 2014.

[39] Phosphatidylethanolamine and related lipids. https://web.archive.org/web/20120821202641/.

[40] Bénédicte Gbaguidi, Pierre Hakizimana, Guy Vandenbussche, and J-M Ruysschaert. Conformational changes in a bacterial multidrug transporter are phosphatidylethanolamine-dependent. *Cellular and molecular life sciences*, 64(12):1571–1582, 2007.

[41] Phosphatidylglycerol and related lipids. https://lipidmaps.org/resources/lipidweb/.

[42] Chijun Li, Brandon K Tan, Jinshi Zhao, and Ziqiang Guan. In vivo and in vitro synthesis of phosphatidylglycerol by an escherichia coli cardiolipin synthase. *Journal of Biological Chemistry*, 291(48):25144–25153, 2016.

[43] Xuemin Wang, Shivakumar Pattada Devaiah, Wenhua Zhang, and Ruth Welti. Signaling functions of phosphatidic acid. *Progress in lipid research*, 45(3):250–278, 2006.

[44] Carol V Robinson, Tibor Rohacs, and Scott B Hansen. Tools for understanding nanoscale lipid regulation of ion channels. *Trends in biochemical sciences*, 44(9):795–806, 2019.

[45] Karin Athenstaedt and Günther Daum. Phosphatidic acid, a key intermediate in lipid metabolism. *European Journal of Biochemistry*, 266(1):1–16, 1999.

[46] Albert L Lehninger. *Lehninger Principles of Biochemistry: David L. Nelson, Michael M. Cox*. Recording for the Blind & Dyslexic New York, 2004.

[47] Annemieke van Dalen and Ben de Kruijff. The role of lipids in membrane insertion and translocation of bacterial proteins. *Biochimica et Biophysica Acta (BBA)-Molecular Cell Research*, 1694(1-3):97–109, 2004.

[48] Kiley Dare, Jennifer Shepherd, Hervé Roy, Stephanie Seveau, and Michael Ibba. Lyspgs formation in listeria monocytogenes has broad roles in maintaining membrane integrity beyond antimicrobial peptide resistance. *Virulence*, 5(4):534–546, 2014.

Chapter 4

Discrimination of Bacteria by MALDI-MS at Single-Cell Level based on Photosensitizer Facilitated Metabolites Profiling on Gold Microchip

4.1 Introduction

Biotyping by means of mass spectrometry (MS) has shown to be very advantageous in several areas, including the food industry and clinical laboratories, overtaking conventional microbiological techniques such as microscopy-based analysis and biochemical tests.[1] Previously, microbial identification and characterization were widely achieved by physiological and biochemical tests, such as morphology assessment and analytical profile index,[2] immune-assay such as enzyme-linked immunosorbent assay,[3] and genetic analysis (DNA sequencing) using polymerase chain reaction[4] and pulsed-field gel electrophoresis.[5] However, most of these laboratory techniques tend to be time-consuming, labor, and cost-intensive, and reduce microbial identification and characterization accuracy. [6]

Advances in technology and the development of specialized facilities have driven innovation, promoting a shift in techniques for identifying and characterizing microorganisms in food. Metabolomics has proven to be a powerful tool in analyzing the chemical diversity of biological systems, and its direct correlation with phenotypes allows for a more sensitive response to subtle differences between species. It provides a holistic method for identifying and comprehensively profiling metabolites that may be present in a system at a specific time.[7][8][9] Different metabolic classes, including sugars, nucleotides, amino acids, and lipids, are associated with the presence and population of pathogenic bacteria. This technique has been established as a viable method for detecting pathogenic bacteria metabolites, including particular biomarkers that might be used to construct quick identification techniques.[10]

Mass spectrometry is often used for metabolomic analysis due to its good sensitivity and capacity to detect and quantify a large diversity of molecules in complex biological samples.[11][12] It is often combined with other high-resolution separation techniques such as LC-MS and GC-MS, but these approaches usually require substantial analytical run times due to complex sample preparation, extraction and typical combination with chromatographic separations.[13] Compared with the traditional method, MALDI-MS offers a rapid turnaround time and relatively simple sample preparation and is a soft ionization technique for accurate measurement of molecules with little or no fragmentation[14][15] This is particularly beneficial for detecting large biomolecules that may be easily destroyed during heating and fragmentation, such as lipids, peptides, and sugars, which are prominent metabolites of bacteria. A critical application of MS-based metabolomics is biotying, which is currently used to identify microbial from cultured microorganisms in clinics. This is achieved by MS1 profiling of ribosomal proteins of bacterial colonies (2,000-15,000 m/z) using MALDI-MS, then the results are searched in a library of MS patterns.[16][17] This biotyping strategy has been applied to environmental microorganisms by data collection in the lower m/z region (m/z 200-2000), where the metabolites are detected. This mass range shows many specialized metabolites or peptides that enable the typing of individual strains.[18][19] Then, multivariate data analysis techniques, such as principal component analysis (PCA)[20][21] and partial least square-discriminant analysis (PLS-DA)[22][23] are utilized for statistical analysis of processed data in order to identify their trends, similarities, and differences in to arrive at a reliable data interpretation.

The MALDI-MS spectrum of a bacterial species gives a unique fingerprint, which makes it possible to reliably identify bacteria at the genus and species levels.[24][25] Some researchers have advocated 6×10^3 CFU/spot as the limit of detection,[26] but in practice, 1×10^5 CFU/spot is typically regarded as the limit.[27][28] However, the bacterial load that potentially occurs in a sample is routinely amplified by culture, which is a time-consuming process that takes up multiple hours and in some cases even several days. Considering the complexity of metabolites and the fact that they sometimes occur in trace concentrations. There are significant challenges in the form of small cell sizes and volumes, and ultrarace metabolite amounts per cell for the detection and quantification. Due to the ultrasmall sample volume, the low abundance of specific metabolites, and the poor ionization efficiencies, metabolite detection, identification, and accurate quantification continue to be formidable obstacles.

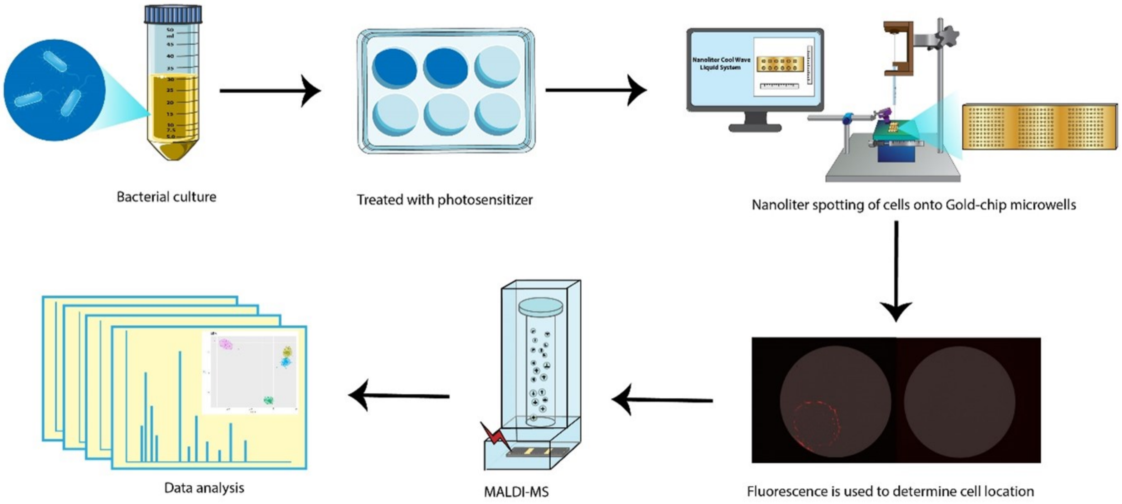

Figure 4.1: Workflow of bacterial metabolite profiling analysis based on MALDI-MS at single cell level

In this study, we show that identification and discrimination of intact different pathogenic bacteria can be achieved at a single cell level combined with our high throughput metal fluorescence enhanced gold-microchip and machine learning algorithms(Figure 4.1). Furthermore, cells can be localized in the wells through their fluorescence, which improves data acquisition effectiveness and simplifies data processing by avoiding unnecessary data collection (Figure 4.2). It is not possible for traditional stainless steel MALDI plates and is particularly useful for studying samples at the single cell level. Moreover, as far as we know, this is the first time that photosensitizer (PS) and MS-based metabolites profiling were combined for intact bacterial discrimination at a single-cell level. Methyl blue (MB) is a cationic phenothiazinium dye and an effective photosensitizer with strong fluorence, an emission peak at 686 nm, and the capacity to absorb light to produce singlet oxygen.[29][30] A series of photo-oxidation/peroxidation reactions induced by singlet oxygen can cause damage to lipid membranes through the breaking of lipid chains and then result in changes in the structural characteristics of the lipids.[31][32][33] We use methyl blue as a fluorescence marker and photosensitizer for facilitated data acquisition and discrimination. We have recently demonstrated a lipidomic study of E.coli under the impact of antibiotics based on our gold-microchip platform. In this work, we further apply this platform to analyze more different bacterial species. Our study demonstrates that a restricted number of bacterial species may be distinguished using single-cell MALDI-MS and machine learning methods based on our bacterial analysis platform.

4.2 Experimental Section

4.2.1 Materials

Super 2,5 - dihydroxybenzoic acid (sDHB), acetonitrile (ACN), LB Broth (Miller) medium, and Methylene blue (CAS 122965-43-9) were purchased from Sigma-Aldrich. BK7

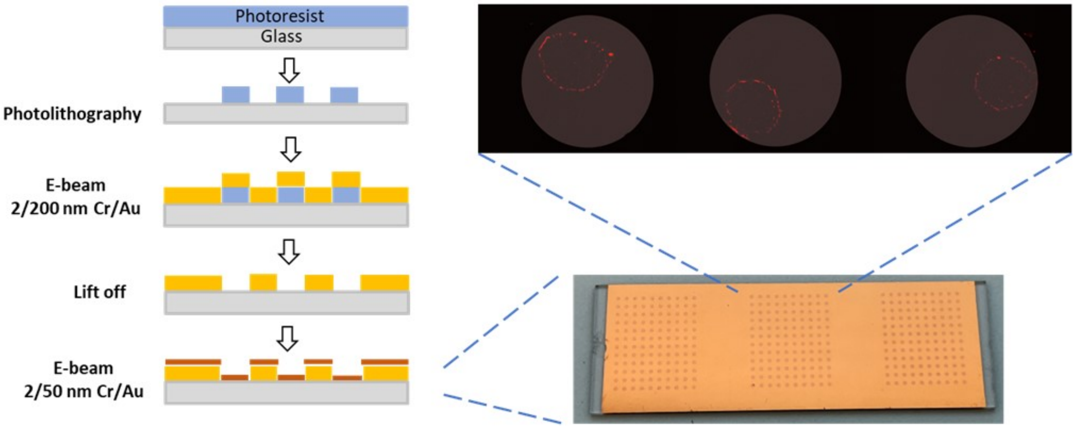

Figure 4.2: Scheme of gold microchip platform for bacterial analysis at single cell level

glass microscope slides came from Fisher Scientific. High-purity water (>18 MΩ cm–1) was obtained from a Barnstead E-Pure water purification system. Matrix solutions (sDHB) were prepared in acetonitrile and water (2:1,v/v) at a concentration of 10 mg/ml. LI-250 radiometer (Li-Cor Inc., Lincoln, NE, USA), lightbox

4.2.2 Fabrication of Gold μchip

The gold microchips array was fabricated in the Cleanroom Facility at UCR.[34] Briefly, gold microchips were fabricated by a photo-lithographic method. The photoresist was spun-coated onto glass slides and baked at 110 °C. A mask aligner and UV light patterned the array into the photoresist. After another baking step, the µchips were cured using UV-light and developed with a developing solution. Next, e-beam deposition was used to deposit 2/200 nm of Cr/Au onto the arrays. Acetone was then used to remove the photoresist, followed by deposition of 2/50 nm of Cr/Au onto the surface to produce a pristine 50 nm gold well array.

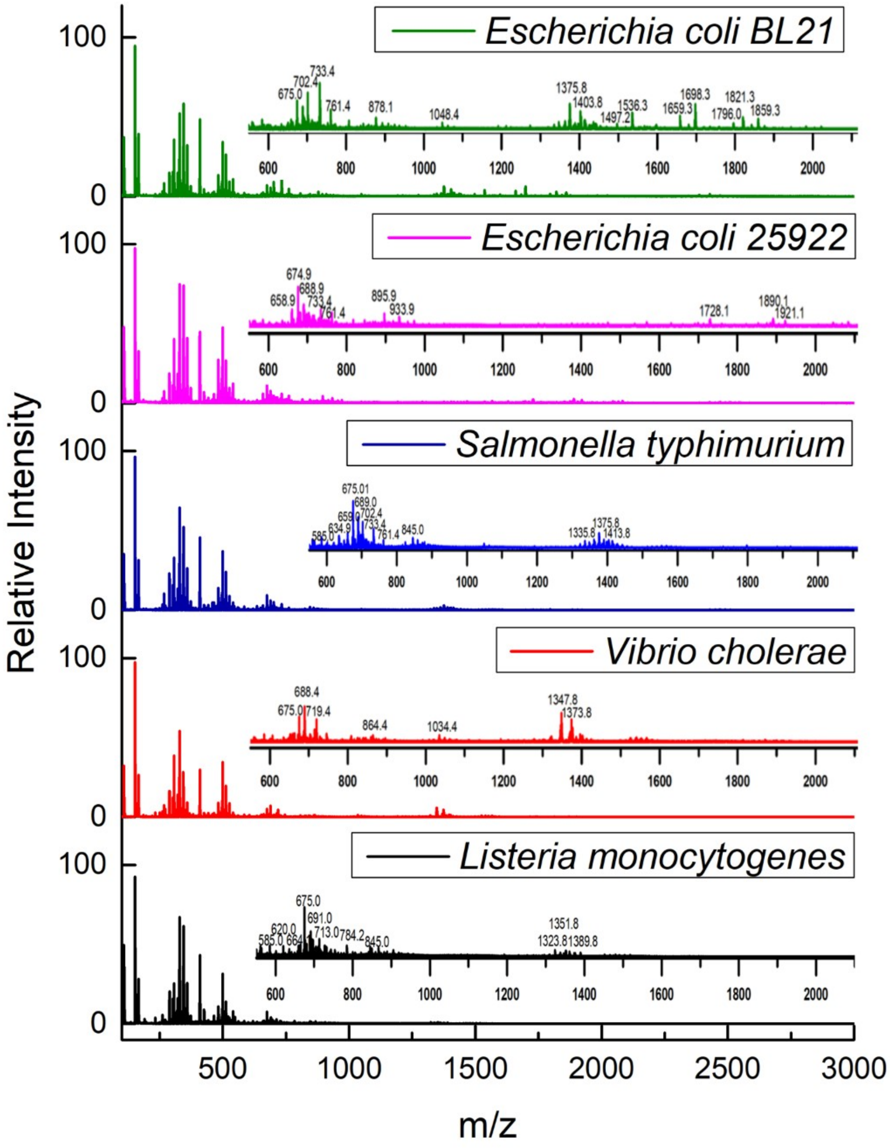

Figure 4.3: MALDI-TOF mass spectra of the metabolites profiling from different bacterial species in negative mode.

4.2.3 Bacterial Strains and Culture Condition

Escherichia coli (E.coli) ATCC 25922 and *Escherichia coli* (E.coli) BL 21, *Listeria monocytogenes* ATCC 19115, *Salmonella Typhimurium* ATCC 14028, and *Vibrio cholerae* ATCC 39315 were purchased from American Type Culture Collection (ATCC, United Stated). All culture media were prepared according to manufacturer instructions, including autoclaving at 121 °C for 30 min to ensure sterility. First-generation bacterial strains were received in the vial as freeze-dried strains and revived according to recommended growth conditions from ATCC. For experimental purposes, all bacterial strains were grown overnight in LB Broth (Miller) growth medium in a 37°C shaker at 220 rpms to the early stationary phase. The turbidity of bacterial suspension was used to determine the cell density in an Agilent spectrophotometer (Cary 60 UV-Vis). The optical density (OD) value was obtained at 600 nm. The bacteria were harvested by centrifugation at 8000 rpm for 10 min and washed with deionized water three times. Finally, the harvested bacteria were resuspended to the particular concentrations in deionized water and used for MALDI-MS acquisition. The same concentration of *E.coli* and *L.monocytogenes* was mixed to make the mixture sample.

4.2.4 Photosensitizer Treatment

Bacteria harvest was suspended(1×10^8) by methylene blue solution with a concentration of 20 μM. The sample was incubated in the dark for 1h under shaking in order to promote the photosensitizer binding to the cells. 1 ml sample solution was added to each well of the 6-well plates, underwent a 90 min period of irradiation (106 Mw/cm2) and stirred every 15 minutes. After illumination by white light, the sample was washed with deionized water 3 times. 1 μL of sample solution was deposited on the MALDI plate covered with 1 μL of sDHB matrix. After drying, the bacteria sample was detected with the MALDI-TOF MS.

4.2.5 Imaging Bacteria on Gold Microchip

The collected bacterial cells were resuspended to particular concentrations and spotted on the wells of the gold microchip quickly and precisely with nanovolume (100 nL) through an electrodeposition instrument (Nanoliter Cool Wave Liquid Systems). Bright-field images and red fluorescence images of cells were obtained using an all-in-one inverted Keyence BZ-X700 series microscope equipped with a camera unit and a Cy5 filter cube. Individual images were assembled into their respective locations on the array by FIJI software.

4.2.6 MALDI-TOF-MS Acquisition

MS experiments were conducted using an AB-Sciex 5800 time-of-flight mass spectrometer equipped with a nitrogen UV laser (337nm wavelength). Diverse bacterial strains, including gram-positive and gram-negative strains, were analyzed using MALDI-TOF-MS. 1μl of the sample per well was added to the gold micro-chip, covered with 1μl of sDHB matrix using a nanoelectronic deposition for data acquisition at single cell level. For bulk measurement as a comparison, the bacteria sample was deposited by hand pipetting. Lipid profiles of bacteria were acquired with a laser fluence of 5900 a.u. on the reflectron detector in negative mode.

4.2.7 Data Analysis

TOF/TOF Series Explorer software version 4.1.0 (AB Sciex) was used to acquire MALDI-MS. MetaboAnalyst 5.0 was used for statistical analysis. For multivariate analysis, partial least squares discriminant analysis (PLS-DA), as a supervised method, was used to find important variables with discriminative power. Linear Discriminant Function Analysis (LDA) was performed as a multivariate test for the determination of categorical variables (different m/z values) to separate different bacteria samples.

4.3 Results and Discussion

Five bacterial species were analyzed using MALDI-TOF-MS, including *E.coli* 25922, *E.coli* BL21, *L.monocytogenes* ATCC 19115, *S.Typhimurium* ATCC 14028, and *V. cholerae* ATCC 39315. Each bacteria strain was analyzed from bulk measurement ($\approx$ 1x10^9) to single cell level (1000 CFU/spot). Typical mass spectra from the analyte ($\approx$ 1x10^9) are shown in Figure 4.3). Visual examination of these spectra reveals that each species has a distinct metabolites profiling in the m/z region 400–2000. The cell-wall molecules ionized in this range will be a mixture of small peptides, teichoic acids, oligosaccharides, and lipids. However, the exact identity of individual m/z values is not known. Despite this, we focus more on the changes in the profile pattern, and the fingerprint patterns generated are reproducible. Moreover, several peaks observed in this area are shared by multiple bacterial species, albeit in varying relative abundances. In order to further test the sensitivity of our bacteria analysis platform, we collected the spectra from a mixture sample of *E.coli* and *L.monocytogenes*. As shown in Figure 4.4a. the spectra on the upper layer are merged from *E.coli* (green) and *L.monocytogenes* (orange), respectively, while the spectra on the lower layer are collected from the mixture sample of *E.coli* and *L.monocytogenes* (red). The results show that the spectra from the mixture sample contain the feature peaks from both *E.coli* and *L.monocytogenes* as labeled in Figure 4.4a with different m/z ranges (600-1100 m/z and 1200-2500 m/z). This result demonstrates that our bacteria analysis platform is sensitive enough to detect more complex samples.

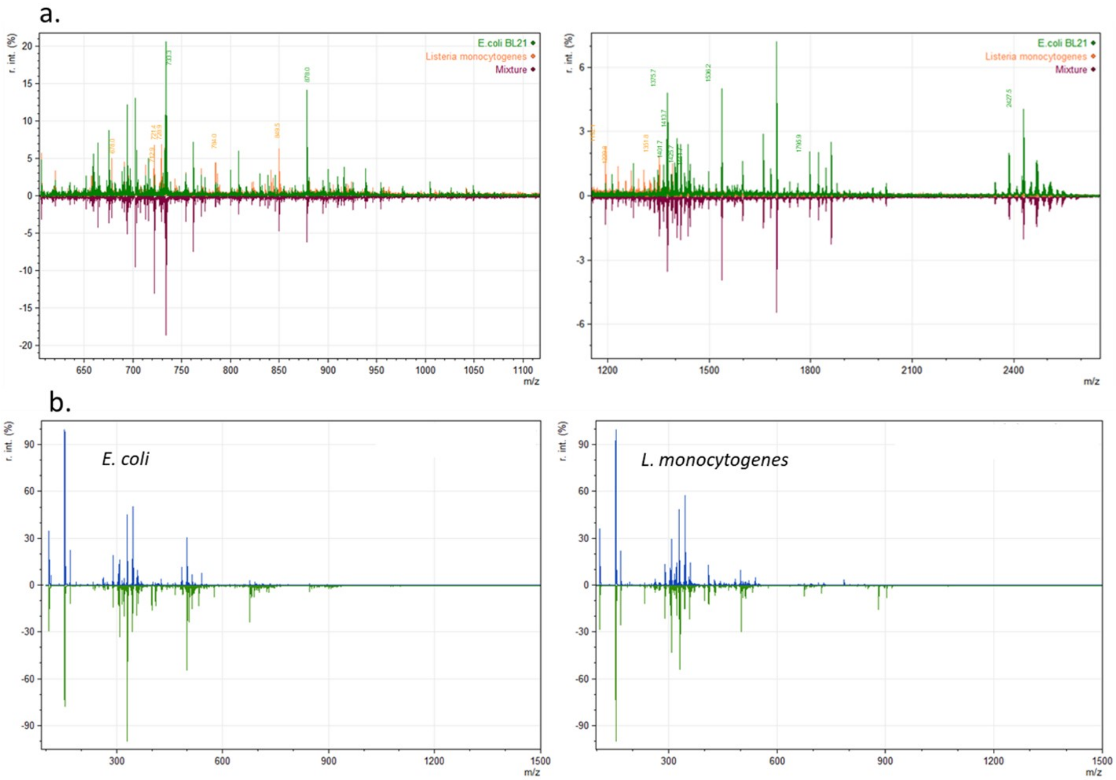

Figure 4.4: Comparison of summed mass spectral data for a. single bacteria species and mixture samples of E.coli and L. monocytogenes in different m/z ranges. Labled peaks with different colors are the unique peaks that only present in the single bacctera species respectively. E.coli in green and L. monocytogenes in orange b. E.coli and L. monocytogenes treated with (green) and without (blue) light excited photosensitizer

Conventionally, the analysis of MALDI-TOF mass spectra depends on a small number of empirically associated characteristics, such as peak height and area under the peak, to identify microbial species. While this is a viable method that works well at the species level, there is plenty of unexplored information in these spectra. To fully leverage the information contained in MALDI-TOF mass spectra, researchers have implemented machine learning methods to enhance species identification.[35][36][37] Machine learning algorisms are able to recognize statistical relationships in data, taking into account nonlinear and interaction effects between characteristics. Consequently, machine learning approaches can unearth unique or undiscovered information hidden within MALDI-TOF mass spectra. This data has been valuable for identifying and distinguishing species, particularly those that are phylogenetically close and sublineages of species.[38][39][40] In this study, Linear Discrimination Function Analysis (LDA) was performed as a multivariate test for the determination of categorical variables (different m/z values) to separate pure *E.coli*, pure *L.monocytogenes*, and the mixture of *E.coli* and *L.monocytogenes* (Figure 4.5). The result shows that the cluster of the mixture sample was well separated from the cluster of *E.coli* as well as the cluster of *L.monocytogenes* Furthermore, the cluster of mixture sample is closer to the cluster of *E.coli* than the cluster of *L.monocytogenes*, because it contains more feature peaks from *E.coli* than *L.monocytogenes*, which can be observed in Figure 4.4a. In addition, to further evaluate the possibility of metabolite profiling for bacterial discrimination, we choose two bacteria strains as blind samples for testing. As shown in Figure 4.5, the cluster of Blind sample (S) from *S.Typhimurium* was not grouped with any of the other clusters, while the cluster of the blind sample (S) from *L.monocytogenes* was grouped with the other cluster of *L.monocytogenes*. It indicated that MS-based metabolite profiling might be useful in predicting or identifying bacterial strains according to a reliable database containing MS-based metabolite profiling without identifying biomarkers in each species.

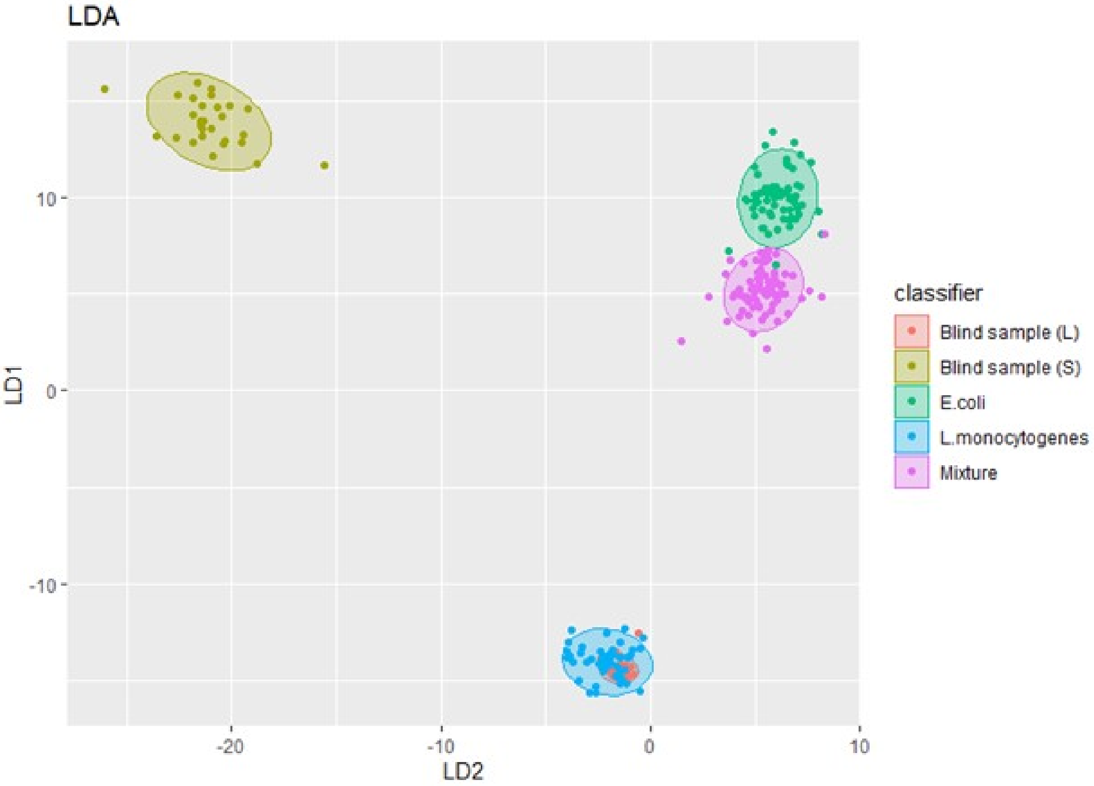

Figure 4.5: Linear discrimination analysis (LDA) for classification of metabolites profiling of different bacteria strains. The x-axis represents the liner discrimination component 2, and the y-axis represents the liner discrimination component 1 differences within the group. Each dot represents a spectrum collected from 3 times experimental replication, and each bacteria group is differently colored (red – Blind sample (L), yellow – Blind sample (S), green – *E.coli* , blue – *L.monocytogenes*, and purple – mixture)

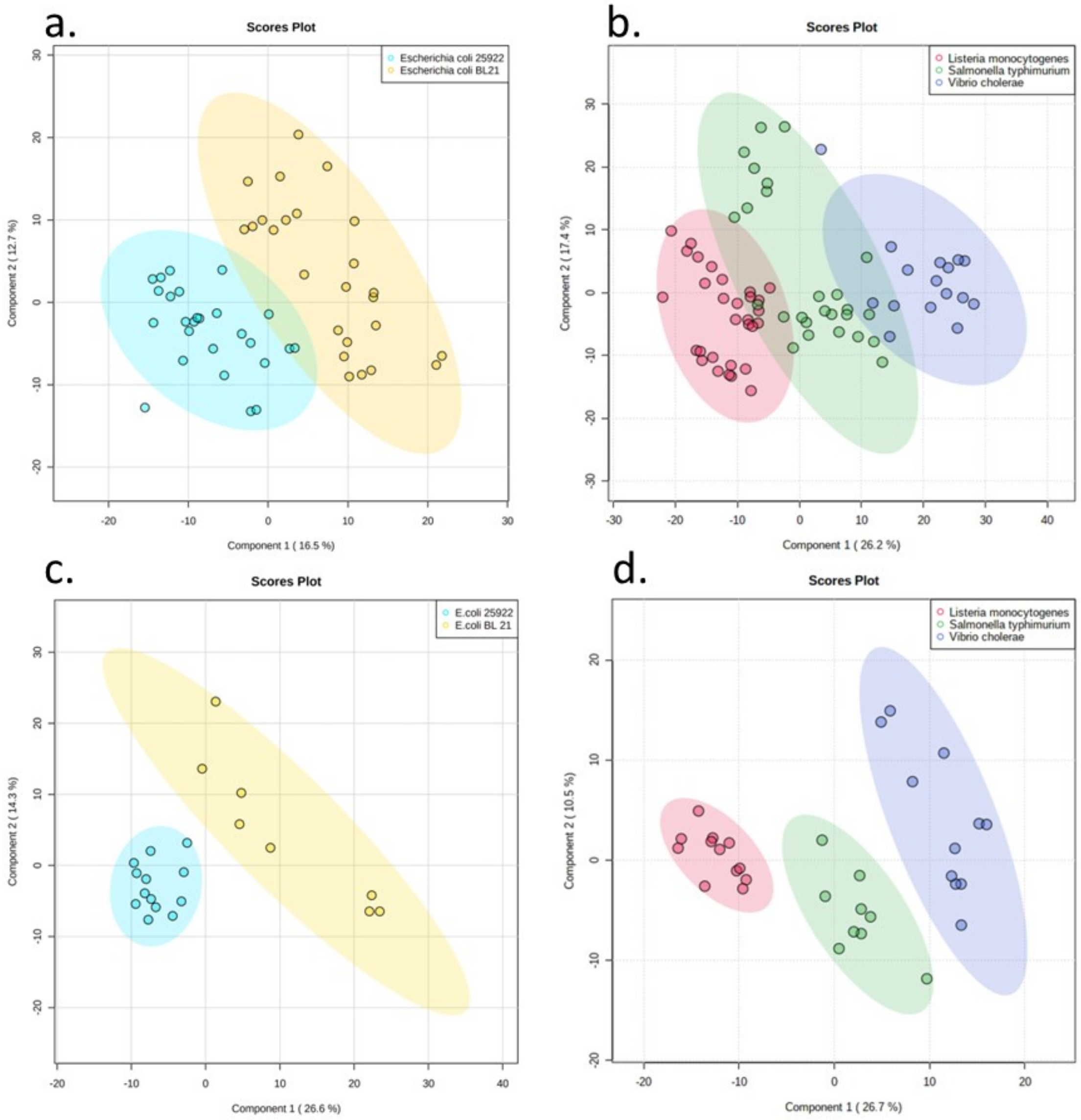

Figure 4.6: PLS-DA plots of a. *E. coli* 25922 and *E. coli* BL21 treated without light excited photosensitizer b. *L. monocytogenes*, *S. typhimurium* and *V. cholerae* treated without light excited photosensitizer c. *E. coli* 25922 and *E. coli* BL21 treated with light excited photosensitizer d. *L. monocytogenes*, *S. typhimurium* and *V. cholerae* treated with light excited photosensitizer.

This study aims to assess the capabilities of our platform for bacterial classification at the single-cell level. Taking into account the challenges involved in extracting the data from the sample because of the restricted number of bacterial cells present in each well. We employed methylene blue as fluorescence dye[29] with an emission peak at 686 nm ($\lambda_e x$ 665 nm) to facilitate the unambiguous location of bacterial cells within wells according to the fluorescence images as shown in Figure 4.2. Our microarray plate with thin gold film has been reported to show a considerably enhanced fluorescence signal due to nonradiative energy transfer and surface plasmon-coupled emission in our previous work.[41] It makes the spatial identification of single cells in wells easier and works as a solution to the widespread issue of signal loss in MALDI that is caused by off-target ionization. This step also eliminated unwanted data acquisitions from wells that did not contain cells for analysis. On the other hand, methylene blue is a cationic photosensitizer[42]. The PS is promoted from the ground state to the excited state upon irradiation at a certain wavelength and then interacts with the substrate by two distinct routes, types I and II.[43] Type I reaction includes electron transfer from triplet state PS to an organic substrate, producing free radicals. These free radicals interact with oxygen at the molecular level, producing reactive oxygen species (ROS) such as superoxide, hydroxyl radicals, and hydrogen peroxide. In Type II reactions, an energy transfer occurs between the excited PS and the ground-state molecular oxygen, resulting in the production of singlet oxygen that may interact with a vast number of molecules in the cell to form oxidized products. It has been reported that MB can bind to bacteria both by type I and type II mechanisms, and consequently, both MB radicals and singlet oxygen are formed.[44] In Figure 4.4b. , it shows the comparison of the averaged spectra that were collected from the samples, *E.coli* (gram-positive bacteria)and *L. monocytogenes* (gram-negative bacteria) as representatives, treated with and without light-excited photosensitizer. The changes in their MS profile can be observed especially in the range of 400-1000 m/z. This might be because in membrane bacteria systems, MB stimulates the generation of singlet oxygen and radical species, which are anticipated to react with double bonds and lipids of the bacteria walls, and due to its hydrophilic and lipophilic properties, MB is thought to bind strongly to the walls of the bacterium. Research has shown that bacteria exposed to ROS are thought to reorganize critical metabolic pathways, and these regulations mainly concern carbohydrate, glutathione, energy, lipid, peptides, and amino acid metabolisms. [45][46] In addition, we found that gram-positive bacteria are more sensitive to MB since more feature peaks and alterations in their MS profiles were observed after exposure to a light excited photosensitizer (Figure 4.4b), which is probably due to the higher resistance that the wall of gram-negative bacteria displays to reactive oxygen species (ROS) versus the gram-positive wall. [47]The teichoic acid residues of the gram-positive bacterial cell wall contribute to the negative charge and consequent binding sites for cationic molecules. Negatively charged LPS molecules in gram-negative bacterial outer cell membranes also have a strong affinity for cations; however, gram-negative bacteria are less susceptible to MB due to the membrane barrier that prevents the uptake of PS. Therefore, MB usually binds stronger to the walls of gram-positive bacteria than Gram-negative bacteria. [44] Based on the MS profiles of each bacterial species ($\approx 1 \times 10^9$ cells/ml) treated with and without a light excited photosensitizer. To better understand the effect of photosensitizer on different bacterial metabolites profiling, we combined machine learning algorism with MALDI-ms for bacterial discrimination. As is shown in the partial least squares-discriminant analysis (PLS-DA) plots (Figure 4.6.), there is a small overlap between the two E.coli subspecies (Figure 4.6a.) as well as in the different pathogen bacteria species (Figure 4.6b.) before the light excited photosensitizer treatment due to insufficient feature peaks presenting in their MS profiles. While as in indicated in Figure 4.6d., data points for each species form separate clusters, allowing species discrimination after the light-excited photosensitizer treatment. This treatment leads to the formation of reactive oxygen species (ROS), which are cytotoxic and capable of oxidizing many biological molecules such as enzymes, proteins, lipids and nucleic acids,[48]which induce more feature peaks in their MS profile and further facilitate the bacterial discrimination based on their metabolites profiling even for the subspecies bacteria strains (Figure 4.6c.)

Considering the results from bulk measurement, we further evaluate different concentrations to confirm the lowest one at which we are still able to detect enough numbers of feature peaks from each species for bacterial discrimination. Figure 4.7a shows the average spectra of E.coli samples with concentrations ranging from 100 to 100000 cells /well. The insets are the fluorescence images of the numbers of bacterial cells in the wells corresponding to each concentration. The spectra show that the signal from the matrix became more dominant, and the signal from bacterial samples decreased as the concentrations of the bacterial samples decreased, as labeled in a red box. Reducing the number of cells analyzed by MALDI-MS in successive dilutions reduces the number of peaks generated. There are some possible reasons why a lower cell density reduces the number of peaks. For densely packed cells, radicals from the initial laser ionization may be involved in interactions that lead to the secondary ionization of nearby molecules, which might have a role in boosting peaks. The concentration of molecules that such a secondary process may ionize is effectively reduced when cells are diluted. Consequently, ionization by this method is decreased in direct proportion to the cell packing density. Alternatively, lowering the number of cells may merely reduce the sampling frequency of the original population. In other words, increasing the number of cells evaluated in a single laser beam enhances the likelihood of discovering cells with more distinct ionizable moieties. A third option is that specific components, present in high concentrations and vast numbers of cells, dissipated or used a significant amount of laser energy. On dilution, the quantity of these components decreases, and a higher proportion of the laser energy is accessible to promote the ionization of entities, which subsequently fragment, resulting in a spectrum with reduced peak intensities.[49]

Even though it was still detectable in the bacterial sample with a concentration of 100 cells/well, the data was poorly reproducible from this concentration. Therefore, we selected a concentration of 1000 cells / well for the study. As cell numbers drop, it is reasonable that only a tiny fraction remains in the path of the laser. Therefore, despite the data collected from the sample of 1000 cells/well, it was considered to be at the single-cell level. Figure 4.7b shows the MS profiles from different bacterial species (1000 cells/well) treated with the light-excited photosensitizer. Due to the limited sample load, there were a limited number of potential peaks of metabolites that could be detected compared with the data from bulk measurements. However, the differences in their MS profiles are still visible. In spite of the discrimination of pathogen, bacteria were not as well as it from bulk

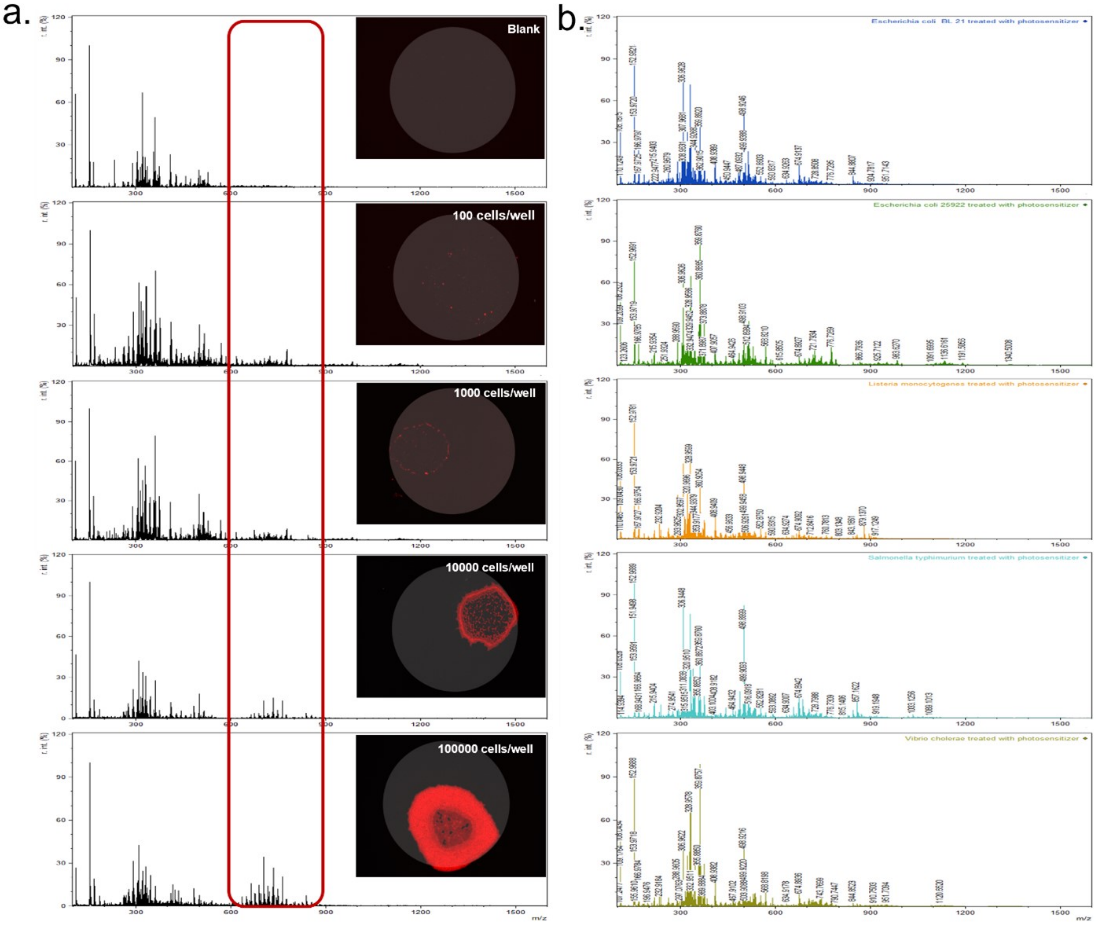

Figure 4.7: MALDI mass spectra of a. different concentrations of bacteria and corresponding images of different numbers of cells /well on a gold chip. b. different bacterial species treated with light-excited photosensitizer at single cell level.

measurements (Figure 4.8, Figure 4.6c and 4.6d) because the limited sample amount gives a reduced number of peaks, data points from different bacteria species as well as subspecies still can be grouped into different clusters (Figure 4.8).

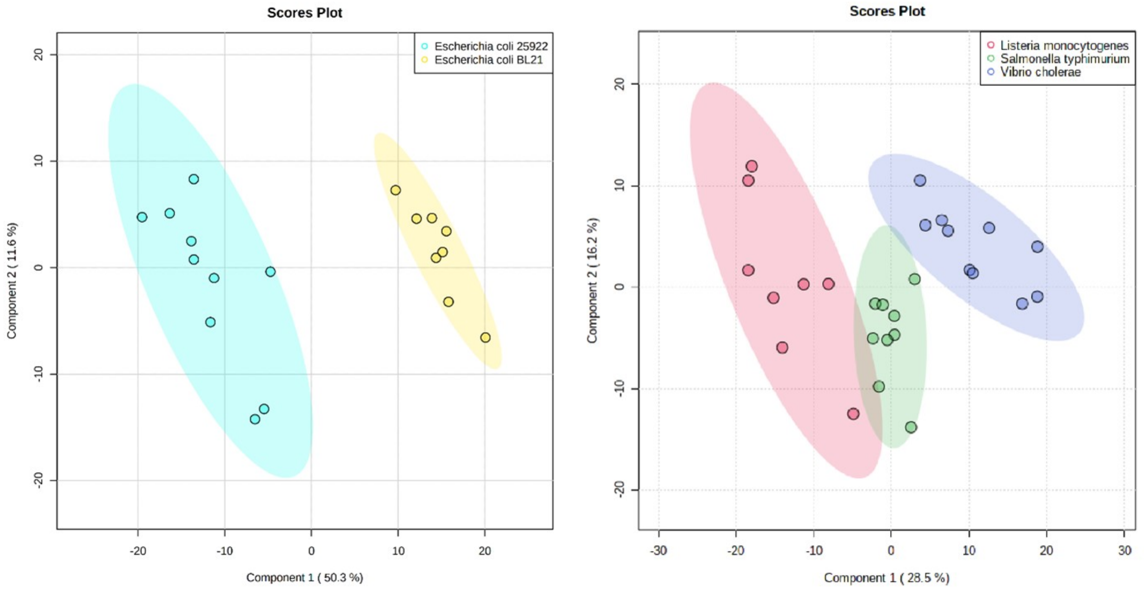

Figure 4.8: Plot of PLS-DA data points for the two principle components using MS profile data from different bacterial species at single cell level

4.4 Conclusion

For the first time, the use of MALDI-MS-based metabolites and cell localization to study how intact bacteria from food-borne pathogens can be told apart at the single-cell level is described. Using methylene blue as a photosensitizer and fluorescence marker for cell discrimination and positioning, we applied the high-throughput MALDI-MS technique to analyze metabolite profiling from whole bacteria, which are major food-borne pathogens with significant implications for food safety and human health. Each species produces a unique metabolite profile in the m/z range of 400–2000, allowing species discrimination without any peak identification from bulk measurements to single-cell analysis. The MS profile of the bacterial species from distinct clusters in PLS-DA is determined by the differences between the MS profiles in each bacterial species. When combined with machine learning algorithms, unique metabolites profiling based on MALDI-TOF-MS obtained from intact cells on our gold microchips without prior extraction or separation steps can be sufficient to distinguish bacterial pathogens and other bacteria at the single cell level. In conclusion, we believe that the potent combination of the whole organism fingerprinting method with sophisticated informatics will provide easy and effective diagnostic and monitoring tools in various fields, including medicine, environment, food, and biotechnology.

References

[1] Etienne Carbonnelle, Cécile Mesquita, Emmanuelle Bille, Nesrine Day, Brunhilde Dauphin, Jean-Luc Beretti, Agnès Ferroni, Laurent Gutmann, and Xavier Nassif. Maldi-tof mass spectrometry tools for bacterial identification in clinical microbiology laboratory. *Clinical biochemistry*, 44(1):104–109, 2011.

[2] B Holmes, WR Willcox, and SP Lapage. Identification of enterobacteriaceae by the api 20e system. *Journal of clinical pathology*, 31(1):22–30, 1978.

[3] Eva Engvall et al. Quantitative enzyme immunoassay (elisa) in microbiology. *Med. Biol.*, 55(4):193–200, 1977.

[4] Sascha Sauer and Magdalena Kliem. Mass spectrometry tools for the classification and identification of bacteria. *Nature Reviews Microbiology*, 8(1):74–82, 2010.

[5] Tadhg F O'Sullivan and Gerald F Fitzgerald. Comparison of streptococcus thermophilus strains by pulse field gel electrophoresis of genomic dna. *FEMS microbiology letters*, 168(2):213–219, 1998.

[6] Ivone Vaz-Moreira, Conceiçao Egas, Olga C Nunes, and Célia M Manaia. Culture-dependent and culture-independent diversity surveys target different bacteria: a case study in a freshwater sample. *Antonie Van Leeuwenhoek*, 100(2):245–257, 2011.

[7] Chunxiu Hu and Guowang Xu. Mass-spectrometry-based metabolomics analysis for foodomics. *TrAC Trends in Analytical Chemistry*, 52:36–46, 2013.

[8] Oluwafemi Ayodeji Adebo, Patrick Berka Njobeh, Janet Adeyinka Adebiyi, Sefater Gbashi, and Eugenie Kayitesi. Food metabolomics: a new frontier in food analysis and its application to understanding fermented foods. *Functional Food-Improve Health through Adequate Food*, pages 211–234, 2017.

[9] Snehal R Jadhav, Rohan M Shah, Avinash V Karpe, Paul D Morrison, Konstantinos Kouremenos, David J Beale, and Enzo A Palombo. Detection of foodborne pathogens using proteomics and metabolomics-based approaches. *fmicb*, 9:3132, 2018.

[10] Gaetan Glauser, Davy Guillarme, Elia Grata, Julien Boccard, Aly Thiocone, Pierre-Alain Carrupt, Jean-Luc Veuthey, Serge Rudaz, and Jean-Luc Wolfender. Optimized liquid chromatography–mass spectrometry approach for the isolation of minor stress biomarkers in plant extracts and their identification by capillary nuclear magnetic resonance. *Journal of Chromatography A*, 1180(1-2):90–98, 2008.

[11] Alexander A Aksenov, Ricardo da Silva, Rob Knight, Norberto P Lopes, and Pieter C Dorrestein. Global chemical analysis of biology by mass spectrometry. *Nature Reviews Chemistry*, 1(7):1–20, 2017.

[12] Biswapriya B Misra. The connection and disconnection between microbiome and metabolome: A critical appraisal in clinical research. *Biological Research For Nursing*, 22(4):561–576, 2020.

[13] Juan M Cevallos-Cevallos, José I Reyes-De-Corcuera, Edgardo Etxeberria, Michelle D Danyluk, and Gary E Rodrick. Metabolomic analysis in food science: a review. *Trends in Food Science & Technology*, 20(11-12):557–566, 2009.

[14] Neelja Singhal, Manish Kumar, Pawan K Kanaujia, and Jugsharan S Virdi. Maldi-tof mass spectrometry: an emerging technology for microbial identification and diagnosis. *Frontiers in microbiology*, 6:791, 2015.

[15] HC Michelle Byrd and Charles N McEwen. The limitations of maldi-tof mass spectrometry in the analysis of wide polydisperse polymers. *Analytical chemistry*, 72(19):4568–4576, 2000.

[16] Anelize Bauermeister, Helena Mannochio-Russo, Letícia V Costa-Lotufo, Alan K Jarmusch, and Pieter C Dorrestein. Mass spectrometry-based metabolomics in microbiome investigations. *Nature Reviews Microbiology*, 20(3):143–160, 2022.

[17] Anja Freiwald and Sascha Sauer. Phylogenetic classification and identification of bacteria by mass spectrometry. *Nature protocols*, 4(5):732–742, 2009.

[18] Chase M Clark, Maria S Costa, Erin Conley, Emma Li, Laura M Sanchez, and Brian T Murphy. Using the open-source maldi tof-ms idbac pipeline for analysis of microbial protein and specialized metabolite data. *JoVE (Journal of Visualized Experiments)*, (147):e59219, 2019.

[19] Chase M Clark, Maria S Costa, Laura M Sanchez, and Brian T Murphy. Coupling maldi-tof mass spectrometry protein and specialized metabolite analyses to rapidly discriminate bacterial function. *Proceedings of the National Academy of Sciences*, 115(19):4981–4986, 2018.

[20] Konstantinos A Aliferis and Suha Jabaji. Ft-icr/ms and gc-ei/ms metabolomics networking unravels global potato sprout's responses to rhizoctonia solani infection. 2012.

[21] Gianfranco Picone, Luca Laghi, Fausto Gardini, Rosalba Lanciotti, Lorenzo Siroli, and Francesco Capozzi. Evaluation of the effect of carvacrol on the escherichia coli 555 metabolome by using 1h-nmr spectroscopy. *Food chemistry*, 141(4):4367–4374, 2013.

[22] Oluwafemi Ayodeji Adebo, Eugenie Kayitesi, Fidele Tugizimana, and Patrick Berka Njobeh. Differential metabolic signatures in naturally and lactic acid bacteria (lab) fermented ting (a southern african food) with different tannin content, as revealed by gas chromatography mass spectrometry (gc–ms)-based metabolomics. *Food Research International*, 121:326–335, 2019.

[23] Xue Zhao, Lin Chen, Ji'en Wu, Yun He, and Hongshun Yang. Elucidating antimicrobial mechanism of nisin and grape seed extract against listeria monocytogenes in broth and on shrimp through nmr-based metabolomics approach. *International Journal of Food Microbiology*, 319:108494, 2020.

[24] Piseth Seng, Michel Drancourt, Frédérique Gouriet, Bernard La Scola, Pierre-Edouard Fournier, Jean Marc Rolain, and Didier Raoult. Ongoing revolution in bacteriology: routine identification of bacteria by matrix-assisted laser desorption ionization time-of-flight mass spectrometry. *Clinical Infectious Diseases*, 49(4):543–551, 2009.

[25] A Bizzini, K Jaton, D Romo, J Bille, G Prod'hom, and G Greub. Matrix-assisted laser desorption ionization–time of flight mass spectrometry as an alternative to 16s rrna gene sequencing for identification of difficult-to-identify bacterial strains. *Journal of clinical microbiology*, 49(2):693–696, 2011.

[26] Sen-Yung Hsieh, Chiao-Li Tseng, Yun-Shien Lee, An-Jing Kuo, Chien-Feng Sun, Yen-Hsiu Lin, and Jen-Kun Chen. Highly efficient classification and identification of human pathogenic bacteria by maldi-tof ms. *Molecular & cellular proteomics*, 7(2):448–456, 2008.

[27] Antony Croxatto, Guy Prod'hom, and Gilbert Greub. Applications of maldi-tof mass spectrometry in clinical diagnostic microbiology. *FEMS microbiology reviews*, 36(2):380–407, 2012.

[28] Food and drug administration. de novo request for evaluation of automatic class iii designation for the vitek ms, 510(k) decision summary. https://www.accessdata.fda.gov/cdrh$_{d}ocs/reviews/K124067.pdf. \quad Accessed \quad :$ 20221022.

[29] Tomasz Cwalinski, Wojciech Polom, Luigi Marano, Giandomenico Roviello, Alberto D'Angelo, Natalia Cwalina, Marcin Matuszewski, Franco Roviello, Janusz Jaskiewicz, and Karol Polom. Methylene blue—current knowledge, fluorescent properties, and its future use. *Journal of Clinical Medicine*, 9(11):3538, 2020.

[30] Robert W Redmond and Janet N Gamlin. A compilation of singlet oxygen yields from biologically relevant molecules. *Photochemistry and photobiology*, 70(4):391–475, 1999.

[31] William P Thorpe, Mehmet Toner, Robert M Ezzell, Ronald G Tompkins, and Martin L Yarmush. Dynamics of photoinduced cell plasma membrane injury. *Biophysical journal*, 68(5):2198–2206, 1995.

[32] Makoto Mitsunaga, Mikako Ogawa, Nobuyuki Kosaka, Lauren T Rosenblum, Peter L Choyke, and Hisataka Kobayashi. Cancer cell–selective in vivo near infrared photoimmunotherapy targeting specific membrane molecules. *Nature medicine*, 17(12):1685–1691, 2011.

[33] K Gollnick. Type ii photooxygenation reactions in solution. *Adv. Photochem*, 6(1), 1968.

[34] Abdennour Abbas, Matthew J Linman, and Quan Cheng. Patterned resonance plasmonic microarrays for high-performance spr imaging. *Analytical chemistry*, 83(8):3147–3152, 2011.

[35] Katrien De Bruyne, Bram Slabbinck, Willem Waegeman, Paul Vauterin, Bernard De Baets, and Peter Vandamme. Bacterial species identification from maldi-tof mass spectra through data analysis and machine learning. *Systematic and applied microbiology*, 34(1):20–29, 2011.

[36] Kévin Vervier, Pierre Mahé, Jean-Baptiste Veyrieras, and Jean-Philippe Vert. Benchmark of structured machine learning methods for microbial identification from mass-spectrometry data. *arXiv preprint arXiv:1506.07251*, 2015.

[37] Marie-Sarah Fangous, Faiza Mougari, Stéphanie Gouriou, Elodie Calvez, Laurent Raskine, Emmanuelle Cambau, Christopher Payan, and Geneviève Héry-Arnaud. Classification algorithm for subspecies identification within the mycobacterium abscessus species, based on matrix-assisted laser desorption ionization–time of flight mass spectrometry. *Journal of clinical microbiology*, 52(9):3362–3369, 2014.

[38] David Moher, Larissa Shamseer, Mike Clarke, Davina Ghersi, Alessandro Liberati, Mark Petticrew, Paul Shekelle, and Lesley A Stewart. Preferred reporting items for systematic review and meta-analysis protocols (prisma-p) 2015 statement. *Systematic reviews*, 4(1):1–9, 2015.

[39] Walter Florio, Arianna Tavanti, Simona Barnini, Emilia Ghelardi, and Antonella Lupetti. Recent advances and ongoing challenges in the diagnosis of microbial infections by maldi-tof mass spectrometry. *Frontiers in microbiology*, 9:1097, 2018.

[40] Irene Burckhardt and Stefan Zimmermann. Susceptibility testing of bacteria using maldi-tof mass spectrometry. *Frontiers in microbiology*, 9:1744, 2018.

[41] Peter V Shanta, Bochao Li, Daniel D Stuart, and Quan Cheng. Plasmonic gold templates enhancing single cell lipidomic analysis of microorganisms. *Analytical chemistry*, 92(9):6213–6217, 2020.

[42] Jaber Ghorbani, Dariush Rahban, Shahin Aghamiri, Alireza Teymouri, and Abbas Bahador. Photosensitizers in antibacterial photodynamic therapy: An overview. *Laser therapy*, 27(4):293–302, 2018.

[43] Julia J Shen, Gregor BE Jemec, Maiken C Arendrup, and Ditte Marie L Saunte. Photodynamic therapy treatment of superficial fungal infections: A systematic review. *Photodiagnosis and Photodynamic Therapy*, 31:101774, 2020.

[44] Jie Chen, Thomas C Cesario, and Peter M Rentzepis. Effect of ph on methylene blue transient states and kinetics and bacteria photoinactivation. *The Journal of Physical Chemistry A*, 115(13):2702–2707, 2011.

[45] Ewelina Wanarska, Karolina Anna Mielko, Irena Maliszewska, and Piotr Młynarz. The oxidative stress and metabolic response of acinetobacter baumannii for apdt multiple photosensitization. *Scientific reports*, 12(1):1–13, 2022.

[46] Nolwenn Wirgot, Marie Lagree, Mounir Traïkia, Ludovic Besaury, Pierre Amato, Isabelle Canet, Martine Sancelme, Cyril Jousse, Binta Diémé, Bernard Lyan, et al. Metabolic modulations of pseudomonas graminis in response to h2o2 in cloud water. *Scientific reports*, 9(1):1–14, 2019.

[47] Saji George, Michael R Hamblin, and Anil Kishen. Uptake pathways of anionic and cationic photosensitizers into bacteria. *Photochemical & Photobiological Sciences*, 8(6):788–795, 2009.

[48] Shiwei Zhou, Guangxue Feng, Shaowei Wang, Guobin Qi, Min Wu, and Bin Liu. Fast and high-throughput evaluation of photodynamic effect by monitoring specific protein oxidation with maldi-tof mass spectrometry. *Analytical Chemistry*, 92(18):12176–12184, 2020.

[49] David J Evason, Martin A Claydon, and Derek B Gordon. Exploring the limits of bacterial identification by intact cell-mass spectrometry. *Journal of the American Society for Mass Spectrometry*, 12(1):49–54, 2001.

Chapter 5

Plasmonic Al-chip Substrate for Analysis of Lipid Metabolite Profiling of COVID-19 Clinical Nasopharyngeal Swabs

5.1 Introduction

The new coronavirus disease 2019 (COVID-19), caused by the severe acute respiratory syndrome coronavirus 2 (SARS-CoV-2) belonging to the β-genus of the coronavirus family, has posed global public health and societal challenge without precedent.[1][2] This reflects the difficulties of removing all disease reservoirs and the possibility for the virus to generate new strains of concern, which might lead to vaccination escape. The SARS-CoV-2 spike (S) protein, which is comprised of S1 and S2 subunits, is important for promoting the virus' entrance into host cells through the surface receptor angiotensin-converting enzyme 2 (ACE2). SARS-CoV-2 entrance into the target cell is facilitated by host protease transmembrane serine protease 2 (TMPRSS2).[3][4][5][6] Since lipids are the structural basis of cellular and viral membranes, they play a crucial role in biology and the pathophysiology of viral illness.[7] To produce lipids for their envelopes, viruses target lipid production and signal modification in host cells.[8] The participation of lipids in membrane fusion, envelopment, and transformation is essential for viral replication. The viruses multiply within the host cell; hence, they must traverse the host cell membrane for entry and exit.[7] Lipids serve as direct and indirect viral receptors, fusion cofactors, and entrance cofactors, among other functions, during a viral invasion.[8] In addition, lipids are a crucial component of the innate and adaptive immune systems during infections.[9] A proteomics study based on mass spectrometry (MS) demonstrated that disruption of lipid metabolism might increase the course of COVID-19.[10][11] Lipids are a major component of the viral envelope and are engaged in crucial replication cycle activities, including the creation of new virions, making them an intriguing molecular target for diagnosing SARS-CoV-2 infection.[12][13]The genetic material of viruses does not code for lipids, but during budding, these molecules are taken away from the cell membranes of their hosts. It is known that the lipid content of the viral envelope derived from the host is unique to the budding site[14] and quantitatively distinct from that of the host membrane and other viruses. [15][16][17][18] Coronaviruses, for instance, proliferate and get their envelope lipids from the membrane of the host endoplasmic reticulum -Golgi intermediate complex,[15]whereas the influenza virus acquires its lipids from the host apical plasma membrane. [19] Altering the total lipid content of infected host cells, viral infections also influence host lipid metabolism to facilitate reproduction during infection. Yan et al. reported that HCoV-229E-infected human cells had much higher levels of fatty acids and glycerophospholipids than healthy cells. [20] Therefore, the dysregulation of very abundant glycerophospholipids in infected host cells and the pathogen's unique lipid composition constitute a prospective diagnostic target.

Currently, reverse transcription polymerase chain reaction (RT-PCR) and serological methods, such as enzyme-linked immunosorbent assay, are mostly utilized for the identification of SARS-CoV-2 and its variations. RT-PCR, which offers great specificity and sensitivity, is now the most well-known and commonly used technique for detecting SARS-CoV-2.[21] However, this method may also have some disadvantages. For instance, the quality of isolated viral RNA might considerably impact the detection sensitivity and accuracy, necessitating the use of competent professionals for extraction. In addition, the high viscosity and high concentration of proteins and other interfering components in the two most often obtained samples, oral swabs, and sputum, provide additional challenges to RNA extraction. [22]More significantly, this method's false negative and false positive outcomes are of concern. [23][24] In addition, the entire analysis usually takes several hours and is done in laboratories with a higher biosafety level (BSL), which limits the use of this method. The objective of serological methods is to identify viral antigens or antibodies. The most obvious advantage of this technology is that goods of portable size are commercially accessible elsewhere, allowing for speedy and on-site identification of anyone carrying them. This method might serve as a supplement to RT-PCR, as the generated antibodies would persist in patients for an extended period, allowing for identifying of moderate and asymptomatic infected individuals. However, this method's sensitivity and specificity are restricted. [25] In addition, it may take a few days after the beginning of symptoms for antibodies to be produced, making this approach less useful for early-stage infection identification.[26]

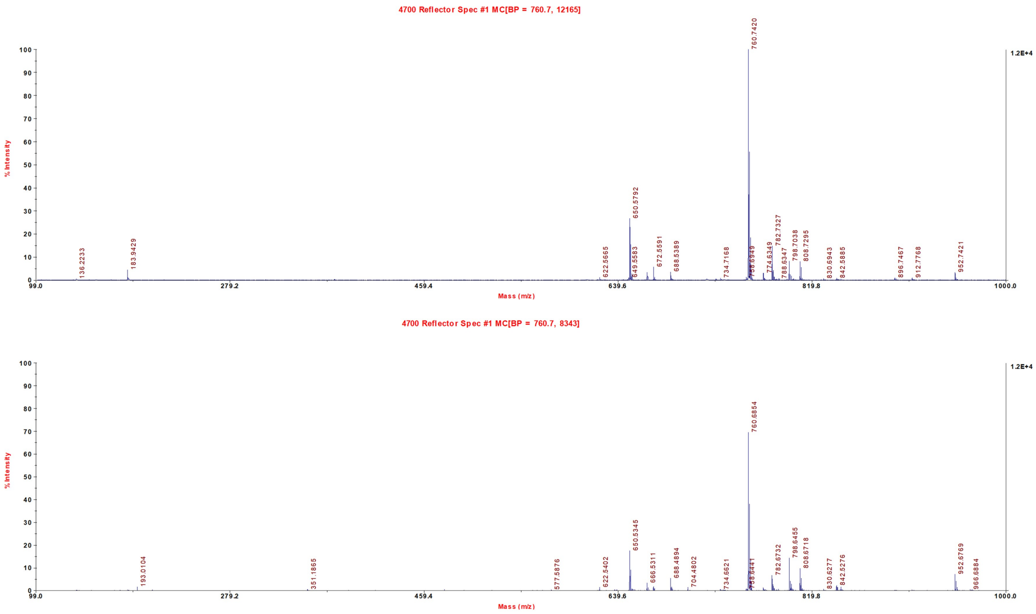

Figure 5.1: MALDI-MS of 4 mg/ml POPC obtained from plasmonic Al substrate (a.) and traditional stainless steel MALDI plate (b.)

Along with the widely used and constantly improving RT-PCR and serological approaches, mass spectrometry (MS) could be an effective method for detecting SARS-CoV-2 because of its speed, sensitivity, specificity, and ability to give qualitative and quantitative information regarding different analytes (such as nucleic acids, proteins, peptides, organic molecules, and elements), which cannot be accomplished using RT-PCR and serological methods. Specifically, proteomics has been utilized extensively to explore several biological pathways and significant illness biomarkers.[27] On the other hand, increasing attention has been paid to the metabolites, volatile organic compounds, and lipid profiles of SARS-CoV-2-infected patients since these may be suggestive of SARS-CoV-2 infection.[28][29] Additionally, the development of viral detection based on increasingly sophisticated instruments has been made possible by the rapid advancement of mass spectrometer speed, sensitivity, and resolution in recent years.

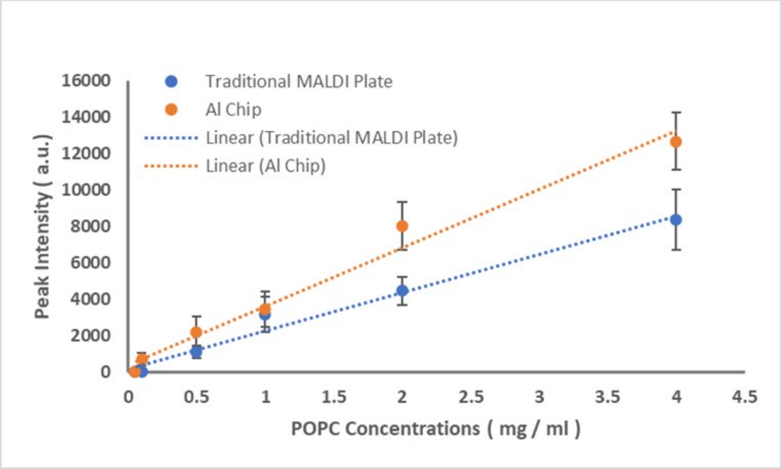

Figure 5.2: Sensitivity comparison between Al microarray and conventional stainless-steel plate

Matrix-assisted laser desorption/ionization mass spectrometry (MALDI-MS) is promising for detecting viruses.[30] The aluminum foil layer and nanostructures as substrates have previously been demonstrated to be beneficial for MALDI-MS with high sensitivity for the identification of proteins and peptides.[31][32][33][34] A study showed that the alumina on Al particles and foils has the ability to extract multi-phosphopeptides selectively,[35] so Al may be used as a method for their enrichment before the quantitative assessment. In addition, a desirable plasmonic feature of Al compared to Au and Ag is its capacity to absorb a greater spectrum of incident photon wavelengths plasmonically. While the plasmonic absorption of Au diminishes significantly at wavelengths below 500 nm, Al can absorb light deep into the UV region.[36] Due to the near-UV lasers commonly employed to ionize sample matrices for desorption, this is particularly significant for MALDI-MS analysis. Our previous studies have revealed the influence of plasmonic Au on MALDI- ionization,[37][38]; therefore, plasmonic Al substrates might be utilized to achieve a comparable result. In this chapter, we report Al thin film as a new substrate for MALDI-MS for the analysis of swab samples, demonstrate its use for rapid and direct lipid analysis, and discuss its potential for COVID-19 screening. The development of this Al thin film for SPR biosensing has previously been reported. [39] In this study, COVID-19 samples are used to test the sensitivity of aluminum microarray chips for studying complicated clinical samples. We investigated the lipid metabolite profiles of COVID-19 samples and compared positive and negative samples. The results indicate that the aluminum chip is a promising substrate for MALDI-MS.

5.2 Experimental Section

5.2.1 Materials and Reagents

Super 2,5 - dihydroxybenzoic acid (sDHB), trifluoroacetic acid (TFA), were purchased from Sigma-Aldrich (St. Louis, MO). 1-Palmitoyl-2-oleoyl-glycero-3-phosphocholine (POPC) was obtained as a powder from Avanti Polar Lipids (Alabaster, AL). Acetonitrile, methanal were obtained from Fisher Scientific (Pittsburgh, PA). Aluminum targets for electron beam physical vapor deposition (EBPVD) were obtained from Kurt J. Lesker (Jefferson Hills, PA). BK-7 glass substrates for E-Beam deposition were purchased from Corning (Painted Post, NY). High-purity water (>18 MΩ cm–1) was obtained from a Barnstead E-Pure water purification system. Matrix solutions (sDHB) were prepared in acetonitrile and water (2:1, v/v) at a concentration of 10 mg/ml. COVID-19 nasopharyngeal swabs (5 positive and 2 negative) were purchased from iSpecimen Inc (Lexington, MA)

5.2.2 COVID-19 Nasopharyngeal Swabs

Preparation and processing of specimens were conducted in a biosafety level 2 (BSL-2) environment, and appropriate personal protective equipment (PPE) was worn by the personnel during all tasks to be conducted, from sample handling to MALDI-MS testing. The mixed swab specimens were suspended in ≈1mL of the iSpecimen company's proprietary collecting medium. Each sample was mixed with the ratio of 1:1 chloroform and methanol for 20min to inactivate virus samples and then vortexed at the speed of 4000 rpm/min for 5min. The chloroform layer was collected and stored in a -80 freezer.

5.2.3 Fabrication of Aluminum Microarray Chip

BK-7 glass microscope slides were cleaned using boiling piranha solution (3:1 $H_2SO_4 : 30\% H_2O_2$) for one hour. After cleaning, the slides were washed with ultrapure water and ethanol, and dried with compressed air. All Al films were deposited using an electron beam physical vapor deposition (EBPVD) machine (Temescal, Berkeley, CA) in a Class 1000 cleanroom facility (UCR Center for Nanoscale Science and Engineering). The fabrication of the microarray substrates for MALDI-MS followed previously reported methods[40]. Briefly, hexamethyldisilazane (HMDS) and AZ5214E were spin-coated at 4000 RPM for 45 seconds on piranha-cleaned glass slides, followed by a one-minute bake at 110 °C. With a photomask and the Karl-Suss MA-6 system, UV exposure was used to generate photopatterning, which was then followed by AZ400K development using standard protocols. 150 nm of Al was deposited using EBPVD, and then the wells were cleaned with acetone. To create the plasmonically active layer in the wells, an additional deposition of 18 nm Al was applied. The final array consisted of a 10 x 12 set of circular wells with a 600 μm diameter.

5.2.4 MALDI-MS Acquisition and Data Analysis

Experiments with MS were performed using an AB-Sciex 5800 time-of-flight mass spectrometer fitted with a nitrogen UV laser (337nm wavelength). MALDI-TOF-MS was used to detect COVID-19 positive and negative samples, which were confirmed via PCR test. 1ul of sample per well was put into the aluminum microchip before being coated with 1μl of sDHB matrix for data capture. Lipid metabolite profiles were collected using a laser fluence of 5900 a.u. on a reflectron detector in positive mode. A sample is defined as the average of m/z values versus intensity (a.u.) obtained in a continuous linear or v-shaped laser pattern during co-crystallization of the COVID-19 sample and matrix. 33 mass spectra from 2 negative samples and 74 mass spectra from 5 positive samples were averaged and normalized via mmass. Data were analyzed using Rstudio (version 3.6.3) via MALDIquant and ggplot package.

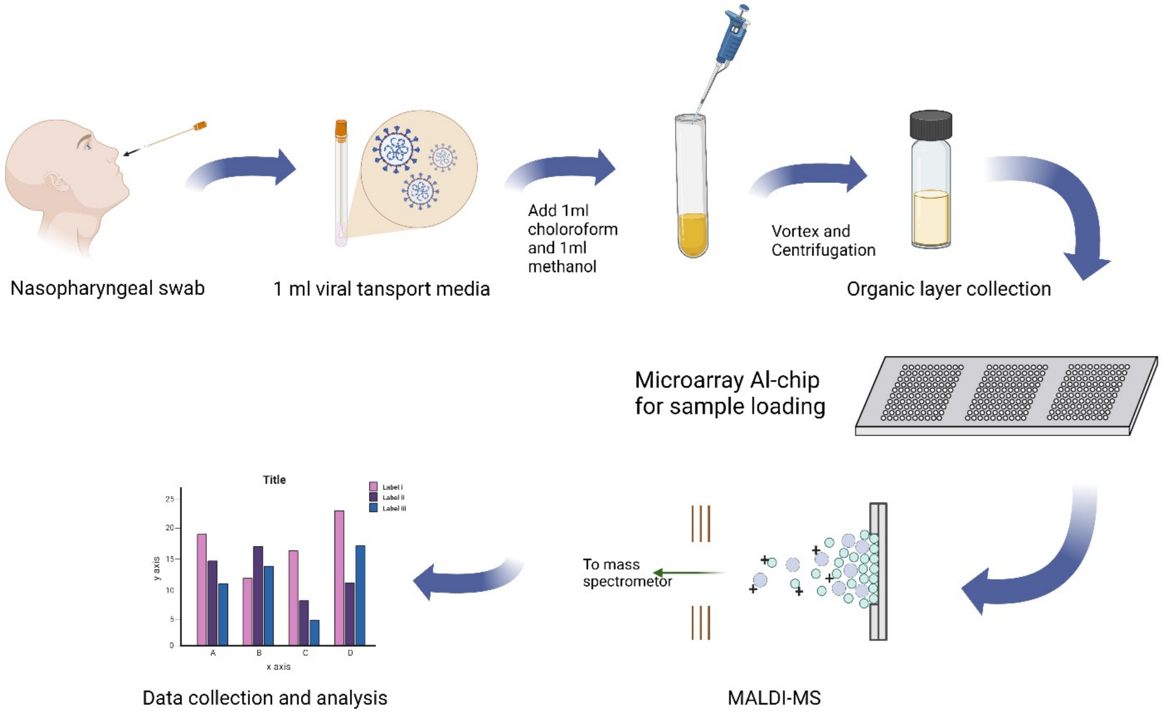

Figure 5.3: Workflow of COVID-19 sample preparation for MALDI-MS analysis. Created with BioRender.com

LC-MS lipidomics analysis was performed at the UC Riverside Metabolomics Core Facility. The analysis was carried out using a Waters G2-XS quadrupole time-of-flight mass spectrometer coupled to a Waters Acquity I-class UPLC system. Separations were conducted using a Waters CSH C18 column (2.1 ×100 mm, 1.7 M). The mobile phase was (A) acetonitrile: water (60:40) containing 10 mM ammonium formate and 0.1% formic acid; (B) isopropanol:acetonitrile (90:10), containing 10mM ammonium formate and 0.1% formic acid. The flow rate was 400 μl/min, and the column was held at 65°C. The injection volume was 2 μl. The gradient was as follows: 0 min, 10% B; 1 min, 10% B; 3 min, 20% B; 5 min, 40% B; 16 min, 80% B; 18 min, 99% B; 20 min 99% B; 20.5 min, 10% B. The MS

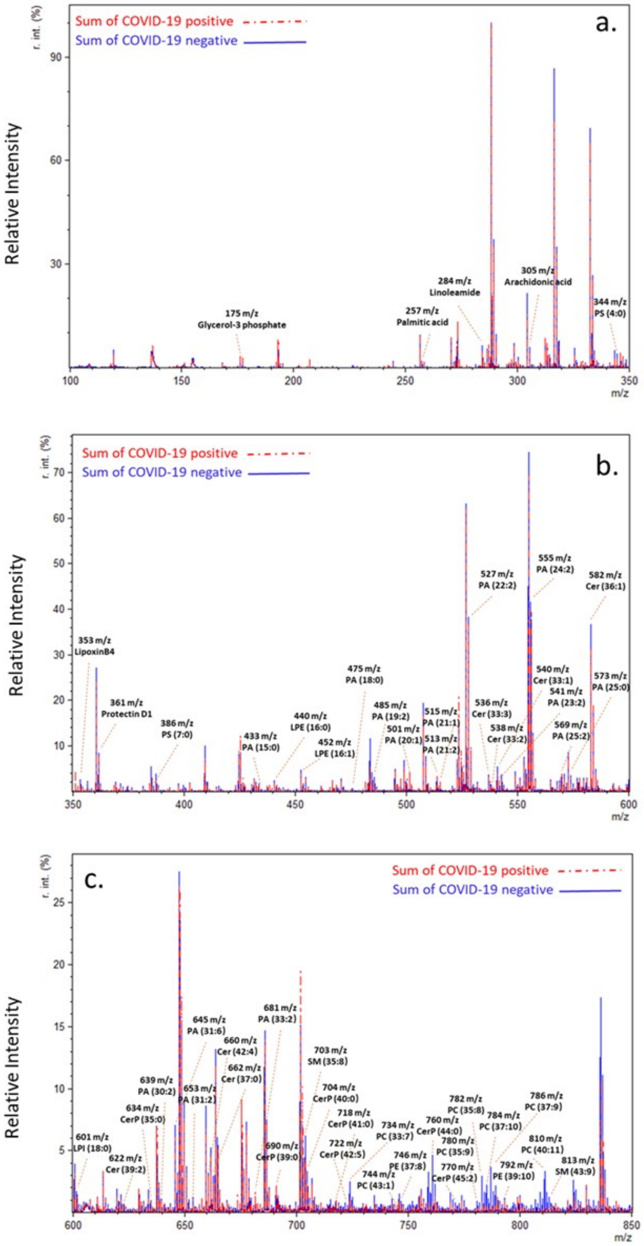

Figure 5.4: Comparison of sum mass spectral data for COVID -19 positive (in red) and negative samples(in blue) with different mass ranges and corresponding potential annotation. (a.) Mass range m/z 100-350 (b.) Mass range m/z 350-600 (c.) Mass range m/z 600-850.

was operated in the positive ion mode (50–1600 m/z) with a 100 ms scan time. MS/MS was acquired in the data dependent fashion. Source and desolvation temperatures were

150 °C and 600 °C, respectively. Desolvation gas was set to 1100 l/h and cone gas to 150 l/h. All gases were nitrogen except the collision gas, which was argon. A quality control sample, generated by pooling equal aliquots of each sample, was analyzed periodically to monitor system stability and performance. Leucine enkephalin was infused and used for mass correction. MS/MS data was analyzed via MSDIAL software.

5.3 Results and Discussion

Plasmonic nanomaterials have been widely investigated in biological and chemical sensing applications due to their distinct surface plasmon properties[41][42] The aluminum foil layer has previously been demonstrated to be an ideal disposable substrate for MALDI-MS with high sensitivity for protein and peptide detection.[31] In our study, this Al thin film microarray substrate has previously been reported to have higher sensitivity for SPR imaging,[39] we further applied it to MALDI-MS for sensitivity evaluation and more complex clinical sample analysis. As is shown in Figure 5.1, it demonstrated that plasmonic absorption of aluminum by the UV laser (337 nm) utilized in MALDI-MS detection enhances the MS signals. Figure 5.2 shows the POPC calibration curve from a Al-chip and a traditional stainless steel MALDI plate. When comparing the sensitivity of the Al-chip to that of the traditional MALDI stainless steel plate, POPC is used as a standard. The concentrations that are increasing are as follows: 0.05, 0.1, 0.5, 1, 2, and 4 mg/ml. In all of the concentrations that were tested, the intensity of the signal coming from the Al-chip was found to be greater than that coming from the traditional MALDI plate. Furthermore, the signal could still be observed at 0.1 mg/ml, whereas it was hardly seen from the traditional plate at that concentration. It suggests that the Al-chip has a greater level of sensitivity in addition to a lower threshold for detection compared to the conventional MALDI plate. The mechanisms that the plasmonic nanomaterials are advantageous for plasmon-enhanced laser desorption/ionization mass spectrometry were reported to be magnified absorption cross section and hot carrier generation at the resonance wavelength[43][44] Particularly, a larger absorption cross section produces a stronger photothermal effect, resulting in a more effective energy transfer to the analytes., the additional energy induces a phase transition of the analytes from the condensed phase to the gas phase, resulting in the production of analyte ions in the gas phase within the mass detector. The production of hot carriers can also stimulate the photo-decomposition of metal ions and small metabolites complexes.[45][46]

After investigating the sensitivity, we further applied this plasmonic Al thin film chip to study more complex clinical samples by MALDI-MS (Figure 5.3). iSpecimen Company provided both positive and negative Covid-19 nasal swab samples in their proprietary collection medium for this assay. After that, the samples were deactivated in a mixture of methanol and chloroform at a ratio of 1:1 for twenty minutes, after which they were vortexed and centrifuged at a speed of 4000 revolutions per minute for five minutes. For the purposes of this investigation, the chloroform layer that was recovered following centrifugation. After that, 1 ul of the sample was spotted onto each well of our Al-chip so that MALDI-MS data could be collected. Positive ion mode was used for the collection of MALDI-MS data.The mass spectra data that were obtained as a result are presented in Figure 5.4. Peak values were determined based on the LIPID MAPS[47] online search tools for lipid research, MS/MS, and literature[48][49][50]. Peak assignment and corresponding adducts are summarized in Figure 5.5a., MS/MS was compared with the referral database for further identification of metabolites (Figure 5.5b). In Figure 5.4, the graphic includes labeling for a total of 51 potential annotations of metabolites. According to the findings of our investigation, it is shown that there were distinctions between the positive and negative test samples. As shown in Figure 5.4, a comparison of summed mass data for test samples of each category depicts downregulated and upregulated metabolites in COVID-19 infected samples. A lipidic profile can mirror a patient's biological status where internal and/or external perturbations activate molecular pathways involved in the immune response and metabolism. Lipids are essential for viruses to cross the host cell membrane. In addition, it is well know that infections caused by viruses modify lipid metabolism in a manner that is beneficial to the reproduction of the virus.[12] Studies on lipidomic profiles have shown that the composition of lipids in infected cells is considerably altered by the coronavirus.[20] Viruses use and alter lipid signaling and metabolism in order to facilitate viral reproduction, since lipids are not only the primary component of membranes but also play essential functions as intercellular signaling agents and energy sources. [51] Replication of enveloped viruses such as SARS-CoV-2, which enter cells by endocytosis and utilize intracellular organelles to manufacture their many components, needs lipid resources.[52] Therefore, investigating how SARS-COV-2 infection affects lipid metabolism and profile might give information on the link between lipid profile and inflammatory processes during COVID-19.

In our study, we focused on several classes of phospholipid species. Previous research has revealed that these phospholipids have key roles in the formation and replication of coronavirus virion,[20][53][54] in addition to their activities as components of the membranes of host cellular organelles. The tentatively identified lipids included glycerophospholipids, such as ceramides, lysolipids, and PE. The details about the changes in metabolite expression due to the virus infection can be observed in the radar charts and bar graphs (Figure 5.6 and 5.7). Radar charts illustrate the abundance of the metabolites. Some metabolites, such as PC (37:10), CerP (42:5), and Cer(33:1), have been shown to be up-regulated in COVID-19 positive samples, whereas others, such as PE (39:10), PA (21:2), and PA (20:1), have been shown to be down-regulated in COVID-19 negative samples. The distribution of the metabolites as well as the ratio of each metabolite between the COVID-19 positive and negative samples are shown using bar graphs. As it is shown in Figure 5.7a,

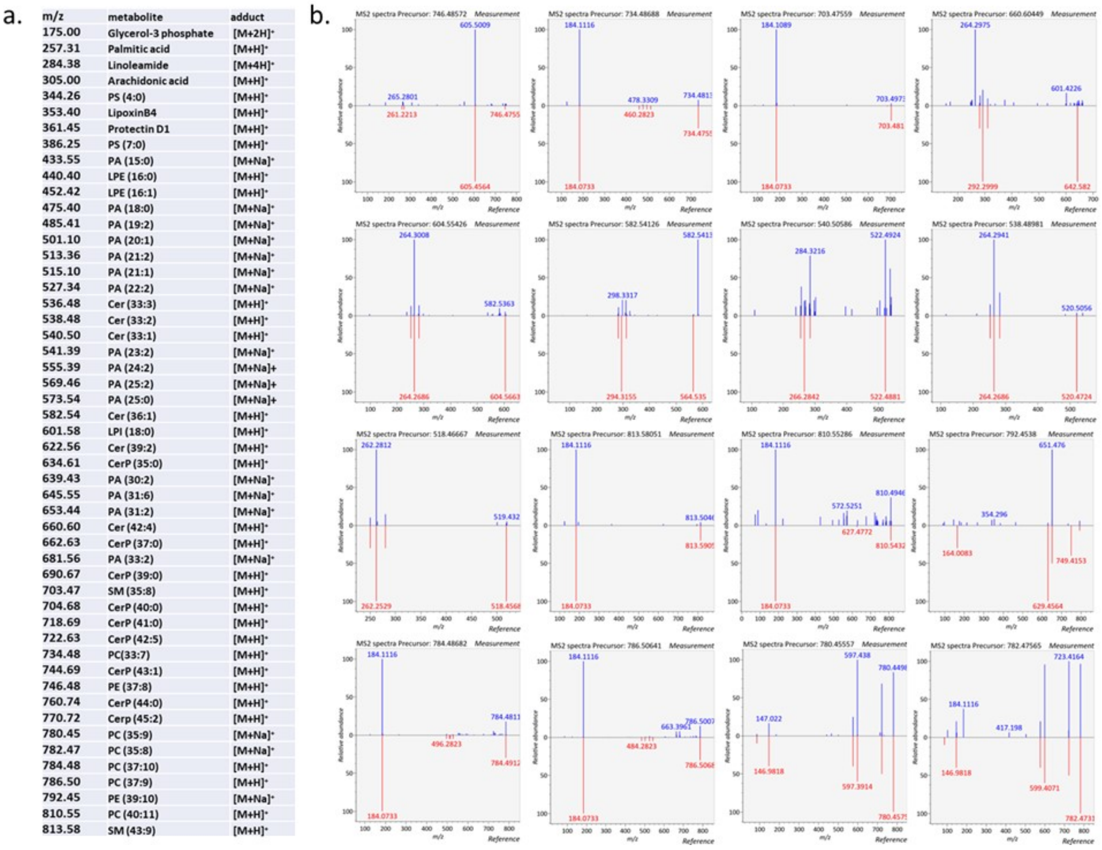

m/z	metabolite	adduct
175.00	Glycerol-3 phosphate	$[M+2H]^+$
257.31	Palmitic acid	$[M+H]^+$
284.38	Linoleamide	$[M+4H]^+$
305.00	Arachidonic acid	$[M+H]^+$
344.26	PS (4:0)	$[M+H]^+$
353.40	LipoxinB4	$[M+H]^+$
361.45	Protectin D1	$[M+H]^+$
386.25	PS (7:0)	$[M+H]^+$
433.55	PA (15:0)	$[M+Na]^+$
440.40	LPE (16:0)	$[M+H]^+$
452.42	LPE (16:1)	$[M+H]^+$
475.40	PA (18:0)	$[M+Na]^+$
485.41	PA (19:2)	$[M+Na]^+$
501.10	PA (20:1)	$[M+Na]^+$
513.36	PA (21:2)	$[M+Na]^+$
515.10	PA (21:1)	$[M+Na]^+$
527.34	PA (22:2)	$[M+Na]^+$
536.48	Cer (33:3)	$[M+H]^+$
538.48	Cer (33:2)	$[M+H]^+$
540.50	Cer (33:1)	$[M+H]^+$
541.39	PA (23:2)	$[M+Na]^+$
555.39	PA (24:2)	[M+Na]+
569.46	PA (25:2)	[M+Na]+
573.54	PA (25:0)	[M+Na]+
582.54	Cer (36:1)	$[M+H]^+$
601.58	LPI (18:0)	$[M+H]^+$
622.56	Cer (39:2)	$[M+H]^+$
634.61	CerP (35:0)	$[M+H]^+$
639.43	PA (30:2)	$[M+Na]^+$
645.55	PA (31:6)	$[M+Na]^+$
653.44	PA (31:2)	$[M+Na]^+$
660.60	Cer (42:4)	$[M+H]^+$
662.63	CerP (37:0)	$[M+H]^+$
681.56	PA (33:2)	$[M+Na]^+$
690.67	CerP (39:0)	$[M+H]^+$
703.47	SM (35:8)	$[M+H]^+$
704.68	CerP (40:0)	$[M+H]^+$
718.69	CerP (41:0)	$[M+H]^+$
722.63	CerP (42:5)	$[M+H]^+$
734.48	PC(33:7)	$[M+H]^+$
744.69	CerP (43:1)	$[M+H]^+$
746.48	PE (37:8)	$[M+H]^+$
760.74	CerP (44:0)	$[M+H]^+$
770.72	Cerp (45:2)	$[M+H]^+$
780.45	PC (35:9)	$[M+Na]^+$
782.47	PC (35:8)	$[M+Na]^+$
784.48	PC (37:10)	$[M+H]^+$
786.50	PC (37:9)	$[M+H]^+$
792.45	PE (39:10)	$[M+Na]^+$
810.55	PC (40:11)	$[M+H]^+$
813.58	SM (43:9)	$[M+H]^+$

Figure 5.5: Peak characterization a. a list of m/z peak value, assignment and adducts detected in the positive ion MALDI-MS. b. LC-MS/MS of experimental spectra (in blue) and referral spectra (in red). Phosphatidyl Choline (PC), Phosphatidyl Ethanolamine (PE), Phosphatidylserine (PS), Phosphatidic acid (PA), Lysophosphatidylinositol (LPI), Lysophosphatidylethanolamine (LPE)

PA (22:2), PA (24:2), and Cer (36:1) have the most abundant with little difference between positive and negative samples, whereas CerP (44:0) has the greatest differences between positive samples and negative samples. Figure 5.7b indicates that Glycerol-3 phosphate, PE (39:10), and SM (43:9) were only observed in COVID-19 positive samples, while CerP (42:5) and PE (37:8) were only observed in COVID-19 negative samples. Other metabolomic studies on COVID-19 disease states show general decreases in phospholipid and free fatty acid abundance in COVID-19 positive patients' blood plasma. [10] In addition, it was reported that glycerophospholipids were the most discriminant between healthy individuals and COVID-19 patients, especially several LPCs, LPC-Os and PC-O which had a progressive decrease in relation to the severity status and were considered a marker of severity for their potential use. [55] As shown in Figures 5.6 and 5.7, our study also observed similar results in PCs' decrease in COVID-19 positive samples. A similar pattern was reported in the case of Ebola virus disease, where liver dysfunction and decay of choline metabolism affect LPCs and PCs synthesis and are associated with the severity of the disease. O'Donnell, V. B et al. reported that activated externalization of PE and PS phospholipids in platelet microvesicles (MV) might account for their elevated exposure in COVID-19-positive nasal fluid swabs. [56] The increased abundance of these phospholipids in COVID-19-positive samples may be attributed to the development of MV for viral replication within the cells. Protectin D1 (PD1), a lipid mediator derived from omega-3 polyunsaturated fatty acids (PUFA), is a strong viral replication inhibitor in Influenza A infections and decreases in severe cases. [57] The decrease in PD 1 is in agreement with our result. Morita, M. et al. also reported that PD1 treatment attenuated the replication of highly pathogenic H5N1 influenza viruses, as assessed by markedly reduced viral M protein mRNA expression, and decreased virus titers in A549 and MDCK cells.[57]

Because our data analysis is based on more than one hundred spectra, we carried out statistical analysis to determine the density and distribution of the data. For the purpose of visualizing the abundance of the metabolites, violin plots, as shown in Figure 5.8, are used. These plots display the data density at every place. In this diagram, the white line indicates the median Q2, while the rectangle depicts the range from the lower

Figure 5.6: Radar plot of normalized metabolites in COVID-19 nasal swab samples. The plot permits the visualization of the similarities and discrepancies between the data from positive (in blue) and negative (in orange) samples. The data are the mean of the normalized values for each metabolite.

quartile all the way up to the upper quartile. Longer quartile intervals indicate that the data are more dispersed, while shorter quartile intervals indicate that the data are more concentrated. The IQR shows the degree of dispersion and symmetry of the normal data. The outer shape of the rectangle is kernel density estimation.The length of the vertical axis of the figure represents the degree of data dispersion, and the length of the horizontal axis represents the data distribution in a certain vertical coordinate position. As it is shown

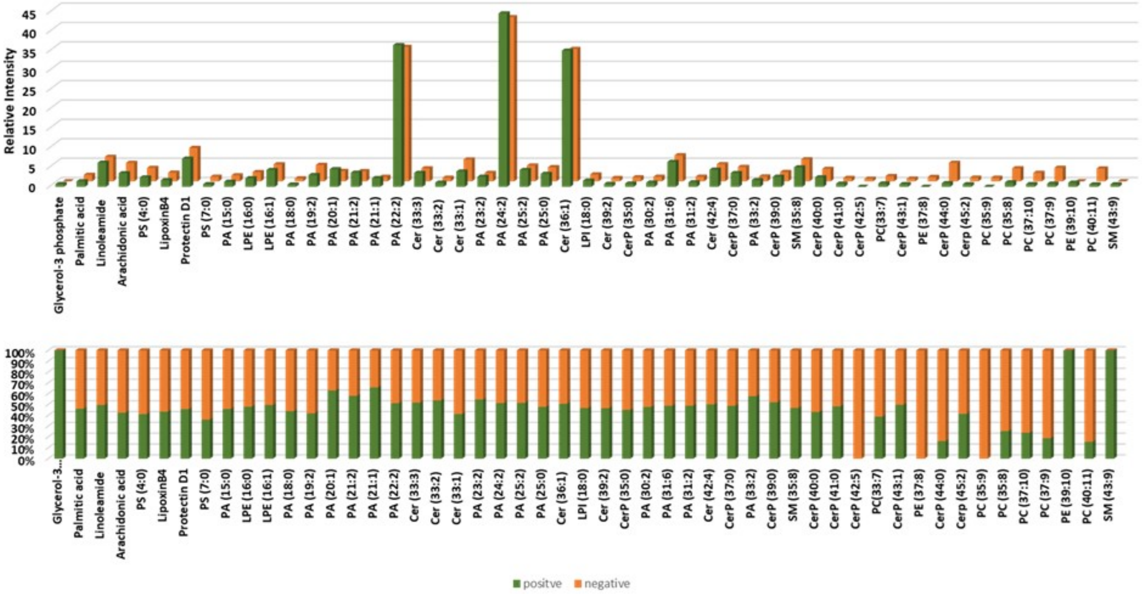

Figure 5.7: Figure 6. Bar graph of a) potential metabolite distribution in covid-19 positive and negative samples. b) The ratio of relative intensity of each metabolite between covid-19 positive and negative samples.

in Figure 5.8, Cer (36:1), PA (22:2), and PA (24:2) present the highest abundance from both positive and negative samples, which can be observed in the bar graph (Figure 5.7) as well. The intensity of CerP (44:0), PC (35:8), PC (37:10), PC (37:9), and PC (40:11) from COVID-19 negative samples has a broad distribution in the vertical direction of the axis, which may be due to the heterogeneity in the individuals. In contrast, more centralized data distribution for these PCs can be observed in COVID-19 positive samples due to the decreases in the abundance of PCs, which was reported previously[55] as well as our results, which are shown in Figure 5.6 and 5.7.

The scatter bubble plot (Figure 5.9) shows the metabolite abundance in each sample. The size of the bubble represents the expression abundance of metabolites. As it is shown in Figure 5.9., PA (22:2), PA (24:2), and Cer (36:1) have much more abundance

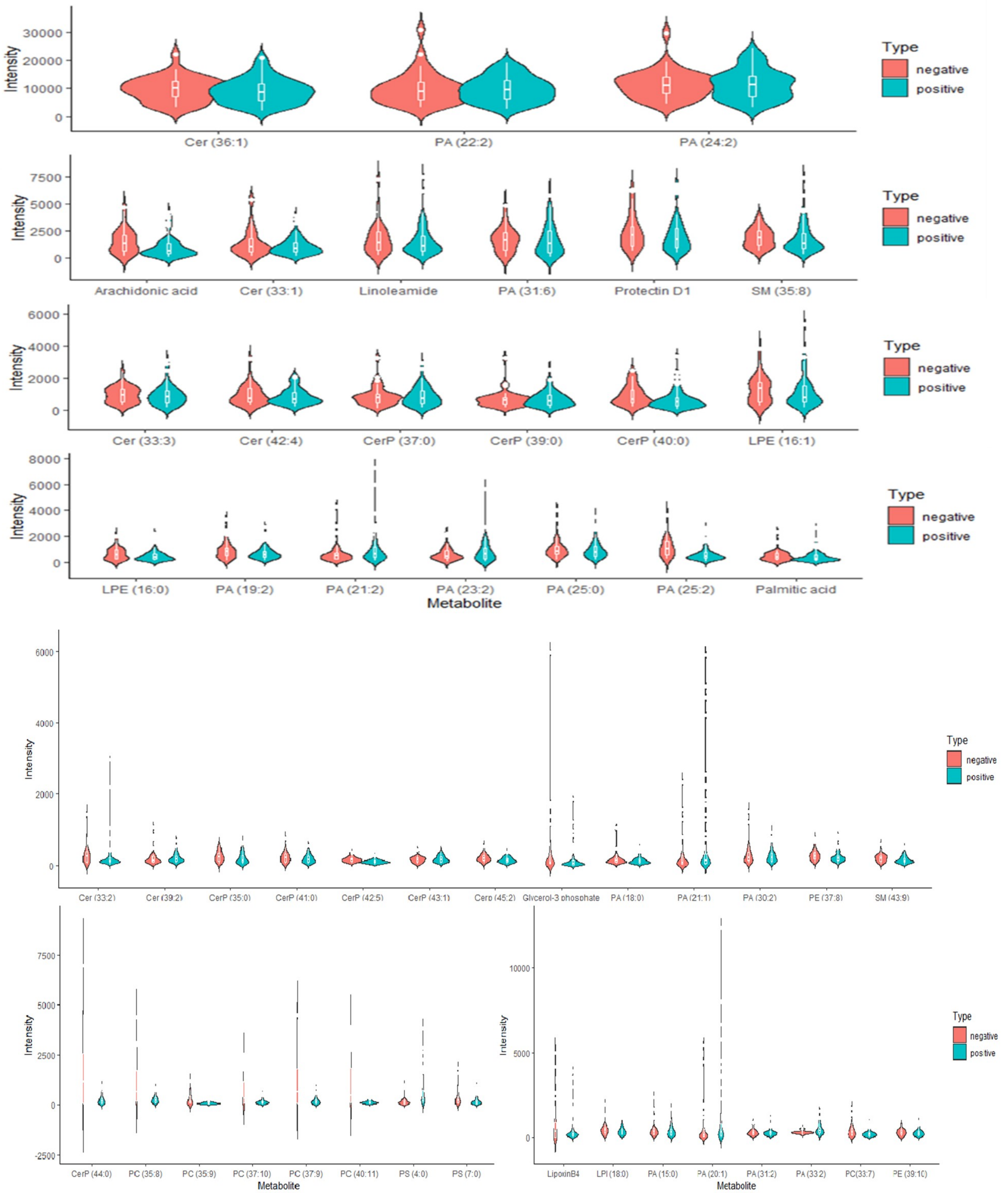

Figure 5.8: Grouped violin plot of data from covid-19 positive (in green) and negative (in red) samples.

than other metabolites in each sample, which is consistent with the radar chart (Figure 5.6) and the bar graph (Figure 5.7). The similarities and differences among each individual sample can be observed from different types of samples in the scatter bubble plot. As shown in Figure 5.9, PA (20:1) and PA(21:2) have more differences among samples which may be associated with the severity of COVID-19, as it reported that PA levels have a role in determining the severity of COVID-19 patients independently from comorbidity, age, and gender.[58] Glycerol-3 phosphate was only observed in COVID-19 positive samples, while CerP (42:5) was only observed in the COVID-19 negative samples. However, in a subsequent study, a greater number of clinical samples will need to be investigated in order to construct a more validation cohort for the purpose of achieving more precise results. This is necessary due to the fact that individuals may express a high degree of heterogeneity in their metabolomic responses under various symptomatic conditions. In addition, viral load information was also unavailable for the patients, preventing the evaluation of a potential relationship between viral burden, molecular information, and diagnostic performance.

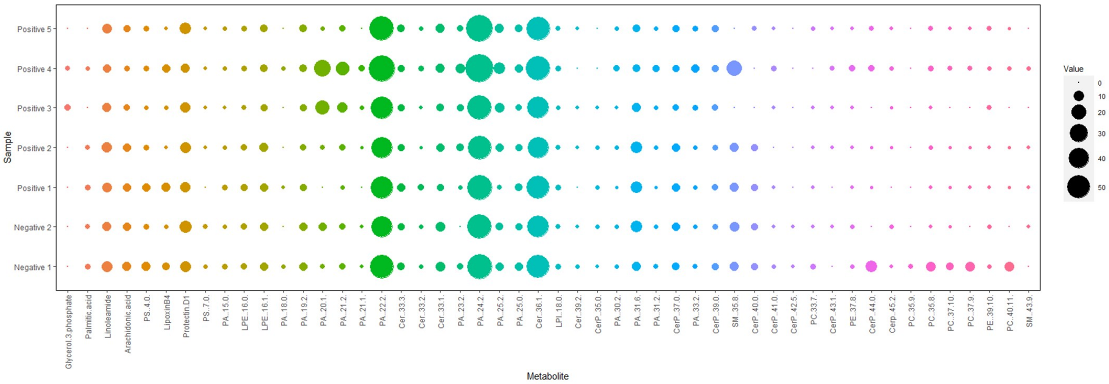

Figure 5.9: Scatter bubble plot of abundance of metabolites in each individual sample. The scale bar on the right side indicates the relative intensity.

5.4 Conclusion

We explored the sensitivity of plasmonic aluminum films microarray chips and their applicability as a viable substrate for MALDI-MS that has improved performance. POPC calibration curve indicated that this Al-chip has a higher sensitivity and lower limit detection than traditional MALDI-MS stainless steel plate. After that, further applications were researched using clinical samples that were more complicated. According to the findings, Al-chips could produce spectra of complex samples that are of a high quality for the purpose of data processing. In addition, infections caused by viruses have a considerable impact on the lipid content of infected cells and may change lipid metabolism in a way that is beneficial to the proliferation of viruses, as lipids are not only the primary component of membranes but also play crucial functions as intercellular signaling agents and energy sources. Therefore, conducting research into how SARS-COV-2 infection alters lipid metabolism and profile might potentially provide information on the link between lipid profile and inflammatory processes that occur during COVID-19. This work presents a rapid MS-based method with a novel potential substrate for analyzing COVID-19 disease directly from nasopharyngeal swabs.

References

[1] Xiaobo Yang, Yuan Yu, Jiqian Xu, Huaqing Shu, Hong Liu, Yongran Wu, Lu Zhang, Zhui Yu, Minghao Fang, Ting Yu, et al. Clinical course and outcomes of critically ill patients with sars-cov-2 pneumonia in wuhan, china: a single-centered, retrospective, observational study. *The Lancet Respiratory Medicine*, 8(5):475–481, 2020.

[2] Tadas Nikonovas, Allan Spessa, Stefan H Doerr, Gareth D Clay, and Symon Mezbahuddin. Near-complete loss of fire-resistant primary tropical forest cover in sumatra and kalimantan. *Communications Earth & Environment*, 1(1):1–8, 2020.

[3] Haibo Zhang, Josef M Penninger, Yimin Li, Nanshan Zhong, and Arthur S Slutsky. Angiotensin-converting enzyme 2 (ace2) as a sars-cov-2 receptor: molecular mechanisms and potential therapeutic target. *Intensive care medicine*, 46(4):586–590, 2020.

[4] Alexandra C Walls, Young-Jun Park, M Alejandra Tortorici, Abigail Wall, Andrew T McGuire, and David Veesler. Structure, function, and antigenicity of the sars-cov-2 spike glycoprotein. *Cell*, 181(2):281–292, 2020.

[5] Hamid Hadi-Alijanvand and Maryam Rouhani. Studying the effects of ace2 mutations on the stability, dynamics, and dissociation process of sars-cov-2 s1/hace2 complexes. *Journal of proteome research*, 19(11):4609–4623, 2020.

[6] Markus Hoffmann, Hannah Kleine-Weber, Simon Schroeder, Nadine Krüger, Tanja Herrler, Sandra Erichsen, Tobias S Schiergens, Georg Herrler, Nai-Huei Wu, Andreas Nitsche, et al. Sars-cov-2 cell entry depends on ace2 and tmprss2 and is blocked by a clinically proven protease inhibitor. *cell*, 181(2):271–280, 2020.

[7] Maier Lorizate and Hans-Georg Kräusslich. Role of lipids in virus replication. *Cold Spring Harbor perspectives in biology*, 3(10):a004820, 2011.

[8] Andrea Murillo, Rosario Vera-Estrella, Bronwyn J Barkla, Ernesto Méndez, and Carlos F Arias. Identification of host cell factors associated with astrovirus replication in caco-2 cells. *Journal of virology*, 89(20):10359–10370, 2015.

[9] Martina Wendel, Rüdiger Paul, and Axel R Heller. Lipoproteins in inflammation and sepsis. ii. clinical aspects. *Intensive care medicine*, 33(1):25–35, 2007.

[10] Bo Shen, Xiao Yi, Yaoting Sun, Xiaojie Bi, Juping Du, Chao Zhang, Sheng Quan, Fangfei Zhang, Rui Sun, Liujia Qian, et al. Proteomic and metabolomic characterization of covid-19 patient sera. *Cell*, 182(1):59–72, 2020.

[11] Di Wu, Ting Shu, Xiaobo Yang, Jian-Xin Song, Mingliang Zhang, Chengye Yao, Wen Liu, Muhan Huang, Yuan Yu, Qingyu Yang, Tingju Zhu, Jiqian Xu, Jingfang Mu, Yaxin Wang, Hong Wang, Tang Tang, Yujie Ren, Yongran Wu, Shu-Hai Lin, Yang Qiu, Ding-Yu Zhang, You Shang, and Xi Zhou. Plasma metabolomic and lipidomic alterations associated with COVID-19. *National Science Review*, 7(7):1157–1168, 04 2020.

[12] Mohamed Abu-Farha, Thangavel Alphonse Thanaraj, Mohammad G Qaddoumi, Anwar Hashem, Jehad Abubaker, and Fahd Al-Mulla. The role of lipid metabolism in covid-19 virus infection and as a drug target. *International journal of molecular sciences*, 21(10):3544, 2020.

[13] Marianna Caterino, Monica Gelzo, Stefano Sol, Roberta Fedele, Anna Annunziata, Cecilia Calabrese, Giuseppe Fiorentino, Maurizio D'Abbraccio, Chiara Dell'Isola, Francesco Maria Fusco, et al. Dysregulation of lipid metabolism and pathological inflammation in patients with covid-19. *Scientific reports*, 11(1):1–10, 2021.

[14] Pavlina T Ivanova, David S Myers, Stephen B Milne, Jennifer L McClaren, Paul G Thomas, and H Alex Brown. Lipid composition of the viral envelope of three strains of influenza virus not all viruses are created equal. *ACS infectious diseases*, 1(9):435–442, 2015.

[15] DP Nayak and EKW Hui. Membrane dynamics and domains: Subcellular biochemistry; quinn pj, ed, 2004.

[16] James P Quigley, Daniel B Rifkin, and Edward Reich. Phospholipid composition of rous sarcoma virus, host cell membranes and other enveloped rna viruses. *Virology*, 46(1):106–116, 1971.

[17] M Kates, AC Allison, DAJ Tyrrell, and AT James. Lipids of influenza virus and their relation to those of the host cell. *Biochimica et biophysica acta*, 52(3):455–466, 1961.

[18] Nathalie Callens, Britta Brügger, Pierre Bonnafous, Herve Drobecq, Mathias J Gerl, Thomas Krey, Gleyder Roman-Sosa, Till Rümenapf, Olivier Lambert, Jean Dubuisson, et al. Morphology and molecular composition of purified bovine viral diarrhea virus envelope. *PLoS pathogens*, 12(3):e1005476, 2016.

[19] Dan Dou, Rebecca Revol, Henrik Östbye, Hao Wang, and Robert Daniels. Influenza a virus cell entry, replication, virion assembly and movement. *Frontiers in immunology*, page 1581, 2018.

[20] Bingpeng Yan, Hin Chu, Dong Yang, Kong-Hung Sze, Pok-Man Lai, Shuofeng Yuan, Huiping Shuai, Yixin Wang, Richard Yi-Tsun Kao, Jasper Fuk-Woo Chan, et al. Characterization of the lipidomic profile of human coronavirus-infected cells: implications for lipid metabolism remodeling upon coronavirus replication. *Viruses*, 11(1):73, 2019.

[21] Antonio Russo, Carmine Minichini, Mario Starace, Roberta Astorri, Federica Calo, Nicola Coppola, et al. Current status of laboratory diagnosis for covid-19: a narrative review. *Infection and Drug Resistance*, 13:2657, 2020.

[22] Mercy R Benzigar, Ripon Bhattacharjee, Mahroo Baharfar, and Guozhen Liu. Current methods for diagnosis of human coronaviruses: pros and cons. *Analytical and bioanalytical chemistry*, 413(9):2311–2330, 2021.

[23] Jamil N Kanji, Nathan Zelyas, Clayton MacDonald, Kanti Pabbaraju, Muhammad Naeem Khan, Abhaya Prasad, Jia Hu, Mathew Diggle, Byron M Berenger, and Graham Tipples. False negative rate of covid-19 pcr testing: a discordant testing analysis. *Virology journal*, 18(1):1–6, 2021.

[24] Paul S Wikramaratna, Robert S Paton, Mahan Ghafari, and José Lourenço. Estimating the false-negative test probability of sars-cov-2 by rt-pcr. *Eurosurveillance*, 25(50):2000568, 2020.

[25] Kevin W Ng, Nikhil Faulkner, Georgina H Cornish, Annachiara Rosa, Ruth Harvey, Saira Hussain, Rachel Ulferts, Christopher Earl, Antoni G Wrobel, Donald J Benton, et al. Preexisting and de novo humoral immunity to sars-cov-2 in humans. *Science*, 370(6522):1339–1343, 2020.

[26] Carolina Lucas, Jon Klein, Maria E Sundaram, Feimei Liu, Patrick Wong, Julio Silva, Tianyang Mao, Ji Eun Oh, Subhasis Mohanty, Jiefang Huang, et al. Delayed production of neutralizing antibodies correlates with fatal covid-19. *Nature medicine*, 27(7):1178–1186, 2021.

[27] Ke Pan, Yulun Chiu, Eric Huang, Michelle Chen, Junmei Wang, Ivy Lai, Shailbala Singh, Rebecca M Shaw, Michael J MacCoss, and Cassian Yee. Mass spectrometric identification of immunogenic sars-cov-2 epitopes and cognate tcrs. *Proceedings of the National Academy of Sciences*, 118(46):e2111815118, 2021.

[28] Xin Wang, Gang Xu, Xiaoju Liu, Yang Liu, Shuye Zhang, and Zheng Zhang. Multi-omics: unraveling the panoramic landscapes of sars-cov-2 infection. *Cellular & Molecular Immunology*, 18(10):2313–2324, 2021.

[29] Baoxu Lin, Jianhua Liu, Yong Liu, and Xiaosong Qin. Progress in understanding covid-19: insights from the omics approach. *Critical Reviews in Clinical Laboratory Sciences*, 58(4):242–252, 2021.

[30] Tomas Do, Roman Guran, Vojtech Adam, and Ondrej Zitka. Use of maldi-tof mass spectrometry for virus identification: a review. *Analyst*, 2022.

[31] Hongyan Bi, Liang Qiao, Jean-Marc Busnel, Valerie Devaud, Baohong Liu, and Hubert H Girault. Tio2 printed aluminum foil: single-use film for a laser desorption/ionization target plate. *Analytical chemistry*, 81(3):1177–1183, 2009.

[32] Alexandra Bondarenko, Yingdi Zhu, Liang Qiao, F Cortes Salazar, Horst Pick, and HH Girault. Aluminium foil as a single-use substrate for maldi-ms fingerprinting of different melanoma cell lines. *Analyst*, 141(11):3403–3410, 2016.

[33] Abdelhamid Hani Nasser and Badr Gamal. Nanobiotechnology as a platform for the diagnosis of covid-19: a review. *Nanotechnology for Environmental Engineering*, 6(1), 2021.

[34] Hani Nasser Abdelhamid and Gamal Badr. Nanobiotechnology as a platform for the diagnosis of covid-19: a review. *Nanotechnology for Environmental Engineering*, 6(1):1–26, 2021.

[35] Liang Qiao, Hongyan Bi, Jean-Marc Busnel, Mohamad Hojeij, Manuel Mendez, Baohong Liu, and Hubert H Girault. Controlling the specific enrichment of multi-phosphorylated peptides on oxide materials: aluminium foil as a target plate for laser desorption ionization mass spectrometry. *Chemical Science*, 1(3):374–382, 2010.

[36] Davy Gérard and Stephen K Gray. Aluminium plasmonics. *Journal of Physics D: Applied Physics*, 48(18):184001, 2014.

[37] Peter V Shanta, Bochao Li, Daniel D Stuart, and Quan Cheng. Plasmonic gold templates enhancing single cell lipidomic analysis of microorganisms. *Analytical chemistry*, 92(9):6213–6217, 2020.

[38] Bochao Li, Daniel D Stuart, Peter V Shanta, Caleb D Pike, and Quan Cheng. Probing herbicide toxicity to algae (selenastrum capricornutum) by lipid profiling with machine learning and microchip/maldi-tof mass spectrometry. *Chemical Research in Toxicology*, 35(4):606–615, 2022.

[39] Alexander S Lambert, Santino N Valiulis, Alexander S Malinick, Ichiro Tanabe, and Quan Cheng. Plasmonic biosensing with aluminum thin films under the kretschmann configuration. *Analytical chemistry*, 92(13):8654–8659, 2020.

[40] Abdennour Abbas, Matthew J Linman, and Quan Cheng. Patterned resonance plasmonic microarrays for high-performance spr imaging. *Analytical chemistry*, 83(8):3147–3152, 2011.

[41] Kun Qian, Liang Zhou, Jun Zhang, Chang Lei, and Chengzhong Yu. A combo-pore approach for the programmable extraction of peptides/proteins. *Nanoscale*, 6(10):5121–5125, 2014.

[42] Vadanasundari Vedarethinam, Lin Huang, Wei Xu, Ru Zhang, Deepanjali D Gurav, Xuming Sun, Jing Yang, Ruoping Chen, and Kun Qian. Detection and inhibition of bacteria on a dual-functional silver platform. *Small*, 15(3):1803051, 2019.

[43] Xuming Sun, Lin Huang, Ru Zhang, Wei Xu, Jingyi Huang, Deepanjali D Gurav, Vadanasundari Vedarethinam, Ruoping Chen, Jiatao Lou, Qian Wang, et al. Metabolic fingerprinting on a plasmonic gold chip for mass spectrometry based in vitro diagnostics. *ACS central science*, 4(2):223–229, 2018.

[44] Lin Huang, Jingjing Wan, Xiang Wei, Yu Liu, Jingyi Huang, Xuming Sun, Ru Zhang, et al. Plasmonic silver nanoshells for drug and metabolite detection. *Nature communications*, 8(1):1–10, 2017.

[45] Luigi Ranno, Stefano Dal Forno, and Johannes Lischner. Computational design of bimetallic core-shell nanoparticles for hot-carrier photocatalysis. *npj Computational Materials*, 4(1):1–7, 2018.

[46] Scott Kevin Cushing, Chih-Jung Chen, Chung Li Dong, Xiang-Tian Kong, Alexander O Govorov, Ru-Shi Liu, and Nianqiang Wu. Tunable nonthermal distribution of hot electrons in a semiconductor injected from a plasmonic gold nanostructure. *ACS nano*, 12(7):7117–7126, 2018.

[47] Lipid maps. http://www.lipidmaps.org/. Accessed: 20221022.

[48] Oihane E Albóniga, Daniel Jiménez, Matilde Sánchez-Conde, Pilar Vizcarra, Raquel Ron, Sabina Herrera, Javier Martínez-Sanz, Elena Moreno, Santiago Moreno, Coral Barbas, et al. Metabolic snapshot of plasma samples reveals new pathways implicated in sars-cov-2 pathogenesis. *Journal of Proteome Research*, 21(3):623–634, 2022.

[49] Imesha W De Silva, Subhayu Nayek, Vijay Singh, Jay Reddy, John K Granger, and Guido F Verbeck. Paper spray mass spectrometry utilizing teslin® substrate for rapid detection of lipid metabolite changes during covid-19 infection. *Analyst*, 145(17):5725–5732, 2020.

[50] Kyana Y Garza, Alex Ap Rosini Silva, Jonas R Rosa, Michael F Keating, Sydney C Povilaitis, Meredith Spradlin, Pedro H Godoy Sanches, Alexandre Varao Moura, Junier Marrero Gutierrez, John Q Lin, et al. Rapid screening of covid-19 directly from clinical nasopharyngeal swabs using the masspec pen. *Analytical chemistry*, 93(37):12582–12593, 2021.

[51] Ilaria Casari, Marcello Manfredi, Pat Metharom, and Marco Falasca. Dissecting lipid metabolism alterations in sars-cov-2. *Progress in lipid research*, 82:101092, 2021.

[52] Philip V'kovski, Hawaa Al-Mulla, Volker Thiel, and Benjamin W Neuman. New insights on the role of paired membrane structures in coronavirus replication. *Virus research*, 202:33–40, 2015.

[53] IL Van Genderen, G-J Godeke, PJM Rottier, and G Van Meer. The phospholipid composition of enveloped viruses depends on the intracellular membrane through which they bud, 1995.

[54] Di Wu, Ting Shu, Xiaobo Yang, Jian-Xin Song, Mingliang Zhang, Chengye Yao, Wen Liu, Muhan Huang, Yuan Yu, Qingyu Yang, et al. Plasma metabolomic and lipidomic alterations associated with covid-19. *National Science Review*, 7(7):1157–1168, 2020.

[55] Michele Ciccarelli, Fabrizio Merciai, Albino Carrizzo, Eduardo Sommella, Paola Di Pietro, Vicky Caponigro, Emanuela Salviati, Simona Musella, Veronica di Sarno, Mariarosaria Rusciano, et al. Untargeted lipidomics reveals specific lipid profiles in covid-19 patients with different severity from campania region (italy). *Journal of pharmaceutical and biomedical analysis*, page 114827, 2022.

[56] Valerie B O'Donnell, Robert C Murphy, and Steve P Watson. Platelet lipidomics: modern day perspective on lipid discovery and characterization in platelets. *Circulation research*, 114(7):1185–1203, 2014.

[57] Masayuki Morita, Keiji Kuba, Akihiko Ichikawa, Mizuho Nakayama, Jun Katahira, Ryo Iwamoto, Tokiko Watanebe, Saori Sakabe, Tomo Daidoji, Shota Nakamura, et al. The lipid mediator protectin d1 inhibits influenza virus replication and improves severe influenza. *Cell*, 153(1):112–125, 2013.

[58] Murat Cihan, Özlem Doğan, Ceyhan Ceran Serdar, Arzu Altunçekiç Yıldırım, Celali Kurt, and Muhittin A Serdar. Kynurenine pathway in coronavirus disease (covid-19): Potential role in prognosis. *Journal of clinical laboratory analysis*, 36(3):e24257, 2022.

Chapter 6

Conclusion and Future Outlook

6.1 Summary of Dissertation Work

The work summarized in the dissertation has primarily focused on applying plasmonic substrate with enhanced MALDI-MS signal for the lipidomic study of microorganisms at the single-cell level. The plasmonic substrate-assisted methodology has been used to identify, quantify, and monitor the lipid changes in diverse samples impacted under different conditions, including algae affected by herbicides, bacteria treated with antibiotics, and clinical samples infected with SARS-CoV-2 virus. This work has demonstrated the potential applications of this advanced technological platform in multiple research fields, including environmental study (Chapter 2) and clinical study (Chapter 3,4 and 5).

The lipidomic analysis based on the plasmonic substrate was demonstrated in Chaper2, 3, and 4. In Chapter 2, we showed a direct, label-free analytical approach to detect lipids and categorize lipid profiles directly on intact algae cells using gold microchip MALDI-TOF mass spectrometry. We have shown that the platform can characterize changes in lipidomic response to several herbicides and revealed some unique herbicide effects on lipid profiles between algae species. Also, machine learning was integrated with MALDI-MS lipid analysis to categorize treatment groups with models. This technology can be used to characterize various cell types and their lipid mass fingerprint for monitoring of environmentally relevant chemicals. In Chapter 3, we applied this platform to the lipidomic study of *E.coli*, a bacterial model system with more complex membrane structures than algae. Compared to HPLC-MS, MALDI-TOF-MS is faster and simpler to implement without the need for sample preparation. A library of 68 lipids was built and a few biomarkers were identified. Our data show that colistin strongly affects *E.coli* lipid expression, which can be differentiated by lipid profiling, and the lipidomic study can help interpret colistin's antibacterial action. This work lays the foundation for the future study of more diverse bacterial species and their identification and classification.In Chapter 4, photosensitizer was selected to facilitate metabolite profile collection for food-borne pathogens using the plasmonic substrate/MALDI-MS platform. Each species was found to form a distinct metabolite profile in the m/z range of 400-2000, enabling species differentiation from bulk samples to single-cell analyses. Combined with machine learning, unique metabolite profiling based on MALDI-TOF-MS can differentiate bacterial pathogens at the single-cell level. Our research has indicated that integrating microorganism fingerprinting with advanced informatics will provide simple and effective diagnostic and monitoring tools in medicine, environment, and food safety studies. In Chapter 5, we investigated a more sensitive and high-performance plasmonic substrate with aluminum thin films, which is low-cost and abundant. COVID-19 clinical samples were studied based on the Al-chips. Results reveal Al-chips can create high-quality spectra of complicated samples for data processing. In addition, viral infections impact the lipid content of infected cells and change lipid metabolism to promote virus multiplication. Examining how SARS-CoV-2 alters lipid metabolism and profile may reveal the relationship between lipid profile and inflammatory processes in COVID-19. This work presents a novel and fast MS-based technique for COVID-19 disease analysis using nasal swabs.

6.2 Future Outlook

Single-cell metabolomics and lipidomics is still a budding field when compared to proteomics. Current limitations of single-cell metabolomics include low throughput for methods to distinguish technical variability from biological variability, a need for higher sensitivity for low abundant metabolites or metabolites with low ionization efficiencies, and a need for improvements in software/databases to identify metabolites of interest and provide biological relevance to the results.[1] However, MS-based lipidomics has already been the most significant method in understanding basic lipid metabolism processes and their changes in pathological states, allowing the discovery of biomarkers for disease diagnosis and drug targets. Almost all lipid species in biological samples can be profiled and quantified by optimizing analytical methods. However, the separation of lipid isomers, the identification of lipid C=C bond locations, and the position of acyl chain branching and stereo-structure are still difficult and would need to be addressed in future development.[2] Furthermore, the integration of multi-omics analytical techniques is critical for better understanding the relationships between individual lipids and lipid classes within a metabolic network, as well as uncovering the role of specific lipid molecules in cellular functions, because the metabolism process in the human body is intertwined with interactions between genes, proteins, metabolites, lipids, and enzymes.[3] Multi-omics analytical methodologies can maximize the power of lipidomics in areas of discovering new lipid biomarkers, understanding disease pathology, and monitoring drug therapy efficacy. [2]

It should be noted that with the fast advancement of metabolomics, there has been an increasing demand for high-throughput, sensitive analysis of small-molecule. LDI MS technology allows for high sensitivity, accuracy, resolution, and throughput in molecular analysis, which has significant potential for metabolomics research. Although significant efforts have been made to generate functional nanomaterials for enhancing the MS readout of biomolecules, the research in this area is still far from mature, and more focus must be placed on the innovation of nanomaterials and the exploitation of in-depth applications. In order to address the rising analytical needs for large-scale identification of many targets in complicated biosamples, more customized nanomaterials with multiple functionalities and improved affinity and specificity need to be developed. [4] Although some nanomaterials have been made that can separate and detect targets simultaneously, the enrichment capacity and desorption/ionization efficiency still need to be improved. For the mechanism investigation, the continuous focus should be placed on elucidating the underlying relationship between the structure of nanomaterials and the desorption/ionization efficiency of analytes, which could lead to the development of nanomaterials with high energy absorption and transfer capacity, and low background interference in MS analysis.[5] From the perspective of the application, the use of nanomaterials in MS characterization should be aimed to address the particular issues inaccessible to conventional approaches. One example is the development of nanoprobes able to monitor the release of endogenous biomarker metabolites or exogenous therapeutic agents in tissues by MS imaging of their molecular weight signals or alternative mass tag signals.[5] In addition, MS can be integrated with other detection methods that offer distinct technological benefits. For instance, developing multimodal procedures that combine MS with Raman spectroscopy, fluorescence, or other analytical techniques might optimize the effective information collected from complicated biomedical materials to fulfill the critical demands and obstacles of clinical diagnosis.[5]

References

[1] Kyle D Duncan, Jonas Fyrestam, and Ingela Lanekoff. Advances in mass spectrometry based single-cell metabolomics. *Analyst*, 144(3):782–793, 2019.

[2] Tianrun Xu, Chunxiu Hu, Qiuhui Xuan, and Guowang Xu. Recent advances in analytical strategies for mass spectrometry-based lipidomics. *Analytica Chimica Acta*, 1137:156–169, 2020.

[3] Ting Hu and Jin-Lan Zhang. Mass-spectrometry-based lipidomics. *Journal of separation science*, 41(1):351–372, 2018.

[4] Kyle D Duncan, Jonas Fyrestam, and Ingela Lanekoff. Advances in mass spectrometry based single-cell metabolomics. *Analyst*, 144(3):782–793, 2019.

[5] Hongmei Xu, Zhenzhen Zhang, Yihan Wang, Weifeng Lu, and Qianhao Min. Engineering of nanomaterials for mass spectrometry analysis of biomolecules. *Analyst*, 2021.